Physik Department

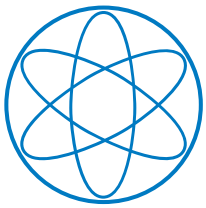

In vitro studies of cytoskeletal structure formation

Dissertation

von

Carina Pelzl

Technische Universität
München

TECHNISCHE UNIVERSITÄT MÜNCHEN

Lehrstuhl für Biophysik E27

In vitro studies of cytoskeletal structure formation

Carina Vanessa Pelzl

Vollständiger Abdruck der von der Fakultät für Physik der Technischen Universität München zur Erlangung des akademischen Grades eines

Doktors der Naturwissenschaften (Dr. rer. nat.)

genehmigten Dissertation.

Vorsitzender:		Univ.-Prof. Dr. M. Zacharias
Prüfer der Dissertation:	1.	Univ.-Prof. Dr. A. Bausch
	2.	Univ.-Prof. Dr. M. Rief

Die Dissertation wurde am 31.08.2015 bei der Technischen Universität München eingereicht und durch die Fakultät für Physik am 25.09.2015 angenommen.

Summary

In eukaryotic cells various functions such as cell division, phagocytosis or cell locomotion rely heavily on the cellular cytoskeleton. The actin cytoskeleton is a complex system that consists mainly of the dynamic protein polymer actin. It is orchestrated by numerous regulatory factors such as cross-linking, nucleation, severing or capping proteins. One of the actin cytoskeleton's main function is to provide mechanical stability for the cell. Especially during locomotion the cytoskeleton constantly rearranges itself. While continuous actin disassembly occurs in the cell interior, regulated actin polymerization at the cell's leading edge takes place. Through this process the cell generates protrusion forces. The dynamic polymerization of the cytoskeleton results here in the formation of various structures such as finger-like filopodia or sheet-like lamellipodia.
Despite the fundamental importance of such structures involved in locomotion, the underlying microscopic mechanisms and their consequences are poorly understood. Specifically, the mechanism of filopodia initiation and force generation remains controversial as well as the structural transition between lamellipodia and filopodia. To understand the individual effects of the involved proteins on the network, it is essential to study the mechanisms underlying the formation of these two actin structures in a more general way. In this thesis, I studied the self-assembly of purified proteins mainly engaged in lamellipodia and filopodia.

The first series of experiments that were performed addresses the self-assembly of proteins involved in filopodia. The network formation depends heavily on the spatio-temporal polymerization of actin, which is influenced by nucleators, capping proteins and especially cross-linkers like fascin. Therefore, the self-assembly and interplay of the participating proteins is studied initially by microscopical bulk measurements.
Since the network assembly in bulk measurements is a simultaneous process of polymerization and cross-linking, I also investigated localized directed actin filament

growth from a spherical surface with and without the addition of fascin. By this means, we gain a better understanding on how the changes in mechanics caused by cross-linking affect the polymerization.

To achieve this the nucleator formin is attached to sepharose beads, from where it nucleates actin filaments. Parallel filaments form a cortex around the bead that steadily grows from the surface radially outwards. The density depends on the amount of formin on the surface. When the filaments in the network are dense and long enough, they get entangled at the far end from the surface. The continuously elongating filaments keep pushing from the center, bend and finally break many filaments at the outside of the cortex simultaneously. However, if the bundling protein fascin is present during polymerization a completely different cortex emerges. With fascin, a spiky dense but thin actin cortex forms around the bead. This clearly demonstrates that cross-linking has a strong impact on the polymerization process.

I investigated the effect of the cross-linking process on the polymerization by subsequent fascin addition to the actin cortex. Upon the addition of fascin a contraction of the actin cortex could be observed starting at the outside and running inwardly for all beads. The growth of the cortex was discontinuous.

To analyze, how exactly cross-linking leads to this arrest of actin filament elongation, I performed elasticity measurements by the means of an optical tweezer set-up. By these experiments I could show that the actin network stiffened through the delayed addition of fascin. I was also able to demonstrate this arrest of elongation with other cross-linkers like alpha-actinin or anillin showing that this behavior is cross-linker independent.

To explain this arrest, I propose a model in which the stiffening of the cortex leads to an opposing force that counteracts the polymerization force at the surface of the bead. This results into the stalling of any further polymerization of the actin filaments. I was able to verify my model by calculations that demonstrate that the change in elasticity gives rise to opposing forces well into the pN range. These forces exceed the stalling force of an actin filament of a few pN. Therefore, I conclude that the polymerization of parallel actin filaments is stalled by an opposing force that is generated by the mechanics of a now cross-linked structure.

These new findings contribute to a better understanding of individual effects of the proteins involved in filopodia mechanics. They provide new perspectives on how filopodia are initiated and how forces are generated.

The second part of this thesis focuses on the structural transition of lamellipodia to filopodia and of the self-assembly of the actin network there. For this, mechanic and dynamic properties of purely branched and cross-linked branched actin networks are addressed by macrorheological experiments with proteins that are mainly involved in the assembly of those two structures, especially the branching protein Arp2/3 complex and the cross-linker fascin.
I observed a non-monotonically increase of the storage modulus during the polymerization process of branches actin networks. For purely branched networks the modulus increases rapidly, shortly decreases then increases again more slowly. This increase could not be observed with cross-linked branched networks. Here, after a steep increase the storage modulus decreases until it reaches a steady state.
I propose for both networks a model in which the newly formed branches by Arp2/3 complex are highly unstable. Very shortly after branching, they dissociate from their mother filaments. For non-cross-linked networks, the ex-daughter branches then diffuse due to their shortness and start to anneal into longer filaments. An entanglement of these filaments then gives rise to a slowly increasing storage modulus. If cross-linkers are present during polymerization, the branches still undergo dissociation. However, since the debranched filaments are cross-linked they cannot diffuse and anneal anymore. Connections are irrecoverably lost as the loose filament ends cannot form new ones. This explains the continuous decrease of the storage modulus after a steep increase in the presence of fascin.
Through this work we gained novel insights about the structural and temporal interplay of the proteins involved in filopodia during polymerization of actin. This will benefit further understanding of the initiation of filopodia and their transition from the lamellipodium.

The present thesis provides new findings about the two cytoskeletal structures involved in locomotion of cell. The physical principles and effects described in this work help to establish a microscopic understanding of both the mechanics of filopodia and the organizational and viscoelastic properties of the structural transition from the lamellipodium to the filopodium.

Contents

1 Introduction

The cellular cytoskeleton is a highly complex and dynamic network that constantly rearranges itself as the cell divides and moves. Locomotion of single cells is crucial for many vital processes in organisms such as fibroblast migration in wound healing [Shaw and Martin, 2009] or tissue patterns in embryogenesis [Gordon, 1994]. In addition, cell locomotion also plays a pivotal role in the formation of cancerous metastases.
During cellular migration regulated actin assembly takes place at the frontal plasma membrane [Pollard and Borisy, 2003, Schafer, 2004, Welch, 1997]. Along with this rearrangement disassembly within the cell interior comes along. Actin filaments need to depolymerize inside to ensure a constant flow of material to the forward-pressing membrane. During locomotion the cell produces broad but thin sheet-like structures, named lamellipodia, and long thin spikes named filopodia through regulated actin assembly.
Filopodia act as antennae for cells to probe their environment. Therefore, they have particular important role in cell migration, neurite growth and wound healing [Mattila and Lappalainen, 2008].

Most cells develop both structures. Other like dendritic cells are dominated by filopodia [Mejillano et al., 2004], while keratocytes grow exclusively lamellipodia [Mogilner and Oster, 1996]. Much is know about the lamellipodia and the filopodia itself, but why certain cells are *in vivo* dominated by just one structure remains elusive besides what determines their preference.
The actin bundling protein fascin is present in particular in the filopodia but abundant in the lamellipodium and the actin related protein 2 and 3 (Arp2/3) complex with its branching capability is only present in the lamellipodium but not in the filopodium, where thick parallel bundles prevail.

Although protrusions of lamellipodia and filopodia are tightly coupled, both structures are organized very differently and generate their filaments in other ways. Fur-

thermore, this organization and generation uses different mechanism to produce force at the plasma membrane. Whereas in the lamellipodia the actin filaments are organized into a flat highly branched network [Pollard and Borisy, 2003, Svitkina, 1999], filaments are assembles into long thick parallel bundles in the filopodia [Svitkina et al., 2003, Resch et al., 2002, Lewis and Bridgman, 1992]. Furthermore, different proteins control the assembly of the structures. Filament generation and branching in the lamellipodia is dominated by the activation the actin-related protein 2 and 3 (Arp2/3) complex [Blanchoin et al., 2000a] by the Wiskott-Aldrich syndrome protein family [Machesky and Insall, 1998, Takenawa and Miki, 2001], followed by simple elongation and barbed-end capping by capping protein [Cooper and Schafer, 2000]. In filopodia on the other hand formin and Ena/VASP is concentrated at the tips of filopodia [Schirenbeck et al., 2005, Applewhite et al., 2007] that promotes persistent elongation of filaments, which are then successively bundled by fascin. This cross-linking process by fascin gives the filopodia the necessary strength and stiffness to protrude into the plasma membrane and overcome its resistance. In both structures the elongating barbed ends face the cell membrane and thus by elongation they are able to push it forward.

Two different mechanism are suggested to explain the formation of the filopodia [Yang and Svitkina, 2011, Gupton and Gertler, 2007].
In the "convergent elongation model" the filopodia are deeply rooted into the branched network of the lamellipodia [Svitkina et al., 2003, Mogilner and Rubinstein, 2005, Yang et al., 2007]. During formation of filopodia, preexisting lamellipodial filaments are associated at their barbed ends with the formin mDia2 and by that elongated continuously. Those filaments then coalesce and converge into bundles by the cross linker fascin and can now protrude as stable filopodia the plasma membrane.
In contrast to this model is the "tip nucleation model" or "*de novo* filopodia nucleation model". Here, proteins of the formin family nucleate new actin filaments directly at the membrane and also promote their elongation. According to this mechanism, bundles do not emanate from the lamellipodia and are not anchored there. The Arp2/3 complex is not needed for filopodia formation.

Besides the fact that the initiation of the filopodia remains controversial, it is also still not fully understood how cells control the transition between lamellipodia and filopodia and what assigns the localization of filopodia formation along the cell membrane. It is very likely that the generation of filopodia is strongly affected by the properties of the branched network in the lamellipodium from where they emerge.

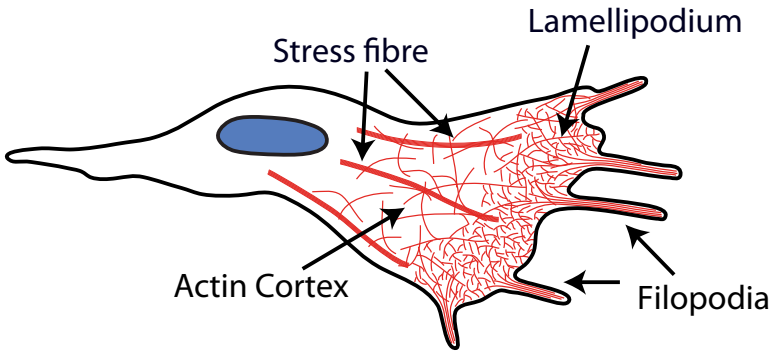

Figure 1.1: Schematic representation of different actin structures in the cell: The actin cortes is a homogeneously cross-linked network that provides mechanical support for the cell and the plasma membrane. Here, stress fibers are embedded. These are antiparallel bundles that are spanning the cell. At the leading edge of the cell, a highly branched network forms the lamellipodium, which is a almost two-dimensional thin broad structure. From there, finger-like protrusions emerge. These so-called filopodia consist of parallel bundled actin filaments and extend beyond the lamellipodium, protruding the cell membrane.

It was shown that the concentration of Arp2/3 complex has a strong effect on these structural properties and influences the formation of filopodia [Korobova and Svitkina, 2008]. Furthermore, the absence of fascin also results in a strong decline of filopodia generation [Vignjevic et al., 2006].
However, it is still not clear how the concentration of Arp2/3 complex in the lamellipodia and the fascin concentration influence filopodia formation.

Biomimetic systems provide a simplified controlled environment for studying the fundamental physical principles concerning self-assembly of proteins and cellular motility. To resolve these issues, it is essential to understand the mechanisms underlying the formation of lamellipodia and filopodia in a more general way. Furthermore, is it necessary to evaluate the factors that play a role in controlling the structure and the dynamics. So here, we studied the self-assembly of purified proteins mainly involved in lamellipodia and filopodia in both bulk and directed growth from a surface without the influence of a plasma membrane.

2 Materials, Methods and Theoretical Background

2.1 Proteins and Labels

2.1.1 Actin

Actin is a 42 kDa globular protein, which is found in almost all eukaryotic cells. It is a key component of the cytoskeleton and plays a major role in cell motility, cell division and cytokinesis, as well as in vesicle transport and muscle contraction.
These processes of the cytoskeleton are all highly dynamic and therefore, actin filaments are permanently rearranged in the cell. At the front, the cell polymerizes actin in the lamellipodia and the filopodia and hence, at the backside of the lamellipodia actin networks need to be dismantled to ensure that enough material is available for new structures. By depolymerization and polymerization a constant flow of actin takes place in a cell.

Actin has a binding pocket for different sorts of nucleotides, mainly ATP and ADP, and can exist in its free monomeric form (G-actin) or polymerize into a filamentous form (F-actin). Polymerization is initiated by the binding of ATP and the presence of ions such as $MgCl_2$. The filaments are two-stranded helical polymers assembled in a polar fashion with their ends distinguishable by their on and off rates for actin, depending the bound nucleotide (Fig. 2.2).
The fast polymerizing end, the barbed or plus end, has an on rate of 11.6 $\mu M^{-1}s^{-1}$ for ATP-actin and only 2.9 $\mu M^{-1}s^{-1}$ for ADP-actin. In contrast, the other end, named the pointed or minus end, binds ATP-actin monomers with an on rate of just k_{on} = 1.3 $\mu M^{-1}s^{-1}$ and ADP-actin with 0.14 $\mu M^{-1}s^{-1}$. Here, for ADP-actin off rate is with k^{-}_{off}(ADP)=0.25 s^{-1} is almost twice a high than its on rate [Pollard, 2007],

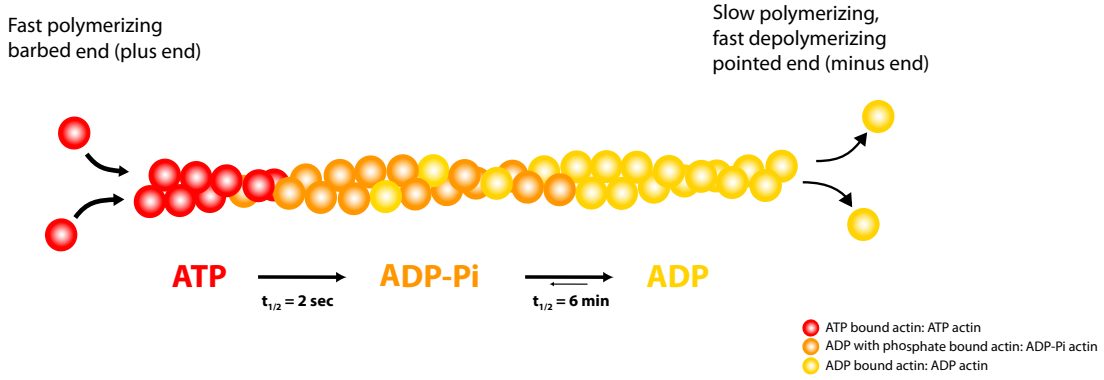

Figure 2.1: Actin mainly elongates at the fast polymerizing barbed end through the addition of free ATP-actin monomers. ATP-actin quickly hydrolyzes into ADP-P_i actin. With time the γ- phosphate dissociates from the filament and actin turns into ADP-actin. The the pointed end, ADP-actin then depolymerizes.

and thus depolymerizing mainly occurs at the minus end.
These different rates lead to a phenomenon that received a lot of interest in scientific publications. This process known as treadmilling is due to the fact that not all actin monomers will be incorporated into filaments. In equilibrium, there is always a constant monomer pool, which is about 0.1 µM, which is denoted by the dissociation constant $K_d = \frac{k_{off}}{k_{on}}$.
The incorporation of one monomer elongates the filament 2.7 nm. So, if the k_{on} rate is applied to a concentration of c_{actin} = 10 µM the filaments grow *in vitro* at an initial speed of 0.3 µm/s.

Actin monomers age within the filament with time and thus monomers bound with different nucleotides are observed along the filament. Newer parts are almost exclusively composed of ATP-actin, whereas older segments consist mainly out of ADP-actin.
The ATP bound to the actin monomer undergoes hydrolysis upon incorporation into an actin filament. The ATP-actin is very unstable once polymerized and the ATP is quickly hydrolyzed into ADP with γ-phosphate P_i still bound to the actin monomer (ADP-P_i actin). The half-life of polymerized ATP-actin is only ∼2 sec. ADP-P_i actin is more stable. The γ-phosphate dissociates slowly from the ADP-P_i actin with a half time of ∼6 min (Fig. 2.1). This reaction is reversible, but the affinity of polymerized ADP-actin for inorganic phosphate is low, with a K_d in the millimolar range [Carlier and Pantaloni, 1988].

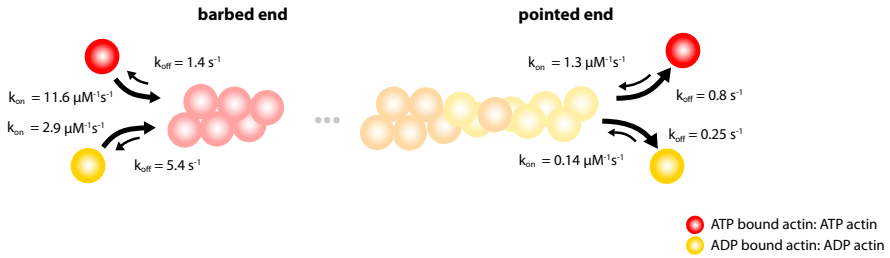

Figure 2.2: Rate and equilibrium constants for association and dissociation of ATP-actin and ADP-actin subunits at both ends of actin filaments.

Purification G-actin is purified from rabbit skeletal muscle by a modified protocol of Spudich and Watt [1971], upon which an additional gel filtration (Sephacryl S-300 HR) step is followed [MacLean-Fletcher and Pollard, 1980]. Actin monomer solution is stored in G-Buffer (2 mM Tris, 0.2 mM ATP, 0.2 mM $CaCl_2$, 0.2 mM DTT and 0.005 % NaN_3, pH 8). The G-actin solutions are kept at 4 °C and used within ten days of preparation. Polymerization is initiated by adding 1/10 volume of a low salt 10x polymerization buffer (100 mM Imidazol, 30 mM $MgCl_2$, 2 mM $CaCl_2$ and 0.05% NaN_3, pH 7.3) and gently but rapid mixing.

Fluorescent labeling

Labeling with phalloidin For fluorescent microscopy experiments actin is visualized by labeled phalloidin. Phalloidin, a cyclic peptide with a molecular weight of 789 Da, is isolated from one of the toxic mushroom Amanita phalloides that binds and stabilizes actin filaments against depolymerization by reducing the rate of subunit dissociation to near zero at both ends of the actin filaments [Dancker et al., 1975]. This changes as well the internal dynamics of actin filaments. Since we do not investigate actin dynamics, visualizing actin by labeled phalloidin is preferred to covalently labeled actin monomers as with phalloidin labeling a much better contrast can be obtained.
Here, both Alexa Fluor 488-phalloidin as well as Alexa Fluor 647-phalloidin (A12379, A22287; Life Technologies) are used.

Covalently labeled actin monomers To directly label actin monomers, an amine-reactive fluorescent dye is attached covalently to the N-terminus as described by [Kellogg et al., 1988]. For pyrene assay experiments, G-actin is labeled at its cysteine

374 with N–(1-pyrenyl)iodoacetamide [Cooper et al., 1983]. The dyes used here are the amine-reactive dye Atto 488 NHS-ester, Atto 532 NHS-ester or Atto 647N NHS-ester (Jena Bioscience, #FP 201-488, #FP 201-532, #FP 201-647N).
To fluorescently label actin, actin is dialyzed against borat buffer (50 mM boric acid, 0.2 mM $CaCl_2$, 0.2 mM ATP, pH 8) before polymerization is induced by addition of 10% polymerization buffer (100 mM imidazole, 10 mM ATP, 30 mM $MgCl_2$, 2 mM $CaCl_2$, 0.05% NaN3, pH 7.2). F-actin is incubated for 1 h with the dye (dissolved in DMSO) in a 1-2 fold molar excess at room temperature, which then covalently binds to amino groups. Afterwards, actin is centrifuged (2 h, 100 000 g, 4 °C) and the pellet is resuspended in G-buffer, homogenized and depolymerized for at least 24 h. Sample is again centrifuged for clarification, lyophilized and stored at -20 °C. Labeling degree can highly vary depending on the utilized dye and its amount. In most cased a labeling degree of $\sim$ 120% for Atto 488 and Atto 647N is achieved as well as 70% for pyrene.

2.1.2 Cross-linking and bundeling proteins

Actin can be cross-linked by many different proteins. Some examples are fascin, α-actinin, or filamin. Depending on the nature and the size of the cross-linker, the actin network is denser or more spacious, its actin bundles are either parallel, antiparallel or crossed over cross-linked. Common to all cross-linkers and bundling proteins is the ability to stiffen the actin network and give rise to more elasticity. For example, in order to generate filopodia the membrane tension can only be overcome by the insertions of fascin. Fascin bundles more than 15 filaments into one thick bundle that now is stiff enough to protrude the membrane.

a) Fascin

Fascin is a 55 kDa monomeric actin cross-linking protein that is *in vivo* mostly localized in filopodia and filopodia-like structures [Vignjevic et al., 2006]. *In vitro* fascin bundles actin filaments to polar, hexagonally packed bundles with a well defined maximum bundle thickness of about 20 filaments [Claessens et al., 2008].
Here, recombinant human fascin is purified from *e.coli* BL21 and stored at -80 °C in 2 mM Tris/HCl (pH 7.4), 150 mM KCl [Vignjevic et al., 2003, Ono et al., 1997].

b) α-Actinin

α-Actinin is a highly conserved large protein, which forms an antiparallel dimer with three actin binding sites on each monomer [Craig et al., 1982]. In its dimerized form it has a molecular weight of 210 kDa. In cells, it is mostly found in stress fibers as well as in adhesion sites [Sjöblom et al., 2008].
α-actinin-2 is expressed recombinantly in *e.coli* strain BL21 RIPL (Stratagene), flash-frozen in liquid nitrogen and stored at -80 °C in 20 mM BIS Tris (pH 6.5), 150 mM NaCl and 2 mM DTT.

c) Anillin

Anillin is an actin-binding protein that cross-links filamentous actin into a branched bundled network [Kinoshita et al., 2002]. *In vivo*, it serves as a linker between myosin and actin by its ability to bind both [Kinoshita et al., 2002].
Here, we use a fragment of Xenopus laevis anillin, spanning amino acids 1-428 that is small enough to be expressed in *e.coli* while still being able to bundle F-actin. The fragment is cloned into a pET-28a vector and then purified from *e.coli* with His-tags on both termini. Anillin 1-428 is stored at -80 °C in 25 mM imidazole (pH 6), 25 mM KCl, 4 mM $MgCl_2$, 1 mM EGTA and 1 mM DTT.

2.1.3 Nucleators and Capping Proteins

a) Formin mDia1 and Profilin mPFN2a

Profilins are abundant proteins, found in all eucaryotes. They cooperate with capping proteins to maintain the vast pool of unpolymerized actin in cells. In addition they regulate the nucleotide bound to actin by stimulating the exchange of ADP for ATP on dissociated monomers and have a discriminating effect on the actin polymerization. Actin monomers bound to profilin have a limited capacity to nucleate new filaments. Furthermore, profilin inhibits elongation at the pointed end, but not at the barbed end. This results from profilin binding to the barbed end of the actin monomer, where it sterically blocks pointed end elongation, but not association of the profilin-actin complex with the barbed end of the filament. After the profilin-

actin complex binds here, profilin rapidly dissociates and by thus leaving the barbed end free to continue growing [Pollard and Earnshaw, 2004].

The formin family is large, diverse and includes many different formins that all have the same similar basic properties, but still differ in fundamental ways. The all nucleate actin filaments, but the fission yeast Cdc12p completely blocks elongation, whereas the budding yeast Bni1p slows elongation and the mammalian formin mDia1 has no effect on elongation [Kovar et al., 2006]. Yet, the addition of profilin changes the dynamics completely.
All formins contain the two formin homology domains FH1 and FH2. While the proline-rich FH1 domains binds profilin and is required for *in vivo* function, the FH2 domain binds actin and is sufficient for actin nucleation *in vitro* [Romero et al., 2004]. Profilin accelerates barbed-end elongation in conjunction with Cdc12p, Bni1p and mDia1 [Kovar and Pollard, 2004b, Romero et al., 2004, Kovar et al., 2003] from about 11 subunits/s up to 47 subunits/s [Kovar et al., 2006].

Purification Here, recombinant shortened mouse formin (mDia1) with a full FH1 and FH2 domaine (549-1255) is expressed in *e.coli* BL21 with auto induction medium for 6 h at 37 °C, then at 15 °C for further 60 h. mDia1 is purified through NiNTA agarose beads, flash-frozen in liquid nitrogen and stored at -80 °C in PBS with 2 mM DTT.
Profilin mouse profilin 2 (mPFN2a) is expressed with a GST-tag in *e.coli* BL21 in a pGex-6p-2 vector with auto induction medium, grown for 6 h at 37 °C before grown for another 72 h at 20 °C. Cells were then pelleted, resuspended in 50 mM Tris (pH 7.0), 150 mM NaCl, 1 mM EDTA, 1 mM DTT, 30% sucrose before lysed. Lysate was cleared by centrifugation (17 000 rpm, 30 min) and incubated with GSH-beads (Glutathione Sepharose 4B, GE Healthcare, 17-0756-01) for 6 h at 4 °C. Beads were washed with cleavage buffer (50 M Tris (pH 7.0), 150 mM NaCl, 1 mM EDTA and 1 mM DTT) and resuspended in same buffer with precision protease (GE Healthcare, 27-0843-01) to remove GST-tag (16-72 h at 4 °C on rotor). Beads are centrifuged at low speed (4000 rpm, 2 min), supernatant centrifuged at high speed (15000 rpm, 2 min). Concentration of profilin is measured with NanoDrop (extinction coefficient: 21 430 $M^{-1}cm^{-1}$. Profilin is flash-frozen in liquid nitrogen and stored at -80 °C in 50 M Tris (pH 7.0), 150 mM NaCl, 1 mM EDTA and 1 mM DTT.

b) Capping Protein

Capping protein is a heterodimeric globular protein that binds to the barbed ends of actin filaments. It has a total molecular weight of 64 kDa with the α-subunit having 33 kDa and the β-subunit 31 kDa. Capping protein inhibits filaments elongation at the barbed end [Kilimann and Isenberg, 1982] by capping the actin filament and thus leaving the only possible polymerization to the pointed end. Capping protein further activates spontaneous nucleation of actin monomers in solution, usually at a concentration of 20–50 nM, by stabilizing the nuclei at their barbed end [Schafer et al., 1996]. Together with profilin capping protein maintains the large unpolymerized pool of actin monomers cells [Kovar and Pollard, 2004a]. Furthermore like formin, capping protein has a very slow off-rate, predicting a half-life for a capped barbed end of an actin filament for about 30 min [Schafer et al., 1996]. Thus, the first protein of either formin or capping protein to bind actin determines the behavior of an extended period of time and so, even actin filaments capped by formin can elongate even in the presence of capping protein [Kovar et al., 2006].

Purification Capping protein's α- and β-subunits are expressed simultaneously in the multi cloning site vector pRFSDuet-1 (Novagen) with a FLAG-tag. Here, the DNA of the two subunits are from different origins: α-subunit is from mouse organism (mus musculus) and the β-subunit is human (homo sapiens). Induction is achieved by addition of 0.5 mM IPTG at 26 °C overnight. Cells are pelleted, resuspended in 20mM TRIS (pH 8.0), 10mM Imidazole, 250mM NaCl, 1mM EDTA 5% Glycerol, 1mM DTT, and lysed. After centrifugation (30 000 rpm, 10 min, 4 °C), supernatant is mixed with 100µl ANTI-FLAG M2 Affinity Gel (Sigma) per 100 ml supernatant, rotated for 90 min at 4 °C and then centrifuged at low speed (500 rpm). Beads are washed several times with same buffer, before adding 100 µl FLAG Peptide (Sigma F3290-25mg lyophilized powder) per 1 ml buffer. After beads rotated for 1 h at 4 °C, they are centrifuged for 2 min at 14 000 rpm. Supernatant with capping protein is dialyzed against 10 mM TRIS (pH 8.0), 50 mM KCl, 1 mM DTT overnight before aliquoted, flash-frozen in liquid nitrogen and stored at -80 °C.

c) Arp2/3 complex and VCA

The actin-related protein 2/3 (Arp2/3) complex is a key component in cells that mediates branched networks [Rouiller et al., 2008]. It is mostly found in the lamellipodium of motile cells, where the Arp2/3 complex produces branched filaments that push forward the leading edge [Pollard and Borisy, 2003].
The Arp2/3 complex consists of seven subdomains: two actin-related proteins, Arp2 and Arp3, which are stabilized by five other other subunits. These are called according to their sizes ARPC1 (a 40-kDa subunit), ARPC2 (a 35-kDa subunit), ARPC3 (a 21-kDa subunit), ARPC4 (a 20-kDa subunit) and ARPC5 (a 16-kDa subunit) [Goley and Welch, 2006]. The Arp2/3 complex has a total molecular weight of 224 kDa, with Arp2 having 45 kDa and Arp3 47 kDa.

Arp2/3 complex initiates new actin filaments at the side of already existing filaments. From this so-called "mother" filament, the Arp2/3 complex forms new barbed ends and can give rise to new "daughter" filaments, which then can also serve in turn as new mother filaments for other branches. Hence, branch formation by Arp2/3 complex is autocatalytic. Here, Arp2 and Arp3, which are structurally very similar to actin monomers, form the first two subunits of the new branching filament [Egile et al., 2005].
Whether Arp2/3 complex binds to the side of existing filament or to its barbed end is still matter of debate. The most compelling experimental evidence supports the side-branching model, since branching form the sides of filaments can directly observed *in vitro* using fluorescence microscopy [Amann and Pollard, 2001]. Support for the barbed-end-branching model comes from polymerization kinetics and electron-microscopic observations [Pantaloni et al., 2000]. However, it was shown that Arp2/3 complex induces conformational changes in both the mother filament and the Arp2/3 complex upon branch formation [Rouiller et al., 2008].
By its branching activity the Arp2/3 complex acts as a nucleator, even though not as a nucleator *de novo* as formin. The Arp2/3 complex must be activated by nucleation-promoting factors (NPFs). Those NPFs are for example the Wiskott-Aldrich syndrome protein (WASp), N-WASP (neuronal Wiskott-Aldrich Syndrome protein) or Scar/WAVE. Common to all of these NPFs are three short functional segments: a V region (verprolin homology), a C sequence (connecting) and an A segment (acidic). These three segments form together the so-called VCA domain [Egile et al., 1999].

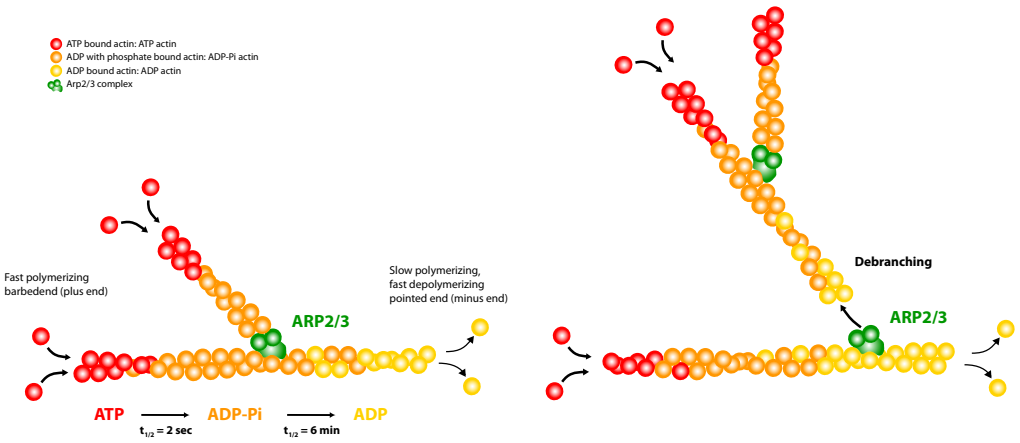

Figure 2.3: Branching and debranching of Arp2/3 complex

Both Arp2 and Arp3 have a binding pocket for ATP, basically the same as actin does. Binding of ATP to Arp2 is enhanced after activation of Arp2/3 complex by VCA and is required for filament branching [Le Clainche et al., 2001]. Due to the affinity of the VC for actin and of CA for the Arp2/3 complex, the VCA brings together the Arp2/3 complex and one actin monomer. This actin monomer then serves after the Arp2 and Arp3 as the third subunit in the daughter filament and with this a new branched end is initiated. Branching requires the hydrolysis of the Arp2-bound ATP. Without this, nucleation cannot be accomplished [Dayel et al., 2001]. After branching, VCA dissociates from both the actin monomer and the Arp2/3 complex on a sub second timescale [Marchand et al., 2000].

If the Arp2/3 complex binds more likely to ATP-actin, ADP-P_i-actin or ADP-actin is until now highly discussed. Most publications favor the binding to ATP-actin [Ichetovkin et al., 2002], whereas others could not prove any difference [Blanchoin et al., 2000a, Mahaffy and Pollard, 2006].
Release of the mother or daughter filament from the Arp2/3 complex, known as debranching, is crucial for recycling actin networks in the cell [Goley and Welch, 2006]. This is happening, through the ATP hydrolysis of either the Arp2/3 complex [Le Clainche et al., 2003] or the first actin monomers of the new daughter filament [Blanchoin et al., 2000b] or both.
The exact pathway of debranching is still a matter of debate, as well as what triggers the disassembly of the branches. However, the ATP hydrolysis plays a very significant role in both the assembly as well as in the disassembly.

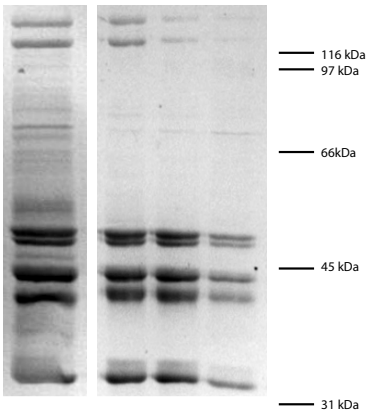

Figure 2.4: SDS-PAGE gel (12% acrylamide) of Arp2/3 complex purification. Left: Purification after old protocol. Right: Purification after new improved protocol. Clearly, the Arp2/3 complex batch on the left is much more contaminated than with the improved purification on the right. In addition, the bands of the different subunits are easily to differentiate. Here, the three lightest subunits with 21 kDa, 20 kDa and 16 kDa are not on the gel anymore. All other four subunits (Arp3: 47 kDa, Arp2: 45 kDa, ARPC1: 40 kDa and ARPC2: 35 kDa) show distinct bands, of which the Arp3 shows a slight double band.

Purification Arp2/3 complex is extracted from pig brain after a slightly modified protocol by [May et al., 1999]. The amino sequence of the peptide for the purification column is "CHERIENDVATILSRRIAVEYSDSEDDSEFDEVDWLE". This sequence is part of the VCA-domain which is known to bind to the Arp2/3 complex [Brackmann, 2011]. The peptide is coupled to CNBr-activated Sepharose and the Arp2/3 complex is purified after [Brackmann, 2011]. Activity of Arp2/3 complex is tested with and without presence of VCA in pyrene assays.

A new protocol was introduced later based on a protocol of Jan Faix (personal communication). Arp2/3 complex is also extracted from pig brain, but now purified with the help of full GST-tagged VCA.
An affinity column is made from CNBr activated Sepharose (GE Healthcare, CNBr Activated Sepharose, #17-0430-01) and 100 mg GST-VCA. VCA is dialyzed against the coupling buffer (0.1 M $NaHCO_3$, 0.5 M NaCl). 5 ml coupling solution per 1 g resin should be used. Sepharose and VCA are rotated for 1 h at room temperature, before removing any excess VCA by washing with a 5-fold volume of coupling buffer. To block any other reactive groups, the resin is transferred to 0.1 M TRIS-HCl buffer (pH 8.0) for 2 h. Sepharose is washed in three cycles of alternating buffers (0.1 M acetic acid/ sodium acetate, 0.5 M NaCl, pH 6.8 followed by 0.1 M Tris-HCl, 0.5 M NaCl, pH 8).

Pig brain is cleaned properly and directly homogenized in a blender with buffer (20 mM Tris-HCl, pH 7.5, 25 mM KCl, 1 mM DTT, 1 mM $MgCl_2$, 0.5 mM EDTA, 0.1 mM ATP-Tris, pH 7.5), and clarified by centrifugation for 1 h at 40 000 g. Supernatant is added to column resin and incubated while rotated over night. The next day column material is washed with buffer and additional 0.2 M KCl. Arp2/3 complex is eluted with buffer containing 0.2 M $MgCl_2$. The protein has to be concentrated to an appropriate volume for gel filtration (Vivaspin20, cutoff 10 kDa). To further increase the purity of Arp2/3 complex, the eluted fractions are separated by size exclusion using a S200 column (HighPrep 16/60, GE), which is equilibrated before with the storage buffer (20 mM Hepes, 150 mM KCl, 2 mM DTT, pH 7.0). Concentration of Arp2/3 complex is determined by spectrophotometrically using an extinction coefficient of 224 480 $M^{-1}cm^{-1}$ at 280 nm and a molecular weight M_W of 224 kDa. Activity of Arp2/3 is verified by pyrene assays before flash-frozen in liquid nitrogen and stored at -80 ° C.

His-tagged VCA is obtained from BL21 *e.coli*. Pre cultures were grown until OD 0.6–0.8 at 37 ° C and 220 rpm. Cultures are then induced with 0.5 mM IPTG and grown for another 7 h at 37 ° C before harvested by centrifugation. Cells are resuspended in 30–40 ml phosphate buffer (50 mM Na_2HPO_4, 50 mM $NaH_2PO_4 \cdot 2\,H_2O$, 300 mM NaCl, pH 8.0), 20 mM imidazole, 200 µL lysozyme (10 mg/ml), 2.5 µL benzonase and a protease inhibitor, before disrupting in the french press. After centrifugation (4 ° C, 17 000 rpm, 30–45 min) and filtration, VCA is purified with a Ni-NTA resin (cOmplete His-Tag Purification Resin, Roche). VCA is dialyzed against VCA buffer (20 mM Tris/HCl, 100 mM KCl, 1 mM $MgCl_2$, 5 mM EGTA, 2 mM DTT, pH 7.0). Concentration of VCA is determined by spectrophotometrically using an extinction coefficient of of 5500 $M^{-1}cm^{-1}$ at 280 nm and a molecular weight of 12 kDa. VCA activation of Arp2/3 complex is verified by pyrene assays, before flash-frozen in liquid nitrogen and stored at -80 ° C.

2.2 Methods

2.2.1 Bulk experiments

Sample chamber Networks in bulk were polymerized in a simple chamber. A ring of vacuum grease was applied to a 60 mm x 24 mm coverslip (Carl Roth), filled

with the sample solution and closed airtight with a smaller coverslip. Samples were not turned up side down and imaged with a 20x oil immersion or 63x immersion oil objective on a confocal microscope (TCS SP5, Leica Mikrosysteme GmbH). We decided against a commonly used flow chamber with a fairly defined height, since in this chamber the filling process gives the early formed filaments a preferred direction and by this changes the overall bulk network can be induced.

NiNTA beads For experiments, where the actin polymerizes from a spherical surface (Chapter 3), formin was attached due to its His-tag to NiNTA beads, commonly used for protein purification (Ni Sepharose 6 Fast Flow, # 17-5318-01, GE Healthcare), which consist of 6% cross-linked agarose and have an average particle size of 90 µm, with a distribution of 45 µm – 165 µm. 10 µl of beads were incubated with the appropriate amount of formin and then diluted with buffer to 100 µl.
About 2 µl beads were added to a total of 200 µl protein solution. This solution is then filled into a sample chamber, which consist of a squared PDMS piece on a coverslip with a 8 mm pierced hole in it and thus can hold about 170 µl. The chamber is closed airtight with another smaller coverslip to avoid major flow and evaporation. Excess solution is absorbed with a tissue. Beads settle quickly at the bottom of the coverslip and there are image with a confocal microscope.

2.2.2 Pyrene assay

The fluorescence intensity of pyrenyl labeled F-actin at 407 nm, after excitation at 365 nm, is enhanced by a factor of about 25 compared to G-actin [Kouyama and Mihashi, 1981]. Hence, by labeling actin monomers covalently with N-(1-pyrenyl)iodoacetamide and measuring the fluorescence over time in a fluorescence spectrometer, polymerization can be directly measured.
Typically 20% of the total actin amount is labeled with pyrene. A higher amount of actin does not necessarily result in a higher intensity value, since scattering increases in a dense meshwork which then again reduces the intensity that is being measured. A big advantage of the pyrene assay is that also very short filaments that cannot be resolved with fluorescence microscopy, strongly contribute to the measured intensities.
Measurements are performed with a fluorescence spectrometer (FP-8500, JASCO

Germany GmbH), where the temperature can be controlled externally by a circulator (Julabo GmbH).

2.2.3 Microscopy

For all fluorescence microscopy experiments a Leica TCS SP5 confocal microscope was utilized, with different objectives such as a 63x/1.4 oil (HCX PL APO CS), a 20x/0.7 oil (HC PL APO) and a long distance objective 10x/0.3 (HCX PL FLUOTAR). Utilized lasers were mainly the Argon laser at 80% power. Scan rate was depending on the sample steadiness between 100 Hz and 400 Hz. Mainly the supersensitive Hybrid Detector (HyD) was used to get pictures at high quality and the smart gain was adjusted for each sample individually, but usually kept at 10% while laser transmission was raised up to 100% if possible.

2.2.4 Rheology

a) Rheological models and basic equations

Viscoelastic materials can be rheologically modeled in order to determine their stress and strain (deformation) dependencies. Different viscoelastic behavior can be described by various linear combinations of elasticities and viscosities, modeled by purely elastic springs and purely viscous dampers, respectively.
The simplest model for a viscoelastic material is the Maxwell model that consists of a spring in series with a damper (Fig. 2.5a). Here, the system will respond to an applied step strain with an immediate stress response that will be completely relaxed over time due to the damper. However, if the stress will not be completely relaxed, the standard linear solid (SLS) model describes this behavior better (Fig. 2.5b). In this model a second spring with E_0 is connected in parallel which is responsible for a remaining stress $E_0\,\varepsilon_0$ in the sample.
When subjected to a constant step stress, viscoelastic materials experience a time-dependent increase in strain. Different materials show different progress of this creep and the various models emulate this behavior as shown in Fig. 2.5 (right).

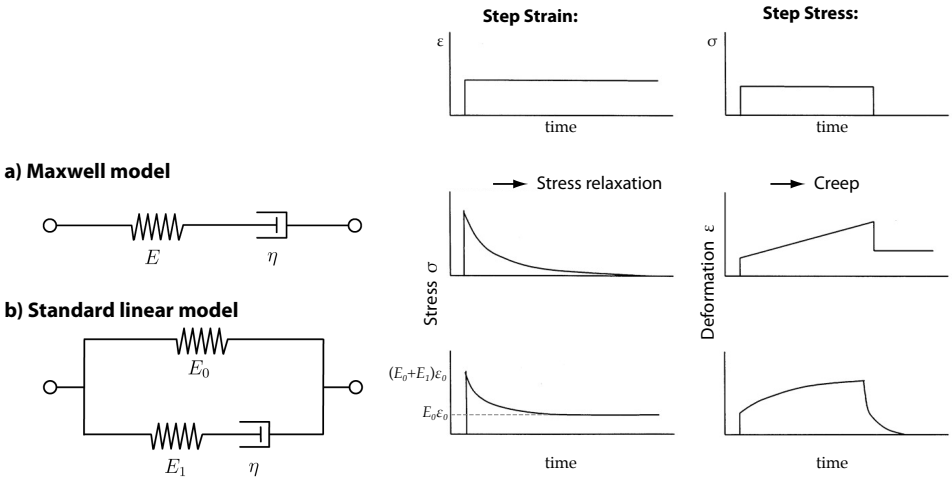

Figure 2.5: Two rheological models to describe viscoelastic materials and their response to a constant strain as well as to a constant stress. a) Maxwell model. b) Standard linear solid (SLS) model.

In rheology stress σ is defined as the force F per cross-section A,

$$\sigma = \frac{F}{A}, \tag{2.1}$$

that leads to a strain or deformation ε, which is a dimensionless quantity and the change of length Δl to its original length l_0,

$$\varepsilon = \frac{\Delta l}{l_0}, \tag{2.2}$$

(Fig. 2.6). For ideal linear elasticities, the elasticity or Young's modulus E can be calculated as the stress divided by the strain,

$$E = \frac{\sigma}{\varepsilon}, \tag{2.3}$$

and the ideal viscosity η depends on the rate of which the deformation is changing,

$$\sigma = \eta \cdot \frac{\partial \varepsilon}{\partial t}. \tag{2.4}$$

In our assays (Section 3.2.6), the protein networks can be rheological described as viscoelastic polymer solutions. The applied strain does not completely relax, instead residual strain persists (Fig. 3.18b) which is best described by the SLS model.
With the rules for series and parallel connection for the components, we can now

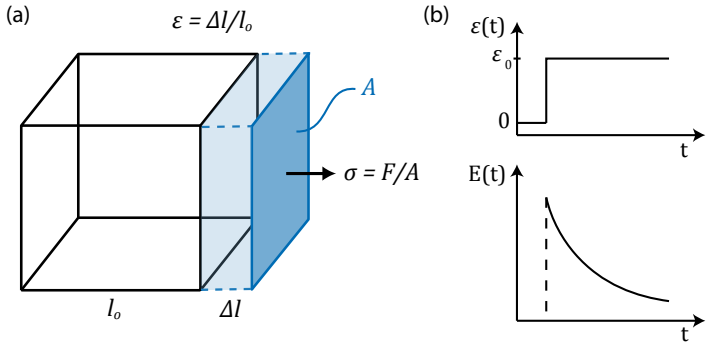

Figure 2.6: (a) Geometric scheme of a sample under linear tensile stress. The stress σ is defined as the applied force normalized by the area F/A and the strain ε as the ratio between the expansion and the original size of the sample $\Delta l/l_0$. (b) Time profiles in a stress relaxation experiment of a viscoelastic material following a sudden step deformation.

describe the applied stress with the SLS model. For series connections the stresses are the same at each parts and the strains sum up to a total strain, which is vice versa for parallel connections. Here, the strains are equal at each parts and the stresses add together.

b) Microrheological step measurements

In Section 3.2.6, the elasticity and viscosity of actin cortices are measured by step strain experiments using a custom built optical tweezer set up described in section 2.2.6. As depicted in Fig. 2.6b during a short time interval τ_0 from $t = t_0 - \tau_0$ to $t = t_0$ a strain of ε_0 with a strain rate of

$$\frac{\partial \varepsilon(t)}{\partial t} = \frac{\varepsilon_0}{\tau_0}. \tag{2.5}$$

is applied (Fig. 2.6b) and from the relaxation time of E(t) the elasticity can be calculated. For these experiments, the stress $\sigma(t)$ can be written as [Maier, 2014]:

$$\sigma(t) = \varepsilon_0 \left(E_1 \cdot exp\left(\frac{-(t - t_0)}{\tau} \right) + E_0 \right), \tag{2.6}$$

where E_0 and E_1 are the Young's moduli and τ is the relaxation time of the viscosity η over the elasticity E_1 in series (Fig. 2.5b):

$$\tau = \frac{\eta}{E_1}. \tag{2.7}$$

For step-strain experiments performed in this thesis the concepts of the Poynting model need to be transferred [Ziemann et al., 1994]. With

$$\sigma \rightarrow F(t) \tag{2.8}$$

$$\varepsilon(t) \rightarrow 6\pi R\Delta l(t) \tag{2.9}$$

$$\varepsilon_0 \rightarrow 6\pi R\Delta l(\tau_0) \tag{2.10}$$

Equation 2.6 becomes

$$F(t) = 6\pi R\Delta l(\tau_0)\left(E_1 \cdot exp\left(\frac{-(t-t_0)}{\tau}\right) + E_0\right) \tag{2.11}$$

$$:= F_1 \cdot exp\left(\frac{-(t-t_0)}{\tau}\right) + F_0. \tag{2.12}$$

Based on Equation 2.11 and 2.12, the force curves obtained by the optical tweezer experiments were evaluated. Elasticities and viscosity of the actin networks can be calculated from fit parameters as described in detail [Maier, 2014].

The data evaluation from the forces of the trap to the cortices' elasticities and viscosities were mainly followed the protocols and routines in the program "IGOR pro" (WaveMetrics, Inc.) established previously in our group [Maier, 2014].

c) Macrorheological shear experiments

Next to microrheology measurements by the means of an optical tweezer, networks were also studies by macrorheology which exerts usually an oscillatory shear stress instead of a linear tensile stress on the sample. Macrorheology is well suited to investigate the mechanical properties of protein networks in both the linear and the non linear regime. In the linear regime only small deformations are applied to the sample, whereas high deformations give information about the non linear regime.

The viscoelastic properties of bulk networks are studied with oscillatory techniques using a rheometer. Here, the complex dynamic or shear modulus G*(ω) is obtained,

with its real part being the storage modulus $G'(\omega)$ and the imaginary part the loss modulus $G''(\omega)$.

$$G^* = G' + iG'' \tag{2.13}$$

The storage modulus G' is a measure for the stored mechanical energy in the sample upon shearing. In addition, the loss modulus G'' provides information about the energy that is dissipated. If $G' \gg G''$, the sample has dominant elastic properties. For $G' \ll G''$ it is dominantly viscous and if $G' \sim G''$ the sample exhibits viscoelastic features.
A rheometric measurement usually applies an oscillatory stress $\sigma(t)$ to the sample and measures the resulting displacement (strain) $\gamma(t)$ besides the phase shift δ between stress and strain. The storage and loss modulus are defined as:

$$G'(\omega) = \frac{\sigma_0}{\gamma_0} \cdot cos(\delta) \tag{2.14}$$

$$G''(\omega) = \frac{\sigma_0}{\gamma_0} \cdot sin(\delta) \tag{2.15}$$

Here, σ_0 and γ_0 are the amplitudes of stress and strain.
The phase shift gives the ratio between elasticity and viscosity. For an angle of $0°$, the material is perfectly elastic and for $90°$ it is perfectly viscous.

Usually, the viscoelastic response of a network is studied by two different approaches that can be consecutively applied to the sample. First of all, the linear response is investigated by a so-called frequency sweep. Here, $G'(\omega)$ and $G''(\omega)$ are probed in an intermediate frequency range, which is typically between an few mHz and several Hz. Secondly, the non-linear response is measured by monitoring the stress-strain response at large applied strains up to several 100%.

In general, for entangled polymer solutions it is assumed that no bonds at all are existing between the individual polymers. There are no attractive forces between them and hence, under small shear forces the macromolecules are able to slowly move and glide along each other. Here, the only occurring forces are the friction forces between the polymer chains. Both G' and G'' are increasing with the frequency.
In contrast, cross-linked polymers solutions exhibit a different behavior. Cross-linking molecules fix the bonds between individual polymers chemically. Thus, polymers chains cannot move along each other without destruction of the network even at small forces. This results in a storage modulus G' which is almost frequency-

independent, i.e. G′ displays a constant line in the whole frequency range. Furthermore, G′ is high relative to the loss modulus G″ [Mezger, 2006].

The non-linear response itself is a very sensitive indicator for molecular interactions present in the network.
Actin filaments are semi flexible polymers, as the typical length of a filament is comparable or less to their persistence length. As a result, the filaments do not form loops and are nearly straight. Their elasticity arises from both entropic and enthalpic contributions. The entropic elasticity originates in the thermal fluctuations of the individual filaments, while the enthalpic elasticity comes from mechanical deformations of the filaments themselves like stretching or bending. When stress is applied to the network the thermal undulations in the filaments get reduced and the elastic modulus increases linearly. This linear response can be quantitatively understood by the tube model [Hinner et al., 1998, Claessens et al., 2006].
At larger stresses near full extension of the filaments, the networks exhibit a non-linear response and thus become stiffer. The widely accepted explanation for this is that the strain stiffening is the result of the non-linear force extension of individual semi flexible filaments, i.e. the filaments resist strongly to further extension [Storm et al., 2004]. This model argues that the non-linear response depends only on the single filament stretching behavior. However, the molecular origin of this non-linear behavior is still highly discussed and it was suggested that the response depends rather sensitively on structural details and molecular interactions [Lieleg et al., 2007].

Measuring protocols Here, a stress-controlled rheometer (Physica MCR 301, Anton Paar, Graz, Austria) is used to measure the viscoelastic response of reconstituted actin networks. The rheometer itself applies a torque to the sample which is converted to the applied stress σ. It reads out the angle and the velocity of the plate which are then translated to rheological values of the strain γ and the shear rate. From these values, all other data is calculated within the rheometer software.
Approximately 450 µl sample volume is loaded into the rheometer using a 50 mm plate-plate geometry. For all experiments the plate separation is kept at 160 µm and the temperature is kept constant at 21 °C. To avoid drying, millipore water is added to the reservoir around the sample plate and the measuring geometry is covered with two metal half-shells. All macrorheology samples undergo a measurement consisting out of three different consecutive phases.
First, the polymerization is monitored by recording the storage modulus G′ over

time t. Polymerization is usually measured for 60 min, but also for just 30 min or up to 90 min according to completion of sample polymerization. Here, measurement of a single datapoint takes 30 s and the frequency is 0.5 Hz. To avoid mechanical disruption of the network only small torques (0.5 µNm) are applied.
After the polymerization, the mechanical response in the linear regime is characterized by measuring the frequency dependent viscoelastic moduli G′(f) and G″(f). Here, the strain or deformation γ is kept constant. A suitable strain should be determined from the final deformation that was applied by the 0.5 µNm during polymerization. For pure or branched actin networks γ is $\sim 5\%$ and for cross-linked actin networks γ is about 0.1–0.5 %. The applied frequencies are applied over three orders of magnitude from 10 Hz down to 0.01 Hz in 20 logarithmically equal spaced steps.
The last phase probes the non-linear response. The sample is deformed up to 500 % with a constants shear rate of $\dot{\gamma} = 0.125\, s^{-1}$. During this phase, the sample will first exhibit a linear stress response upon deformation, then eventually a non-linear response (stress-stiffening or stress-softening), before it will exhibit a plastic and irreversible deformation and detach from the rheology plate.

2.2.5 Nucleation seeds

To enhance polymerization of actin in rheology assays, nuclei in form of actin seeds were added. Seeds were obtained by polymerizing the desired amount of actin monomers into filaments, which are then dismantled into small pieces by shearing. Here, we used 1 %, 5 % and 25 % seeds, respectively, which corresponds to 0.1 µM, 0.5 µM and 2.5 µM actin. Actin was polymerized for 1h in polymerization buffer and then sheared 30 times through a 25 Gauge needle (25GA1 05x25 N.18, Sterican®, Braun). The resulting seeds were mixed with buffer and optionally with the Arp2/3 complex and VCA as well as actin monomers immediately before the experiments.

2.2.6 Optical Trap

The elasticity and viscosity of the cortices in Chapter 3.2.6 are measured by the means of microrheology using a custom built optical tweezer set up, which is depicted in Fig. 2.7 [Maier, 2014] and previously described in [Gebhardt et al., 2010].

The trapping laser is a 4W linear polarized diode pumped Nd:YVO_4 laser emitting 1064 nm (Spectra-Physics, California, USA) which can be deflected by an AOD, and which intensity is regulated by an $\lambda/2$-plate. The collimated laser beams is focused by a 60x water immersion objective (CFI Plan Apo IR 60x/1.27 WI, Nikon) in the sample plane, where it can thus trap dielectric objects in the micrometer range. Bead deflection was detected by a PSD (Silicon Sensor). Trapped polystyrene beads had a diameter of 1 µm. The stiffness of the trap was adjusted to 0.06 and 0.31 pN/nm between different experiments. Data were recorded and saved at a sampling rate of 150 kHz (National Instruments, Texas, USA).

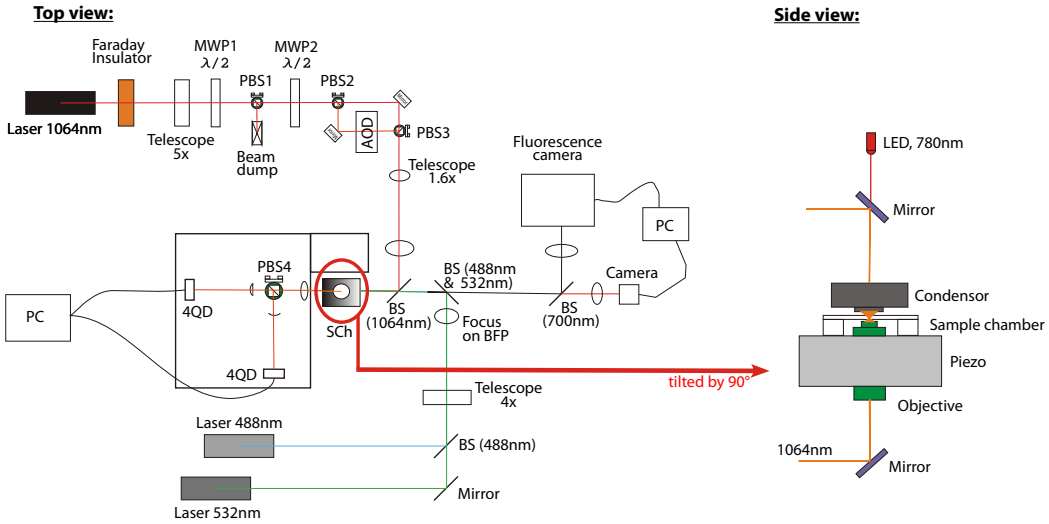

Figure 2.7: Schematic view of the optical tweezer set up. Left: Top view. Right: Detailed side view of sample chamber.
MWP: Motorized wave plate with a $\lambda/2$ plate. PBS: Polarizing beam splitter cube. AOD: Acoustic optic deflector. BS: Beam splitter. 4QD: Four quadrant diode. BFP: Back focal plane. PC: Personal Computer. SCh: Sample chamber.

3 Growth of artificial actin cortex and effect of cross-linker addition

3.1 Introduction

The cytoskeleton is a highly dynamic network that can develop various structures like filopodia or lamellipodia. Network formation depends heavily on spatiotemporal polymerization of actin. Many proteins contribute to this formation of sheet-like or finger-like structures by their participation in nucleation, elongation and cross-linking.

Depending on the kinetic interplay of these competing processes, different networks form. The speed of nucleation influences for example whether chemically identical networks will either be composed of sparse thick bundles or dense thin bundles in the presence of alpha-actinin [Falzone et al., 2013]. Polymerization enhances the arrest of filament mobility and is as such a competing process to bundling, which only occurs in a fluid microenvironment. Therefore, the kinetics of polymerization and bundling determines the final structure of the network which is far away from thermodynamic equilibrium [Falzone et al., 2012, Schmoller et al., 2009].

Most research in this field focuses on the simultaneous processes of nucleation, elongation and cross-linking. So far the only way to investigate the temporal dependence between these is to enhance or reduce the nucleation and elongation rate, since the cross-linking cannot be delayed. Thus it remains elusive how the cross-linking itself effects the polymerization process and how it changes the mechanics of the network.

Here, we try to gain a better understanding on how the changes in mechanics caused by cross-linking then in return influence the polymerization. For this the consecu-

tive effects of nucleation, elongation and cross-linking are studied. We focus on the formation of filopodial structures. Parallel actin filaments nucleated from a surface by formin are cross-linked by the bundling protein fascin. By the means of confocal microscopy the structure formation of actin networks is studied in the presence of different nucleation, elongation, capping and bundling proteins.
We show that the cross-linking process arrests filament elongation by changing the mechanics of networks through a change in elasticity. The polymerization of parallel filaments is stalled by an opposing force that is generated by the mechanics of a now cross-linked structure.

3.2 Results

The interplay of the different proteins involved in this experiment, i.e. actin, formin, profilin, capping protein and fascin, has a quite complicated mutual interdependence on elongation, nucleation and bundling as mention to some extend in Chapter 2. Their full interactions are studied here in detail. First of all, actin networks are characterized in bulk solution in different combinations with its actin binding proteins to better understand their interplay.
The effect of elongation and nucleation are only indirectly distinguishable in bulk by the interplay of different nucleation and elongation factors. Here, the polymerization is non-localized, which means it is happening throughout the sample. Furthermore, both the polymerization and the bundling process happen simultaneously and so, filaments which emerge in the sample are being bundled at the same time.
All of this leads to the question how spatial and temporal polymerization and bundling cues can be differentiated and thus be further investigated.

The proteins used in this assay are the nucleation promotion factor formin (mDia1), mouse profilin (mPFN1), capping protein and the cross-linker fascin. The actin concentration is held constant at 5 µM. The concentration of the other proteins are either 0 µM or they are 1 µM for formin, 10 µM for profilin, 150 nM for capping protein and 1 µM for fascin.

3.2.1 Nucleators and cross-linkers and their interplay in bulk

Pure actin without other proteins develops in a tightly entangled dense meshwork. The combined interplay of capping protein and profilin results in a mainly suppressed polymerization besides some fragments of filaments. By addition of formin polymerization is restored through formin's ability of de novo nucleation (3.1a). The meshwork looks similar to a pure actin meshwork.
Fascin arranges actin filaments into long bundles (Fig. 3.1c). Formin with fascin results in a much denser network with thinner bundles, due to formin's nucleation ability (Fig. 3.1b-A). More nucleation sites lead to more filaments and hence also to more bundles which are thinner. In contrast, profilin with fascin gives rise to fewer but thicker bundles (Fig. 3.1b-E). Profilin's hindrance of actin nucleation causes a high mobility of filaments that do form and these can then develop thicker bundles over time [Falzone et al., 2013]. Filaments capped by capping protein also demonstrate a high mobility du to their short nature and accordingly fascin can bundle these pieces of filaments into thick short frayed bundles, which also remain mobile (Fig. 3.1b-C).
Formin and capping protein together with fascin show a similar picture with also frayed yet longer bundles. Since the FH2 domain of mDia1 and capping protein bind both to the barbed ends of actin filaments and dissociate only slowly from these ends, the first protein that binds a filament determines its behavior for an extended time [Kovar et al., 2006, 2005]. Hence, formin and capping protein give rise to a class of long as well as short filaments simultaneously. Fascin then bundles the short capped filaments and the formin-dominated filaments into long frayed bundles, which again are mobile and do not interconnect to a space-spanning network (Fig. 3.1b-B). The addition of both capping protein and profilin suppresses again the polymerization regardless of the bundle protein fascin. Nevertheless, due to the slow dissociation rate of capping proteins, filaments can still grow over the course of 24h well into the µm range and then be cross-linked by fascin into very thick clusters rather than bundles (Fig. 3.1b-D, Fig. 3.1d).

A simple estimation proves that capped filaments can still grow up to 10 µm within a day: The on-rate of capping protein is 3.0 $\mu M^{-1}s^{-1}$ [Schafer et al., 1996]. At a concentration of 150 nM, this predict a half-life for a free barbed end of $t_{1/2} = ln\,2\,/\,(k_{on} \cdot c_{CP}) = 1.54$ s. The off-rate constant for the dissociation of a capping protein from a barbed end is $4 \cdot 10^{-4}\,s^{-1}$. With this, the half-life of a capped barbed end is rather long with $t_{1/2} = ln\,2\,/\,k_{off} = 1733$ s = 28.9 min. Over the

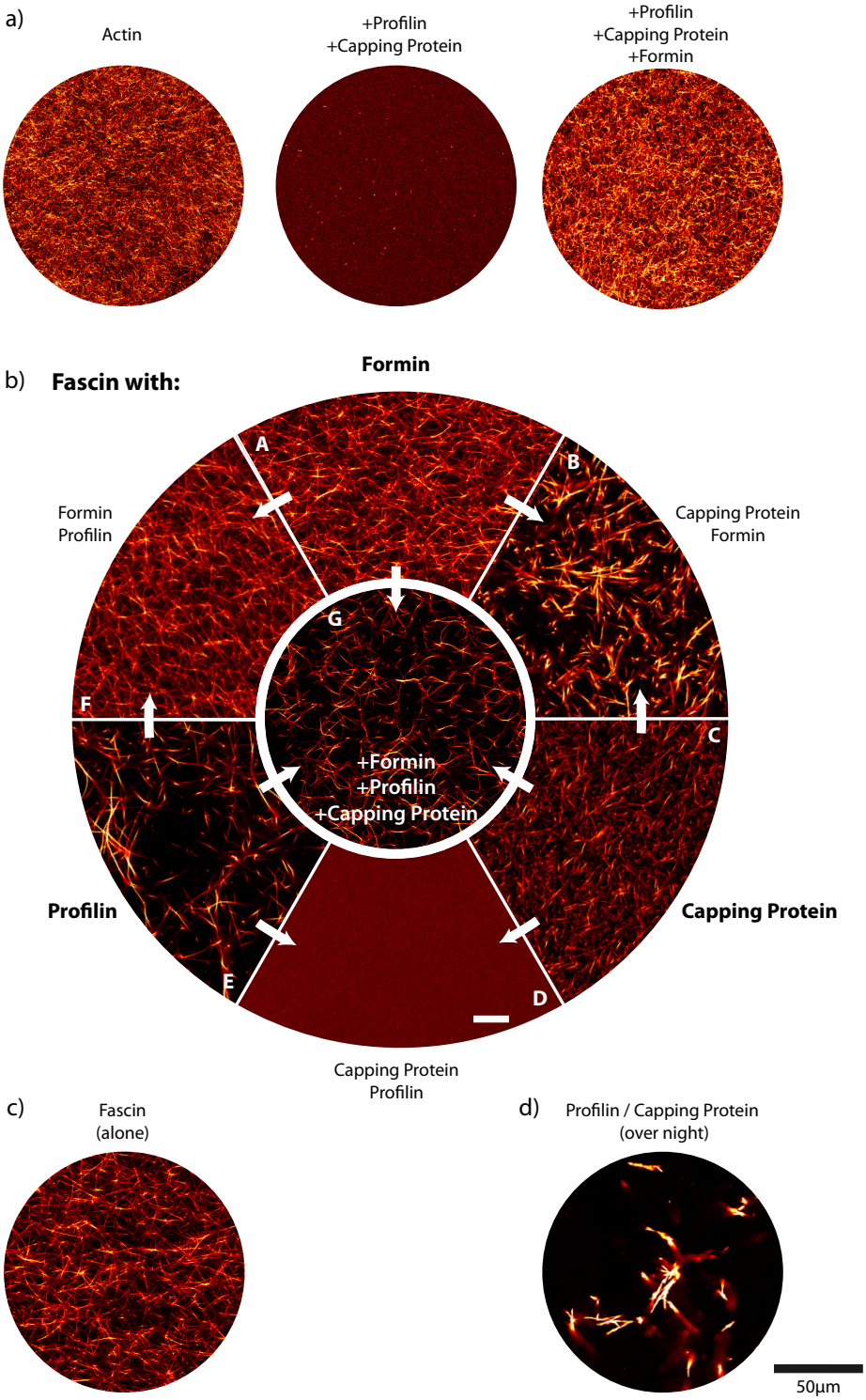

Figure 3.1: a) Bulk polymerization picture of an entangled actin network. Additional profilin and capping protein suppresses mainly the polymerization, but formin can restore the polymerization again. b) Actin-fascin networks with the addition of formin and/or profilin and/or capping protein. c) A pure actin-fascin network with long straight bundles. d) Sample with profilin, capping protein and fascin. Mini-filaments grow and cluster over night. Scale bar 20 µm.

time course of 24 h, roughly ever 30 min an unbinding event of a capped filaments occurs, which will then stay free for 1.54 s. Profilin-actin has an elongation rate of 10 subunits/s [Kovar et al., 2006] and every monomer adding 2.7 nm length to an actin filament. The elongation rate is directly proportional with the actin concentration, hence for $c_{actin} = 5$ µM, the elongation is at 50 subunits/s. Therefore, within a day the filament can grow up to $(24\,\text{h} \cdot 2/\text{h} \cdot 1.54\,\text{s} \cdot 50 \cdot 2.7\,\text{nm/s}) = 10$ µm (Fig. 3.1d). Formin with profilin does not change much in the actin fascin network compared to a simple formin-fascin network. The densities of the networks are very similar, suggesting that the nucleation rate of mDia1 does not change with or without profilin. Even though mDia1 has a four fold barbed end elongation rate with profilin (47 subunits/s, Kovar et al. [2006]), this is not reflected in the microscopy pictures (Fig. 3.1b-F).

3.2.2 Localized polymerization without cross-linker

To investigate how spatial cues affect the polymerization of a non-cross-linked network, formin is attached to NiNTA beads. In solution, the polymerization in solution is suppressed due to the presence of both profilin and capping protein. Capping protein binds to the fast polymerizing plus end of actin filaments and prevents elongation here. Thus the only possible polymerization to the minus end is assigned, which is not feasible for profilin-actin. Formin nucleates and elongates actin filaments from the bead surface.

Different formin concentrations

Consequently, NiNTA beads are incubated with different formin concentrations. Whereas the incubated bead volume remains constant at 10 µl, the amount of formin changes. Since the concentration of beads is unknown and with this how much volume is excluded by them, in this section $c_{formin} = 12.5$ µM will be referred to as 10 µl of NiNTA beads that are mixed with 10 µl of formin ($c^{stock}_{formin} = 25$ µM). Likewise, $c_{formin} = 16.7$ µM to 10 µl beads mixed with 20 µl. Beads are incubated for 10 min and then diluted with buffer to 100 µl.

To check the binding, coverage and dependence of the his-tagged formin, beads were incubated with His-GFP at the same concentrations as formin. Intensity measure-

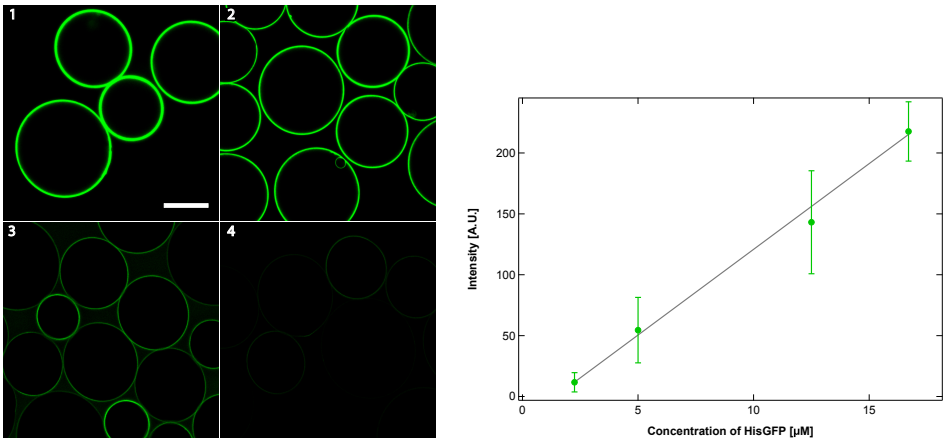

(a) (b)

Figure 3.2: His-GFP intensity measurements: a) NiNTA beads with different concentrations of His-GFP attached to the surface, (1) 16.7 µM, (2) 12.5 µM, (3) 5 µM, (4) 2.25 µM. Scale bar 50 µm. b) Linear correlation of intensity measurements versus His-GFP concentration in incubation solution.

ments were performed with the confocal microscope at constant laser power and with same exposure times (Fig. 3.2a). For each concentration the maximum intensity value was taken of approx. 170 line scans across the bead surface. In Fig. 3.2b the concentration of His-GFP over the intensity is plotted. The correlation is highly linear and hence, the amount of proteins in the incubation solution is directly proportional to the surface density.

Depending on the amount of formin attached to the bead, cortices of different densities form. For 2.25 µM formin isolated filaments start growing from the surface in a non-coordinated fashion (Fig. 3.3a). They wiggle and bend and the background stays rather bright. More filaments develop for 5 µM, but they are only in loose contact with each other. Above a certain concentration the characteristic of the cortex dramatically changes. With more formin, here $c_{formin} = 12.5$ µM (Fig. 3.3b), the actin cortex is very dense and its structure is highly ordered and parallel. All filaments face radially outwards and they are tight enough to guide each other's growth. In the beginning the area doubles within 3.5 min independent of the bead radius (Fig. 3.15, orange). Furthermore, the contrast between cortex and background increases with polymerization time since the proteins and hence phalloidin-488 are recruited to the cortex.

While growing, the filaments will primarily align to the local flow in the sample chamber. This flow is inevitable due to the experimental set-up and the quick onset of polymerization. The beads need time to sediment to the surface and even if

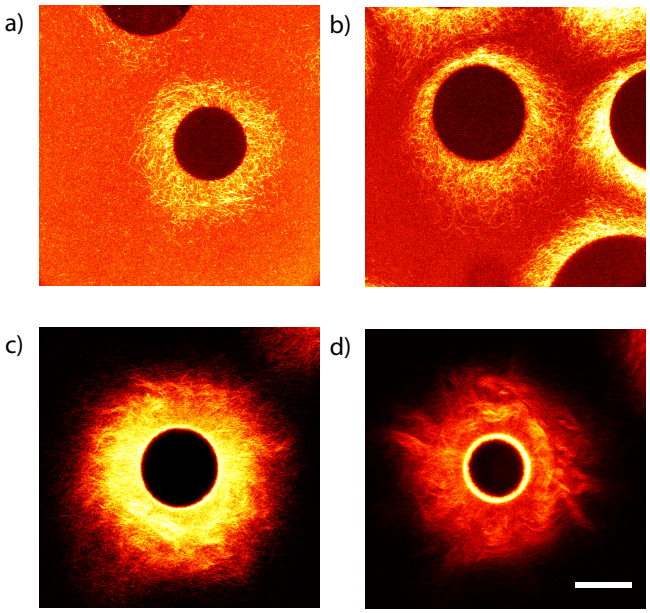

Figure 3.3: Actin cortices with different formin concentrations on the bead surface. The more formin there is on the surface, the denser the cortex. a) 2.25 µM, b) 5 µM, c) 12.5 µM, d) 16.7 µM. Scale bar 50 µm.

the chamber is closed right after pipetting the sample, local drift cannot completely eliminated. This flow can bend filaments on one side of the beads and aligns and straightens those on the other side.
In the beginning, the filaments can slide past each other, since they are rather short. The persistence length of actin filaments is 15 µm and hence, they are stiff enough to overcome friction forces. After the cortex grows to about half its final size, neighboring filaments start to get entangled. The further elongating filaments keep pushing from the center, bend and finally break the outer filaments combined in a bunch simultaneously (Fig. 3.4). This bending and breaking of filaments can also be observed if the local flow in the chamber changes and thus leading to a change of main direction in the filaments' growth. This behavior is even more amplified at a formin concentration of 16.7 µM (Fig. 3.3d).

Proof of polarity

With the formin attached to the beads, the polarity of the filaments should be with the plus end on the surface at the formin and the minus end facing outwards. To proof that this is indeed the case the supernatant with all the excess actin and other

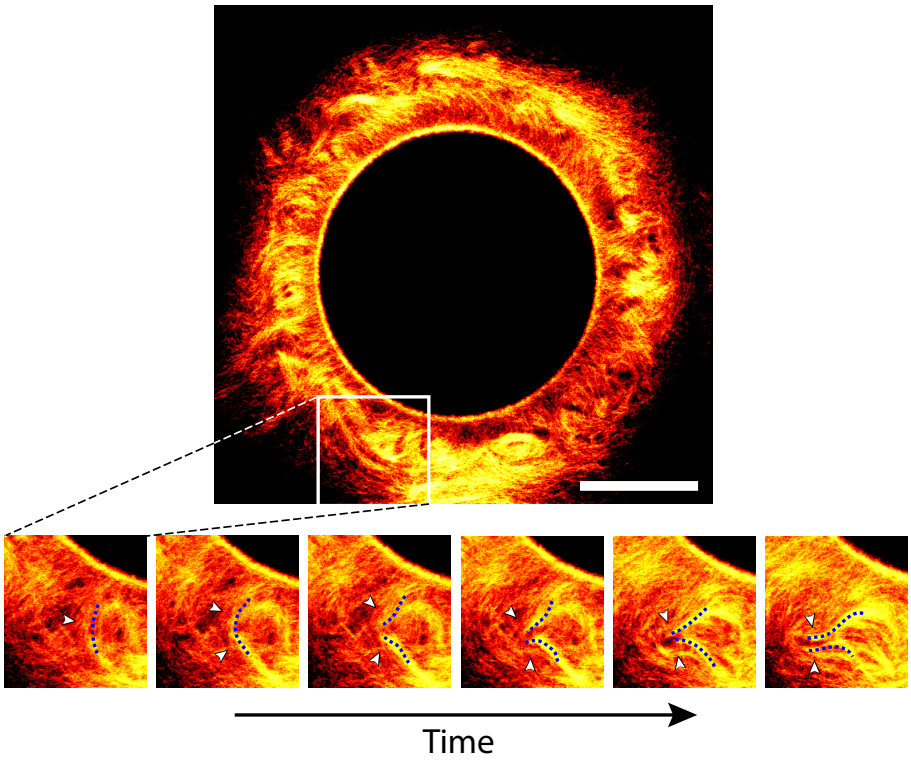

Figure 3.4: Top: Cortex with bunches of broken filaments. Bottom: Time series of several parallel filaments that are elongating radially outwards. If they are long enough, they start to get entangled. Due to friction forces and further elongation forces from the bead surface they break (arrows, dashed lines to guide the eye). c_{actin} = 5 µM, c_{formin} = 16.7 µM. Scale bar 50 µm.

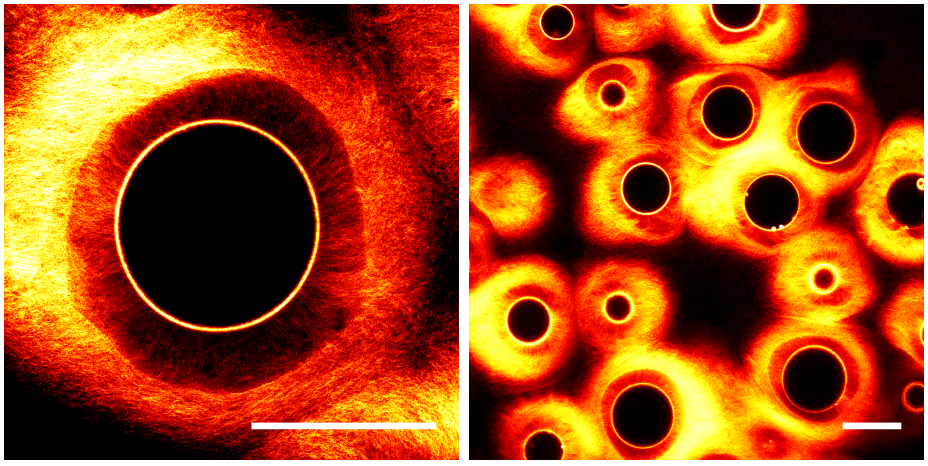

Figure 3.5: Upon addition of actin monomers after moderate washing and thus removing of excess phalloidin Atto-488, actin filaments polymerize further from the bead's surface. Dark rings form at the surface due to missing labelling molecules. c_{actin} = 5 µM, c_{formin} = 12.5 µM. Scale bar 100 µm.

protein is substituted during the polymerization process with exactly the same protein mixture but exclusive of phalloidin-488. Actin polymerization is again revived from the bead surface as can be seen by dark rings (Fig. 3.5). The rate of growth is about the same rate as before.
The cortex growth arrests as soon as the actin monomers in the samples are depleted to the critical concentration. Beads that are monitored for 4–6 h after arrest of growth, will also exhibit dark rings around the surface of the beads. These rings are not as symmetric as it is the case if the protein solution is exchanged after several minutes after initiation of polymerization. Actin that is not stabilized by phalloidin will depolymerize, and those monomers then again polymerize at the formin site at the surface of the bead.

Labeling actin with phalloidin instead of covalently

If actin was labeled covalently with a dye, these rings would not appear 4–6 h after growth of the cortex is terminated. However, the issue with covalently labeled actin in this assay is that the cortex is not as clearly visible with labeled actin as with labeled phalloidin.
When 20% of actin monomers are replaced by monomers covalently labeled with Atto 488 only a diffuse cloud around the beads is detectable (Fig. 3.6a). If none of the monomers are labeled and phalloidin is instead used as a label, the cortex with its filaments emerges again clearly.
Since dyes differ in some specifications and also the Atto and Alexa dyes have different properties even at the same excitation and emission wavelengths, we tested other labels as well. Nevertheless, the same results of a diffuse cloud and a distinct cortex was obtained with actin is labeled covalently with Atto 647N and Alexa Fluor 647N-phalloidin. For these reason, the cortex was exclusively labeled with phalloidin.

3.2.3 Localized polymerization in the presence of cross-linker

If the cortex polymerizes in the presence of fascin, a thin dense layer of actin forms with numerous spikes (Fig. 3.7a). At the very beginning of the polymerization, some actin filaments appear at the surface and start growing. Soon after at t = 2 min a light cortex forms around the bead, which continues to increase in intensity,

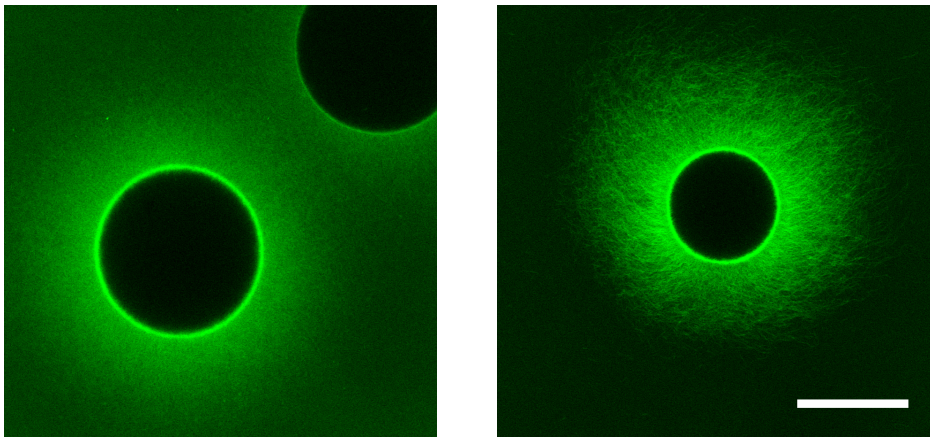

(a) Covalently labeled with Atto 488 (b) Alexa Fluor 488-phalloidin

Figure 3.6: Actin cortex around NiNTA beads coated with formin (c_{formin} = 12.5 µM). Left: 20% actin is labeled covalently with Atto 488 (R = 0.2). Right: Cortex is labeled with 0.5 µM Alexa Fluor 488-phalloidin (R = 0.1). Protein concentrations were 5 µM actin, 1 µM profilin and 150 nM capping protein. Scale bar 50 µm.

but however does not thicken much (Fig. 3.7b). After having reached a certain length, which allows the initial single filaments to bend enough, they bundle with their neighboring filaments as soon as they touch each other. When the far ends of the filaments are in contact, they start to zip together (Fig. 3.7b, Overlay: Fig. 3.7c, t_1 - green, t_2 - blue, t_3 - red), until the actin filaments cannot bend any further towards each other. This sticking and zipping of the filaments results in the observable long spikes in the end of the polymerization process.
The kinetic of the polymerization process is similar to the bulk measurements of the same protein mixture. Here, the main structures, i.e. bundles, are also already visible after 2 – 4 min and from there simply continue to thicken until the polymerization process is finished, which is in agreement with the pyrene data (Fig. 3.8, [Falzone et al., 2012]).

The thickness of the actin cortex that is polymerized in the absence and presence of fascin is extremely different. That raises the question, what effect does the cross-linking process have on the polymerization.
Since all the material polymerizes at the bead surface, we expect that more material will lead to thicker cortices even in the presence of fascin. If the density of the nucleation sites does not change, meaning the number of actin filaments at the surface is kept constant, a higher concentration of actin must alter the filament

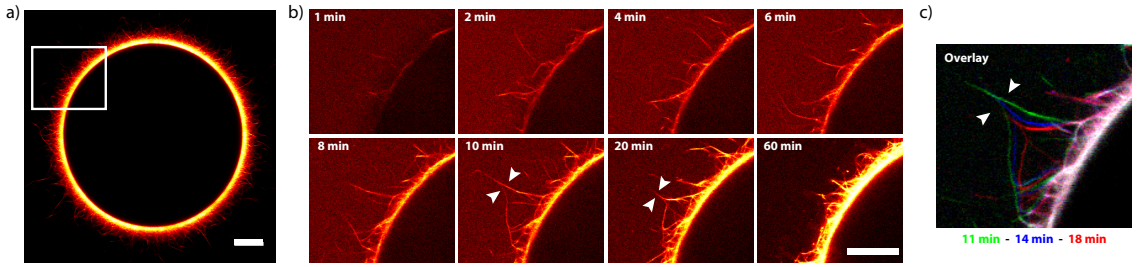

Figure 3.7: a) Final polymerized state of actin cortex in the presence of fascin. b) Time-resolved growth of cortex: 1 min, 2 min, 4 min, 6 min, 8 min, 10 min, 20 min and 60 min. After a thin dense layer of actin forms around the bead, filaments form. As soon as these reach a certain length, they touch and start to zip together. c) Overlay of the zipping process (green: 11 min, blue: 14 min, red: 18 min). Scale bar 20 µm.

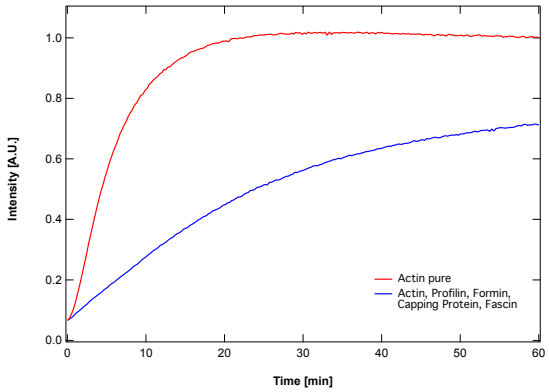

Figure 3.8: Pyrene assay with pure actin (red) and actin, profilin, capping protein, formin and fascin (blue). c_{actin}= 5 µM, c_{prof} = 10 µM, c_{cap} = 150 nM, c_{form} = 1 µM and c_{fascin} = 1 µM.

length. Therefore, we investigated the thicknesses of cortices with our standard protein composition (c_{actin}= 5 µM, c_{prof} = 10 µM, c_{cap} = 150 nM and c_{fascin}= 1 µM) and its fourfold.

Cortex thicknesses were analyzed by plotting the radial profile. The thickness and the radius of the bead were extracted at a certain intensity threshold which was kept constants for all measurements. In Fig. 3.9 the thickness is plotted against the radius. For our standard protein composition, thicknesses are between 6 µm and 10 µm. Beads with a radius smaller than 40 µm show a quite linear dependency of their cortex thickness to their radius. The thicknesses scatter more for large beads. On the contrary, if four times the amount of protein (c_{actin}= 20 µM, c_{prof} = 40 µM, c_{cap} = 600 nM and c_{fascin}= 4 µM) is polymerized around formin coated beads in the presence of fascin, the cortex is between 5 µm and 7 µm broad. The cortex thickness

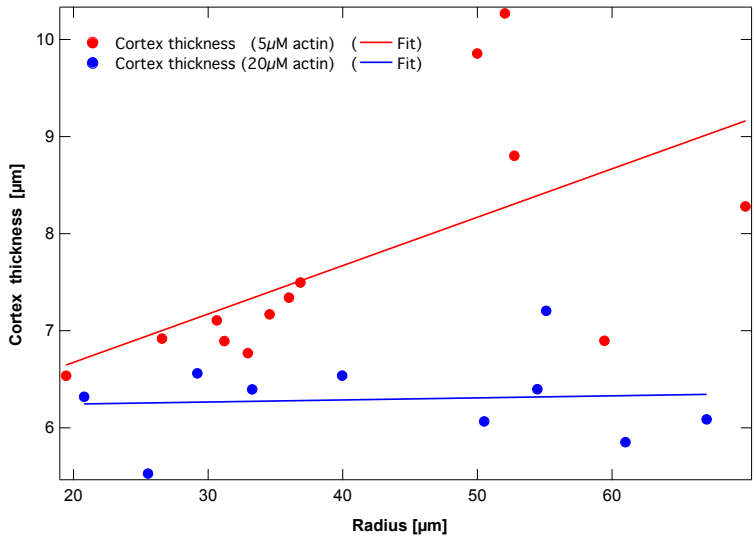

Figure 3.9: Cortex thicknesses plotted against the radius of the corresponding beads. The formin concentration on the NiNTA beads is kept constant at 12.5 µM. Red: Standard concentration of protein for experiments (c_{actin} = 5 µM, c_{prof} = 10 µM, c_{cap} = 150 nM, c_{fascin}= 1 µM). Blue: Four times as much protein (c_{actin} = 20 µM, c_{prof} = 40 µM, c_{cap} = 600 nM, c_{fascin}= 4 µM).

does not show any size dependency of the bead radius.
These results are unexpected. Although a higher concentration of actin should lead to a thicker cortex, we observed that instead more protein and thus more actin lead contrariwise to a smaller cortex that is independent of the bead size. The data is not sufficient to draw any conclusions and therefore, which effect the cross-linking has on the polymerization of the actin cortex, needs to be further investigated.

3.2.4 Time delayed addition of fascin induces contractions

To further study the impact that bundling has on the formation of the actin cortex, we added fascin subsequently to the polymerizing actin cortex at various points in time and also to various densities of nucleation sites. i.e. formin concentrations.

Upon the addition of fascin into the supernatant of polymerizing actin beads without cross-linker, described in Section 3.2.2, the filaments in the cortex start to bundle. Bundling occurs from the outside to the inside. If several beads are in vicinity to each other and their cortices touch, fascin takes longer to diffuse in between them, but then also bundles the filaments there, provided that enough fascin is present in the sample.

The cross-linking process initiates a contraction of the whole cortex (Fig. 3.10, top). The contraction starts also from the outside of where the bundling sets in until the whole cortex is cross-linked. Although, depending on where the fascin is added, cortices can even contract from left to right or right to left according to cross-linker diffusion. Larger actin cortices that had more time to grow, will also exhibit larger cross-linked cortices.

Time dependent addition of fascin

The size of the bundled cortex depends strongly on when the fascin is added after initializing the polymerization. To examine how the contraction evolves depending on the point in time when fascin is added, experiments were done after 3 min, 10 min and 20 min polymerization without cross-linkers.
At all points in time a contraction of the cortices can be observed (Fig. 3.10), but the longer the filaments had time to grow the less they contract. After 3 min the cortical area is reduced to 60 ± 11%. Likewise after 10 min it scales down to 59 ± 7%. For longer polymerization times however, the cortex does not contract as much anymore. Here, with a fascin addition after 20 min of polymerization the cross-linked cortex still covers 89 ± 6% of the initial non-bundled cortex (Fig. 3.10, bottom).

Furthermore, beads whose cortical filaments are entangled sufficiently are drawn to each other upon fascin addition (Fig. 3.10-A and -B). If this is not the case, the cortices are just contracting independently and their filaments disentangle.

Different formin concentrations

In Section 3.2.2 is was already shown that different formin concentrations on the NiNTA beads have different effects on the unbundled actin cortices. Higher formin concentrations lead to denser actin filaments and this high density then causes the filaments to polymerize orderly in a parallel fashion, since they guide each other's direction of growth.
To study the effect of the filament density on the contraction, beads were incubated at different formin concentrations and fascin added after the actin cortex had sufficient time to grow. For the incubation, we used here the same formin concentrations of 2.25 µM, 5 µM, 12.5 µM and 16.7 µM as in Section 3.2.2 and added always the same amount of 1 µM fascin per sample.

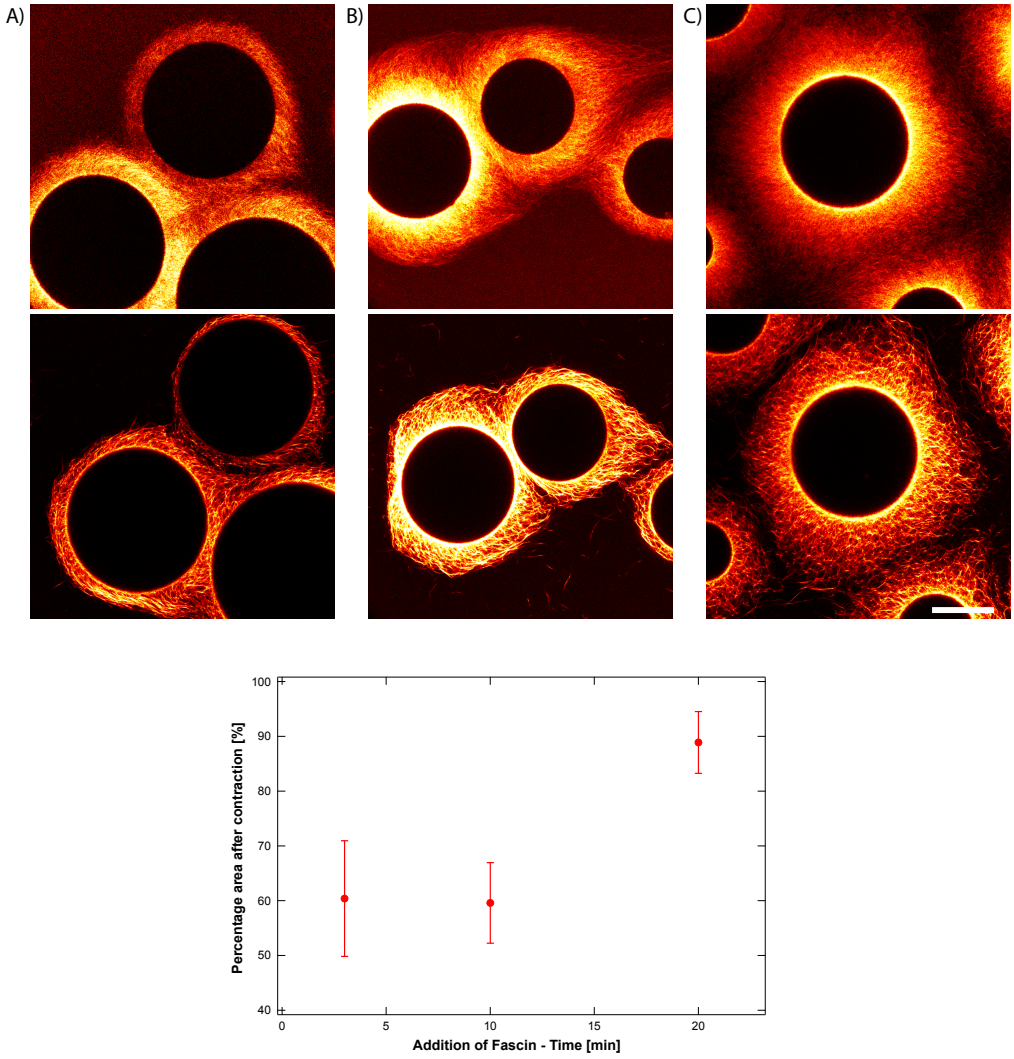

Figure 3.10: Top: Addition of fascin after different polymerization times. A) after 3 min, B) after 10 min and C) after 20 min. Scale bar 50 µm. Bottom: Percentage area of contraction against polymerization times after which fascin was added. c_{formin} = 12.5 µM, c_{fascin} = 1 µM.

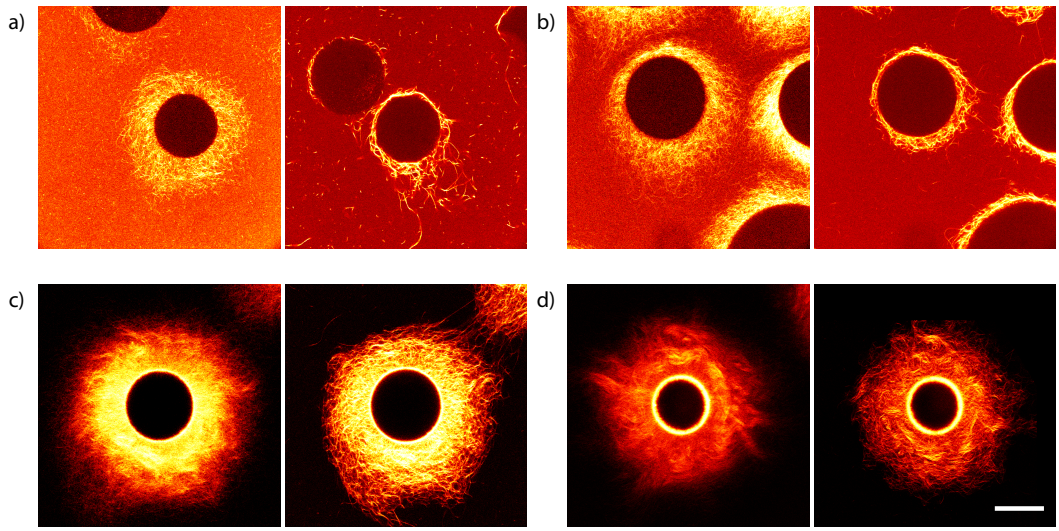

Figure 3.11: Contraction with different formin concentrations on the bead surface. a) 2.25 µM, b) 5 µM, c) 12.5 µM, d) 16.7 µM. Left: Before addition of fascin. Right: After addition of fascin. Scale bar 50 µm.

If now fascin is added these non-cross-linked actin cortices at different densities, contraction can be as well observed at all of them (Fig. 3.11). The contractions for different formin concentrations are of varying strength. But for all of them, the inner shell of the cortex is gaining intensity (Fig. 3.12), which means that here, the filaments become more tightly packed. Simultaneously the outer part of the cortex shrinks. This shrinkage is less pronounced for higher formin concentrations.
Whereas for low amounts of formin (2.25 µM) the cortex after fascin addition is just 31 ± 12% of its original size, the strength of contraction decreases for 5 µM to 45 ± 7% to 77 ± 5% for 12.5 µM until the cross-linked cortex covers as much as 95 ± 4% for 16.7 µM. If these values are plotted versus the formin concentration of the sample, we get a strikingly linear correlation in these concentration regimes (Fig. 3.13).
The fact that the error (the standard deviation) is larger for small formin concentrations, arises on the one hand from the small distances and thus larger percentage errors in the measuring process. The cortex around these beads are on the other hand much more heterogenous, which also contributes to the error. In addition those samples have a worse background to noise signal, since only little actin is polymerized at the bead and thus a lot of protein is still in solution, which makes it more difficult to decide on the outline of the cortex.

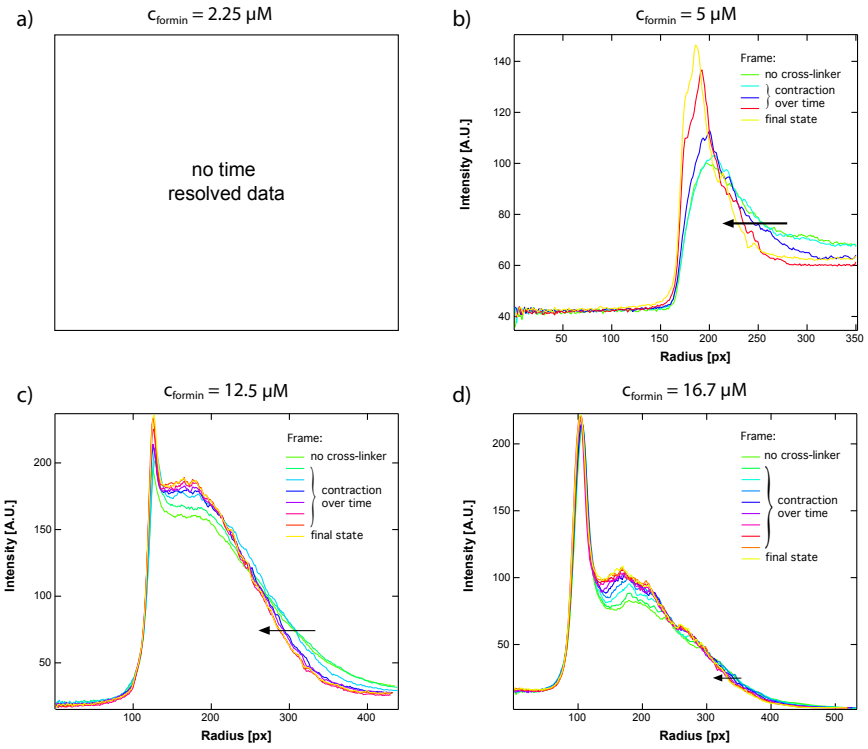

Figure 3.12: Contraction evaluated over time. Radial intensity profile averaged over 360°. Green curve denotes the initial cortex intensity and the cortex intensity is rainbow color coded to the final state in yellow. The intensity gain near the surface of the bead and the intensity loss at the outside cortex shows a clear contraction of the cortex. The more formin there is, the less powerful the contraction is. Besides with less formin the bulk intensity is higher as not all actin is polymerized. a) 2.25 µM, b) 5 µM, c) 12.5 µM, d) 16.7 µM.

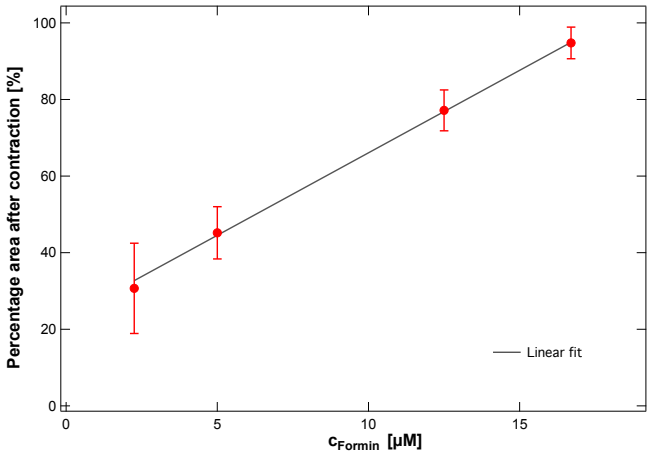

Figure 3.13: Percentage contraction of cortices resulting from different formin concentrations on the bead surface.

Discussion

The later fascin is added to the system, the longer the actin cortex had time to grow and the larger the overall cross-linked cortex will be. This behavior is probably due to the length of the filaments. After 20 min the filaments grew well above their persistence length of $l_p = 15$ µm and hence exhibit a certain flexibility. Due to this flexibility longer adjacent filaments have a higher possibility of being entangled at the outer domain of the cortex. If then fascin diffuses into the network from the outside, it links these loose connection points between all actin filaments and therefore stabilizes the cortex. This might counteract a strong contraction.
For shorter younger filaments, we propose a different explanation for the strong contraction. After 3 min the filaments are just a little longer than their persistence length and are thus stiffer. This might however contradict the increased contraction. But here, the contraction mostly arises from the filaments getting bend towards the surface of the bead.

Furthermore, the density of actin filament also has a strong influence on the contractility of the cortex. The more formin and hence actin filaments there are, the less contractile the cortex is. A most likely explanation for this behavior that the dense filamentous structure stabilizes itself. Filaments do not have enough space to bend. Besides, due to their vicinity, the cross-linkers can bind adjacent filaments without bending them much. Both leads to a less pronounced contraction.

So, in conclusion more actin, especially longer and denser filaments in the cortex are working against contractile forces and stabilize the cortex.

3.2.5 Cortex growth stops upon fascin addition

An interesting observation is that regardless of fascin's addition to the actin beads after 3 min, 10 min or 20 min, after bundling and contraction of the filamentous actin cortex, the polymerization is terminated. Even monitored for up to 12 hours the network around the beads remained unchanged (Fig. 3.14c, Fig. 3.15 – yellow).

We propose that the addition of the cross-linker causes an arrest of polymerization due to stiffening of the network. The cross-linking of filaments into bundles results in an opposing force at the filament's plus-end at the bead surface and hence, formin

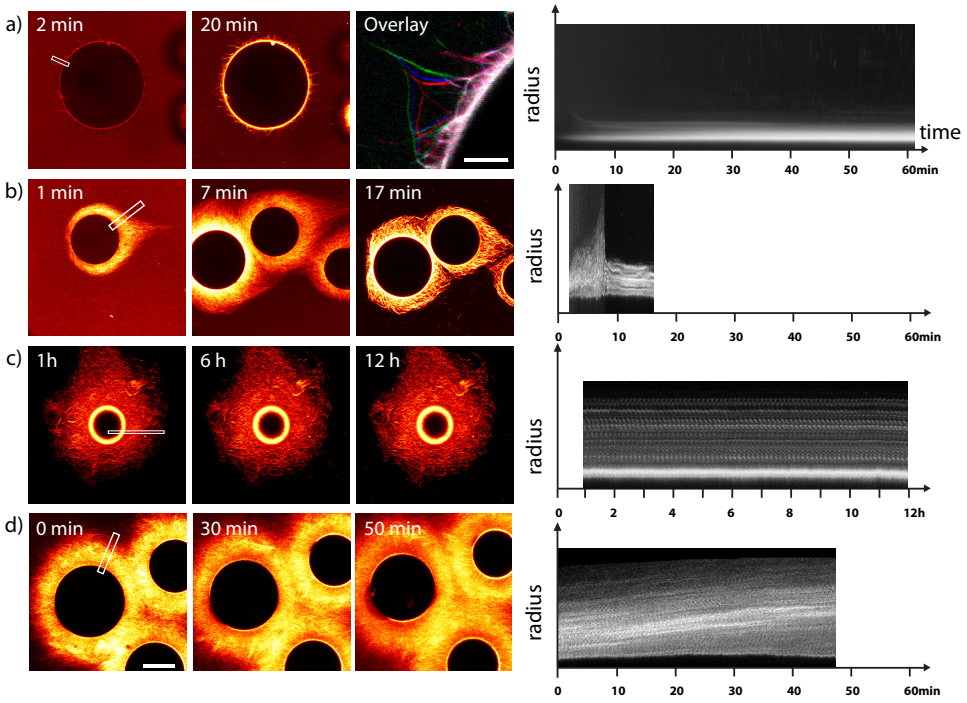

Figure 3.14: Overview of different experiments: Left: Microscopy pictures of temporal cortex evolution. Right: Corresponding kymographs of marked areas over time. a) Polymerization of cross-linked beads. b) Growth of a non-cross-linked bead until the addition of fascin at $t = 7\,\text{min}$. After the addition the cortex contracts and further polymerization is terminated. c) Longterm measurement of cross-linked beads. Size of cortex remains constant over the time course of 12 h. d) Non-cross-linked beads upon the addition of more actin monomers.

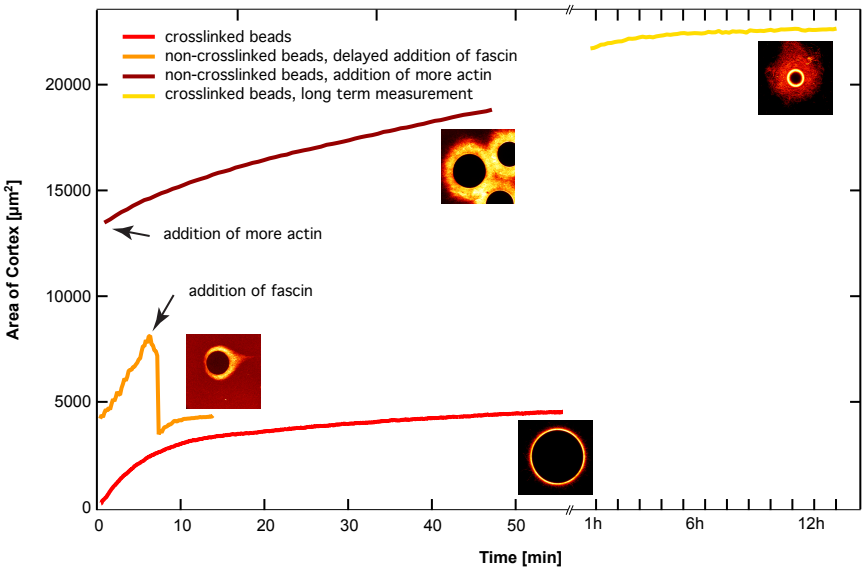

Figure 3.15: Evolution of cortical area over time. Red: Growth of cortex in the immediate presence of fascin in the sample. Orange: Growth of cortex without any cross-linker. After 7 min fascin is added to the sample upon which the cortex contracts fast. This can be seen in the steep decrease in the curve. Dark red: Fully polymerized non-cross-linked beads in the sample, where in a distant area fascin was present. After the addition of more actin monomers, the beads start polymerizing further, but at a slower velocity than initially observed. Yellow: Long term measurement of cross-linked beads. The cortex remains stable for a time span of up to 12 h.

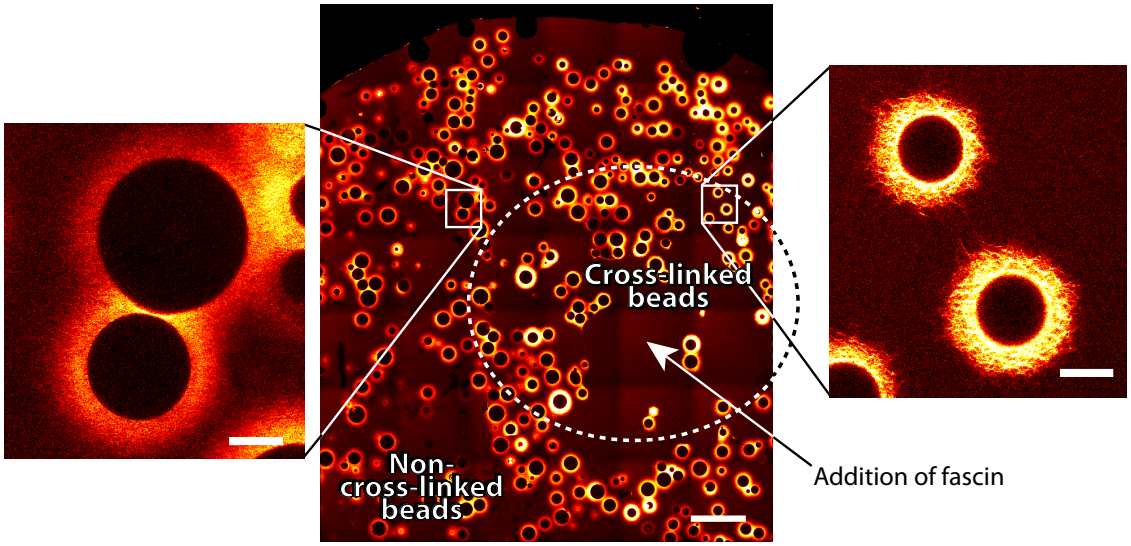

Figure 3.16: Center: Overview of a large part of the sample. Tiled appearance due to stitching of 775 µm x 775 µm pictures. After polymerization 0.1 µM fascin was added as indicated. Cross-linked cortices appear only in vicinity of fascin addition. Scale Bar 500 µm. Left: Non-cross-linked cortices. Right: Cross-linked cortices. Scale bar 50 µm.

cannot further polymerize actin.

To test this hypothesis, an assay was performed where only little fascin (0.1 µM) was added subsequently to the sample. At this low concentration only the beads that are in vicinity of where fascin is added, manifest a cross-linked cortex (Fig. 3.16). Fascin diffuses through the sample and bundles the first and closest actin filaments that it encounters. On the timescale, during the experiments were performed, fascin does not detach.

If more actin monomers are added to the sample after polymerization has ceased, the beads which exhibit a bundled cortex remain the same before and after further addition of monomers. By contrast, further polymerization at the non-cross-linked beads is initiated (Fig. 3.14d).

3.2.6 Elasticity measurement by means of optical tweezer

To determine the elasticity of the cortex after the addition of fascin, step strain experiments with an optical tweezer set up were performed on the cortical network (Section 2.2.4). Step strain measurements were carried out at a distance of 12 µm and 20 µm, respectively, to the surface (Fig. 3.17), in either radial or tangential direction

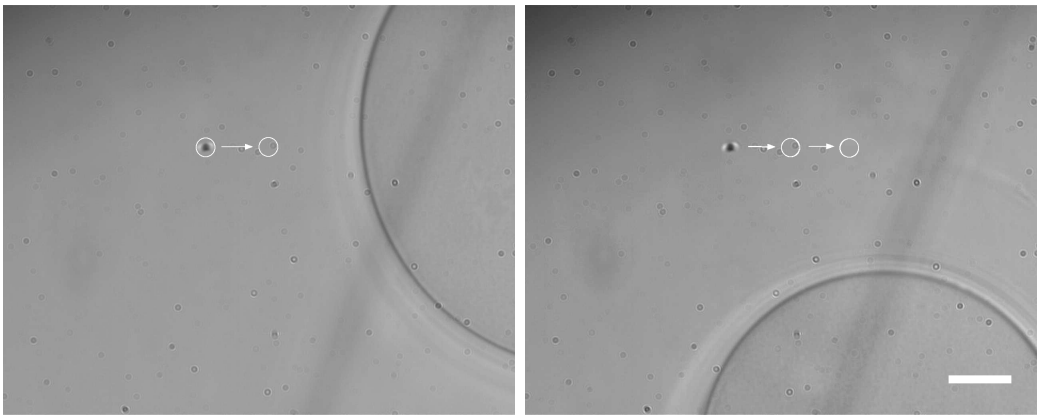

Figure 3.17: Examples of bright field pictures with beads (ø 1 µm) trapped by an optical tweezer and their path of measurement. Left: Radial measurement in a pure actin cortex of a NiNTA bead with diameter of 75 µm. Distances to surface from 24 µm - 12 µm. Right: Tangential measurement in a fascin actin cortex of a NiNTA bead with diameter of 58 µm. Distance to surface ca. 20 µm. Scale bar 10 µm.

before and after the addition of fascin. Typical response curves are shown in Fig. 3.18. The differences of the force curves are easily observable between measurements in a pure actin cortex and a cross-linked actin-fascin cortex. Whereas the response for actin is disguised in the SNR and the network's elastic response is visually not detectable at the time magnification in these data plots (Fig. 3.18), the response is easily recognizable for the cross-linked network.
To extract the Young's modulus of the networks, the decay after the peak is fitted with a double exponential (Section 2.2.4b). For radial actin measurement in total 39 steps were fitted, and for fascin 46 steps. Furthermore, 70 steps were fitted for tangential data of actin and 57 for actin-fascin cortices.

For the pure actin cortex the elasticity in radial direction is 0.005 ± 0.25 Pa and in tangential direction 0.14 ± 0.35 Pa. This is in the same magnitudes of order in agreement with macrorheology data (Chapter 4: Fig. 4.1a). Here, 10 µM actin displays an elastic shear plateau modulus of $G_0 = 0.2$ Pa [Lieleg et al., 2007], whereas in microrheology data 24 µM actin shows a plateau modulus of also $G_0 = 0.2$ Pa and 7 µM show 0.01 Pa [Gardel et al., 2003]. In our system the local concentration of actin is much higher in the cortex as the bulk concentration, a lower Young's modulus is measured. Since the elastic shear modulus G' relates to the Young's modulus with $G' = G_0 = E/2(1+\nu) = E/3$ for incompressible materials (Poisson number $\nu = 0.5$), the values differ even slightly more.

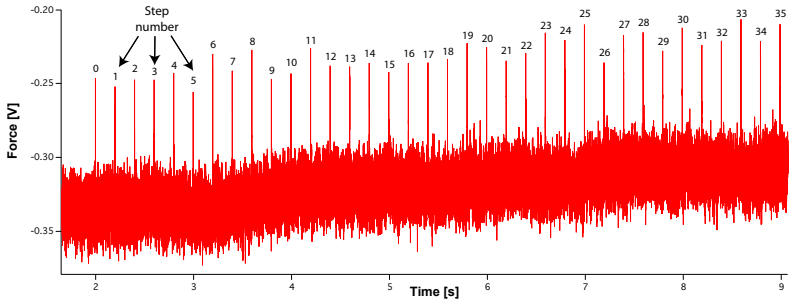

(a) Step Strain response of an actin cortex

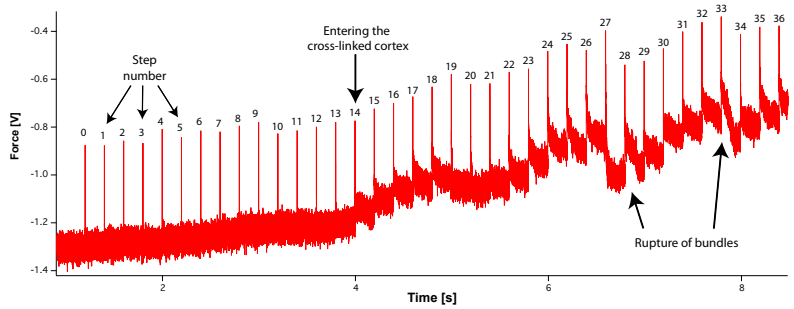

(b) Step Strain response of an actin-fascin cortex

Figure 3.18: Typical stress responses to a step strain in a tangential direction within a pure actin cortex (a) and a fascin cross-linked cortex (b).

The actin-fascin cortices show different step strain curves. In Fig. 3.18b for example steps 0 – 13 are relatively homogeneous, similar to the ones of actin. From step 14 on the step strain curves have a different appearance an the exponential decay is much slower. Here, the trapped bead enters the cross-linked cortex. The difference of these two regimes can also be clearly seen in the overlay of the curves (Fig. 3.19a). Here, steps 0 – 13 are very similar and differ only very little (reddish curves). The regime after entering the cross-linked cortex is noticeably separated (yellow greenish curves) by higher force curves. This difference is also observable in the Young's Modulus, which is also much higher after step 14 (Fig. 3.19b). In step 28 an 33 we see a decay of the curve over a longer time, which indicates probably a rupture of bundles that piled up at the trapped beads while dragging it through the network.

For the fascin cortex a Young's Modulus of 1.0 ± 1.6 Pa in radial direction was measured, as well as 4.3 ± 2.4 Pa in tangential direction. In tangential direction only E_0 measurements were taken for the average that are definitely within the cortex.
In our assay we have 5 µM actin with 1 µM fascin, which results in a ratio $R = 0.2$. For these concentrations and that ratio, a plateau modulus of $G_0 \simeq 6\,Pa$ was macrorheologically measured [Lieleg et al., 2007].

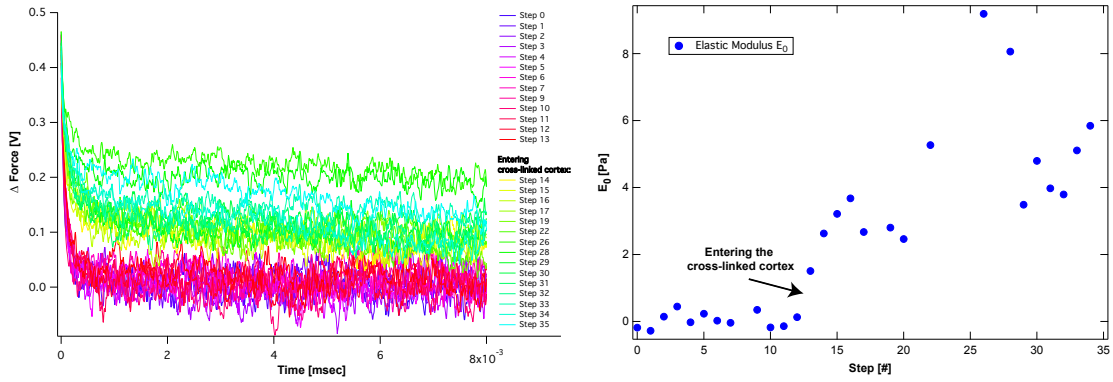

(a) Overlay of step decays of Fascin

(b) E_0 step by step

Figure 3.19: (a) Overlay of step decays of Fascin (Fig. 3.18b). The entering of the trapped bead into the cross-linked cortex is clearly distinguishable by higher force curves (yellow greenish).
(b) Young's Modulus E_0 per step. Entering the cross-linked cortex can also here clearly be detected by a steep rise in the modulus' value.

This is the same order of magnitude. But we have to take into account that the local concentration of cortical actin filaments around the bead is a lot higher. Therefore, we can extrapolate measurements by Lieleg et al. [2007]. If we assume that we have local concentrations within the cortex of a few hundred micro molar and that the ratio of fascin is locally between 0.1 and 0.2, we get with $G' \sim c_a^{2.4}$ [Lieleg et al., 2007, MacKintosh et al., 1995] a modulus of $\approx 3-8\,\mathrm{kPa}$.
With this, we need to conclude that the elastic modulus of the actin fascin cortex differs a lot to macrorheological bulk measurements. This might be due to the very different architecture of the actin-fascin cortex formed around the beads. Here, the actin filaments grow radially outward, are thus mostly parallel oriented and not entangled. Therefore, fascin can cross-link actin filaments efficiently due to their alignment and their vicinity in one direction but not in the other. That is the reason for the different elastic moduli in radial and tangential direction and might also be the reason for the huge differences to bulk measurements, where the network is homogenous in all directions.

Moreover, as can also be extracted from Lieleg et al. [2007] the elasticity of the network depends strongly on the ratio R of fascin to actin. The more fascin there is, the higher the elastic modulus. Since, in our assay, fascin is added to the sample after or during polymerization to the solution without inducing much flow, distribution of fascin mostly happens by diffusion and is thus not homogeneous (Fig. 3.16).

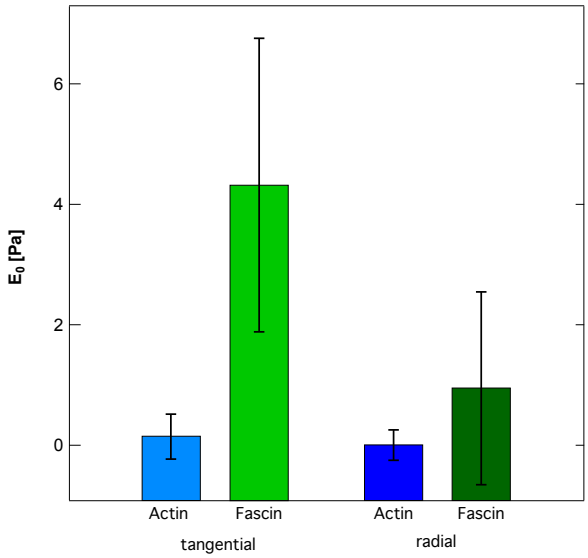

Figure 3.20: Elasticities measured by optical tweezer set up in radial and tangential directions, respectively for both pure actin cortices and cross-linked actin-fascin cortices.

Therefore, the elasticity of the beads' cortices depends also on their amount of cross-linkers and by that on their location in the sample.

3.2.7 Same behavior for other cross-linkers

This arrest of elongation also proves true for other cross-linkers. Similar behavior was shown for the cross-linking proteins alpha-actinin as well as anillin (Fig. 3.21). For alpha-actinin the outline is frayed and single bundles are pointing outwards, similar to fascin cortices. The cortex mesh is regular and contraction can also be observed (Fig. 3.21a).

For anillin, however, the outline is smooth. Bundles pointing outwards at the border of the cortex cannot be observed. In contrast, actin bundles arrange themselves parallel to the bead surface and imbed them (Fig. 3.21b, top left). Aside from that, beads in vicinity to each other with slightly entangled cortices will form structures that resemble long stretched fibers that are under tension (Fig. 3.21b, bottom left). The addition of 1 µM anillin did not result in an equally strong cross-linking as with fascin and alpha-actinin. However, cross-linking can be further initiated, if more anillin is added (Fig. 3.21b, right). Upon addition, the actin filaments between the beads will also cross-link and contraction continues.

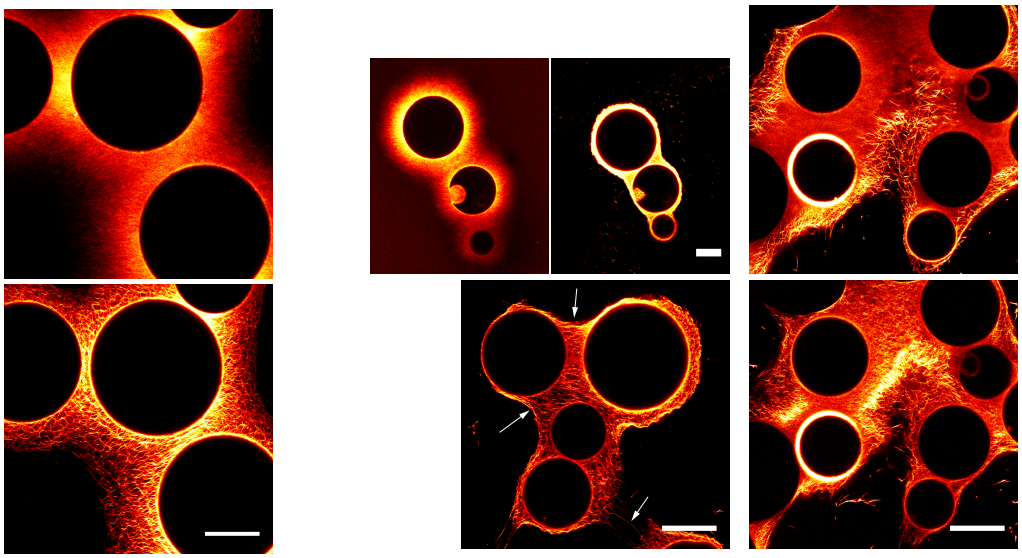

(a) Alpha-actinin (b) Anillin

Figure 3.21: Both the addition of alpha-actinin and anillin terminate the elongation and growth of the actin cortex. (a) Alpha-actinin leads to a frayed cortex. Top: Before addition of alpha-actinin. Bottom: After the addition of alpha-actinin. (b) An anillin cortex around a bead depicts a very smooth surface. Top left: Before and after the addition of anillin. Bottom left: Long stretched actin fibers between close beads (arrows). Top right: After the addition of 1 µM anillin. The actin filaments between the beads are not yet fully cross-linked. Bottom right: After a further addition of a total of 5 µM anillin, actin completely cross-links and further contraction of the beads can be observed. Scale bar 50 µm.

3.3 Discussion

The thickness of the actin cortex that is polymerized in the absence and presence of fascin is extremely different. Therefore, the question is, what overall effect the cross-linking process has on the polymerization. For this, the different effects of nucleation, elongation and bundling and their interplay are investigated, by initiating bundling consecutively through subsequent addition of fascin later to the assay.

We suggest a model by that the cross-linking process of fascin leads to a stiffening of the cortex. Due to the bundling of the filaments, single growing filaments cannot slide past each other anymore. By this hardening the cortex exerts an opposing force on the actin filaments on the surface of the bead, where actin filaments are polymerizing with the help of formin. This opposing force results in stalling of the

elongation and thus polymerization. Hence, the cross-linking changes clearly the basic mechanics of the network, which then leads to an arrest of filament elongation.

It was already theoretically shown that polymerization of actin filaments can be slowed down and eventually stalled by an opposing force F_{max} [Hill and Kirschner, 1982, Peskin et al., 1993]:

$$F_{max} = \frac{k_B T}{\delta} \cdot ln\left(\frac{C}{C_{crit}}\right), \tag{3.1}$$

where k_B is the Bolzmann's constant, T is the absolute temperature, δ is the filament's elongation by adding one actin monomer (2.7 nm), C is the concentration of actin monomers in solution and C_{crit} is the critical concentration for polymerization (about 0.1 µM).
With estimations of free actin concentrations C in living cells between 10 µM to 100 µM and the same effective *in vivo* critical concentration C_{crit} as *in vitro* [Pollard, 1986], the theoretical maximum force that could be generated in a living cell is about 9 pN for the elongation of an actin filament. Given that in *in vitro* assays, mostly a far smaller amount of actin is used, here, the stall forces should be significantly lower.

There have been two published measurements, which determine the force that a single actin filament can generate. Footer et al. [2007] used an optical trap to directly measure the force that few parallel-growing actin filaments generate by elongation. Here, they attached an acrosomal bundle at a 2-µm-diameter polystyrene bead, brought the end of the bundle in close proximity with a micro fabricated wall that serves a rigid barrier and then introduced actin monomers that start to polymerize at the end of the bundle. By this, they could measure the polymerization-driven displacement of the bead and as such the force. They showed that approximately eight parallel-growing actin filaments can be stalled by a relatively small force on the order of 1 pN, which suggests that the force generated by a small bundle is limited by dynamic instability of a single actin filament.
Kovar and Pollard [2004a] measured the polymerization force of actin filaments that elongate between an immobilized formin and a second anchor point. The elongation buckled filament segments as short as 0.7 µm which demonstrates that the polymerization produces forces of at least 1.3 pN.

Both theoretical calculations and experimental measurements point out that actin

filament elongation can be stalled by an opposing force in the pN-range. To support our hypothesis that the cross-linking induces forces on the surface of the bead that terminate the polymerization, we need to estimate the forces that act there.

Noireaux et al. [2000] calculated the stress that an external actin gel is executing on a spherical beads. To do this, they only assume three things: Firstly, the stress tensor $\sigma(r,t) = \mathrm{diag}(\sigma_r, \sigma_\perp, \sigma_\perp)$ in spherical coordinates, with σ_r being the radial component and $\sigma_\perp$ the tangential components of the stress tensor, must obey the equilibrium condition,

$$\nabla \cdot \sigma(r,t) = 0, \tag{3.2}$$

Secondly, at time $t = 0$, the thickness

$$e = r_e - r_i \tag{3.3}$$

of the actin gel is 0, i.e. $r_e(t=0) = r_i$ (Fig. 3.22) and finally, the absence of external normal stress on the gel surface is given by:

$$\sigma_r(r_e, t) = 0 \tag{3.4}$$

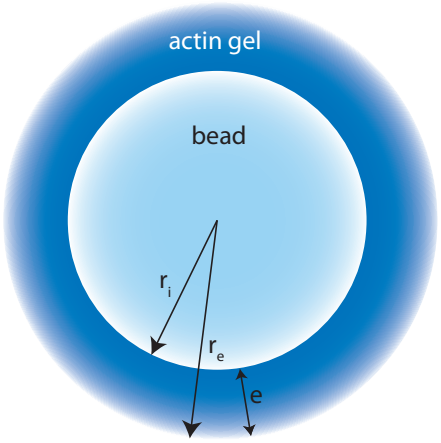

Figure 3.22: Solid bead with radius r_i from which surface an actin gel is growing of thickness e. The total radius of bead with the actin gel is then r_e.

With these three basic assumptions they can calculate the stress $\sigma_r(r = r_i, t) := \sigma(t)$ that the gel exerts on the bead surface:

$$\sigma(t) = 2C\left[\frac{r_e^2(t)}{r_i^2}\left(\frac{r_e(t)}{3r_i} - \frac{1}{2}\right) + \frac{1}{6}\right], \tag{3.5}$$

where C is the elastic modulus of the gel. With $r_i + e = r_e$ (Fig. 3.22), this then can be further simplified, for $e \ll r_i$:

$$\sigma(t) = C\left(\frac{e}{r_i}\right)^2 + \frac{2}{3}C\left(\frac{e}{r_i}\right)^3 \cong C\left(\frac{e}{r_i}\right)^2, \tag{3.6}$$

saying that the stress depends on the squared fraction of the gel thickness to the bead radius.

Moreover, the polymerization rates of the actin gel at the barbed end $\omega(\sigma)$ can be related to the stress-free rates $\omega(0)$ with rate equations [Kramers, 1940]:

$$\omega(\sigma) = exp\left(\frac{-\xi_{nucl}^2 a\sigma}{k_B T}\right) \cdot \omega(0) \tag{3.7}$$

Here, ξ_{nucl} is the distance between nucleators on the bead surface and hence $1/\xi_{nucl}^2$ their density, a is the size of an actin monomer addition, k_B is the Bolzmann's constant, and T the absolute temperature.

Finally, for $r_i \geq e$ Noireaux et al. [2000] derive the following correlation between the gel thickness e and the bead radius r_i:

$$\frac{e}{r_i} \cong \left(\frac{\Delta\mu}{C\xi_{nucl}^2 a}\right)^{1/2}, \tag{3.8}$$

where $\Delta\mu$ is the chemical potential difference per monomer, i.e. it represents the chemical energy released in the polymerization process. Eq. 3.8 states that the growth of the actin gel will stop, if e has reached a certain thickness.

One can understand Eq. 3.8 also in terms of a somewhat more direct physical approach. The polymerization process terminates, when the chemical energy gained in the polymerization process E_χ equals the elastic energy cost for adding a new monomer E_{el}. Thus energetically, further polymerization is not favorable anymore:

$$E_\chi = E_{el} \tag{3.9}$$

The total chemical energy is the chemical energy $\Delta\mu$ released per monomer addition times the number of nucleators on the bead surface:

$$E_\chi = \Delta\mu \cdot \frac{4\pi r_i^2}{\xi_{nucl}^2} \tag{3.10}$$

With the elastic energy being the force F times the distance Δx, which is here a, the addition of an actin monomer (2.7 nm), and Eq. 2.1, we get:

$$E_{el} = F \cdot \Delta x = \sigma_{rr} A \cdot a = \sigma_{rr}\, 4\pi r_i^2 \cdot a \tag{3.11}$$

Inserting Eq. 3.10 and Eq. 3.11 into Eq. 3.9, gives

$$\Delta\mu \cdot \frac{4\pi r_i^2}{\xi_{nucl}^2} = \sigma_{rr}\, 4\pi r_i^2 \cdot a \tag{3.12}$$

and with the approximation of Eq. 3.6,

$$\Delta\mu \cdot \frac{1}{\xi_{nucl}^2} = C\left(\frac{e}{r_i}\right)^2 \cdot a \tag{3.13}$$

one derives the same correlation as in Eq. 3.8:

$$\frac{e}{r_i} = \left(\frac{\Delta\mu}{C\xi_{nucl}^2 a}\right)^{1/2}. \tag{3.14}$$

These calculations can now be applied to estimate the forces that act on the actin filaments on the bead surface in our assay, after the addition of fascin to the growing actin filaments that terminates the polymerization.
First of all, to estimate the distance of the nucleators ξ_{nucl}, i.e. formin, on the NiNTA beads, the thicknesses of the cortices e as a function of the bead radius r_i were measured in Section 3.2.3 (Fig. 3.9) for the polymerization process in the presence of the cross-linker fascin. Here, we get an average for $e/r_i = 0.21 \pm 0.06$. Since it is not possible to measure the elasticity of the thin cortex with an optical trap due to the laser beam's deflection in vicinity of the bead surface, as a rough estimation serves the elastic modulus of the *Listeria* comet tail, given that the structure of the actin gel is similar. Its elasticity was measured with about $C \approx 10^4$ Pa [Gerbal et al.,

2000]. If we rewrite Eq. 3.8,

$$\xi_{nucl} = \sqrt{\frac{\Delta\mu}{Ca}} \cdot \frac{r_i}{e} \ , \tag{3.15}$$

and take into account $\Delta\mu \simeq 14\ k_BT$ [Gordon et al., 1976] and the elongation distance per monomer addition $a = 2.7\,\text{nm}$, we get $\xi_{nucl} \approx 230\,\text{nm}$, which is a reasonable average distance for the formin molecules on the bead surface.

From the density of nucleators, we can now estimate the forces that act on a single actin filament at the surface, after the addition of fascin.

Based on the definition of the stress (Eq. 2.1), moreover, the fact that all the stress will only be applied to the collectivity of actin filaments on the surface and finally the approximation of Eq. 3.6, we can calculate the force acting on a single filament:

$$\begin{aligned} F &= \sigma \cdot A \\ &= C\frac{e^2}{r_i^2} \ \cdot \ \frac{4\pi r_i^2}{\xi_{nucl}^2}\ a^2\pi \\ &= \frac{C}{\xi_{nucl}^2}(2\pi a \cdot e)^2 \end{aligned} \tag{3.16}$$

With the measurements of the elasticity of the subsequently cross-linked actin cortex (Section 3.2.6), we get an elastic modulus of $C \sim 1\,\text{Pa}$. Furthermore, the cortices are after contraction between $30-50\ \mu\text{m}$ thick. Lastly, we take the density of nucleators calculated in Eq. 3.15.
Thereby, for $e = 50\,\mu\text{m}$ we get a force of

$$F \simeq 23\ \text{pN} \ , \tag{3.17}$$

and even for $e = 30\,\mu\text{m}$ we still get 8 pN. Both forces are well in the pN-range and above or similar to the stalling force of theoretically possible 9 pN. Experimentally measured were forces of at least 1 pN with and without formin [Kovar and Pollard, 2004a, Footer et al., 2007]. As such, the attachment of formin at the end of an actin filament does not have a big impact on the stalling forces.

In Fig. 3.2 it was shown that the binding of HisGFP to the NiNTA beads varies throughout the same sample up to ±20% (Fig. 3.2b). In conclusion the surface density ξ_{nucl} of formin will also vary to the same extent and thus will the density

of actin filaments in the cortex as well. This is most likely due to the fact that the formin is added to the beads in a concentrated form. Since the amount of formin molecules do not saturate the beads, more formin molecules will bind to the beads in vicinity to the pipette tip. This variance will of course directly affect the actin filament density, thereby the stiffness of the cortex, assumed that the fascin is uniformly distributed in the sample . If we thus assume as a lower bound that we have up to ten time less formin molecules on the surface, we still calculate forces of several pN.

It also has to be mentioned that the theoretical model is based on a homogenous actin gel i.e. elasticity in all directions are the same. Here, the actin cortices have different elasticities in radial and tangential directions. However, since the magnitudes are the same, the approximations are still valid.

Therefore, we arrive at the conclusion that our estimations of the forces acting on the actin filaments are quite robust to different uncertainties like filament density and thus reliable. With this we have shown successfully that our hypothesis is applicable: The cross-linking process stiffens the network, which results in a higher elastic modulus and by this, we get a polymerizational arrest, since the polymerization energy cannot overcome the elastic energy to further elongate.

The same behavior could also be reproduced with other cross-linkers like alpha-actinin or anillin as well, which supports as well our hypothesis. The arrest in elongation does not depend on a specific cross-linker but only on the change in elasticity. If the cortex is stiffened by cross-linkers of any kind, polymerization is terminated due to a balance of forces.

3.4 Outlook

A very interesting approach would be applying the described system on the surface of vesicles. Vesicles unlike beads have a deformable membrane. The forces of the polymerizing actin filaments might be high enough to overcome the membrane tension typically in range between 5 pN and 30 pN [Sheetz, 2001]. By this filopodia like structures can be achieved.
Experiments with a polymerizing cortex on the outside membrane of a vesicle will

lead to a further insight into the mechanics of filopodia formation. The investigation of the vesicle shape and size upon pure actin polymerization will illuminate the involved forces.
If the fascin is added later to the entangled actin cortex, it will be interesting to see, if the pressure of the contraction might be strong enough to deform the vesicle on the whole or if filopodia like structures will protrude into the vesicle interior. In this case the work of elasticity can eventually overcome the membrane tension at some points, polymerization will prolong and protrusion will form.

4 Rheology on branched and cross-linked branched actin networks

During cell locomotion, the cytoskeleton is constantly reorganizing itself. Regulated actin polymerization at the leading edge takes place while continuous disassembly deeper in the cell interior occurs. This polymerization results in the formation of lamellipodia and filopodia. In the previous chapter (Chapter 3) we focused on the mechanics of filopodia. We showed that the elongation of filaments polymerized by the nucleator formin, which is mainly present in the filopodia tip, can be arrested through the addition of the cross-linker fascin, which is also present in the filopodia. The change in elasticity generated through the cross-linking process leads to a change in the network mechanics and by thus the growth of the filaments at the formin end can be stalled.

Now we focus on the transition between lamellipodia and filopodia. The lamellipodium consists of a network that is highly branched by the Arp2/3 complex. In contrast, the filopodium is a parallel bundled structure by the cross-linker protein fascin that is completely absent of the Arp2/3 complex. It is still not clear how these two proteins interact structurally at the transition and how the structure of lamellipodia and the fascin concentration control filopodia formation. It remains elusive how the network arranges itself at the interface of the two structures.

Therefore, it is essential to gain further knowledge about the self-assembly of these actin-based structures and the factors controlling these processes in a more general way. Here, we studied the interplay of actin in the presence of the proteins that play a major role in the assembly of lamellipodia and filopodia respectively. We investigated the self-assembly of actin with Arp2/3 complex activated by VCA microscopically and rheologically both with and without fascin. In particular we studied the dynamics of the polymerization process.

We observed a peculiar non-monotonically increasing course of the storage modulus G′ during polymerization for networks both with and without fascin. For this, we provide a model showing that the newly formed branches of the actin network are highly metastable and dissociate of their mother filaments on a fast time scale. In the absence of fascin the short daughter filaments freely diffuse and then anneal rapidly to longer filaments. The filaments formed by annealing contribute also to the elasticity of the final network and are in part responsible for the increase of the storage modulus.

Arp2/3 complex is different to "real" nucleators, like for example formin. Other than formin, the Arp2/3 complex is not a nucleator *de novo*. It needs an actin mother filament, where it can bind to and subsequently nucleate another filament, the daughter filament [Pollard, 2007]. By this the Arp2/3 complex accelerates not only nucleation but is also a branching protein, since it organizes filaments into y-branched networks. The Arp2/3 complex is the only protein that is known of that can generate branches of actin filaments and hence is especially very important in the lamellipodium in a cell, where is it dominantly present and where it is crucial for actin-based motility [Pollard and Borisy, 2003].

4.1 Rheological investigation of branched actin networks

4.1.1 Addition of Arp2/3 complex alters the polymerization of actin

a) Rheological characterization

Actin at a concentration of 10 µM polymerizes to a plateau storage modulus G′ of usually less than 1 Pa for low frequencies [MacKintosh et al., 1995] (Fig. 4.2a). Here, we used a medium ranged frequency of 0.5 Hz to monitor the polymerization process of actin networks. In the beginning the storage modulus shows a steep increase and then flattens after around 20 min at a value of about 0.6 Pa (Fig. 4.1a). Polymerization is thus rheologically completed. The completion of polymerization is not fully in agreement with the information that pyrene assays reveal about the

polymerization process of actin. Here, the intensity curve of actin takes only about 12 min to converge to its final value (Fig. 4.1b). So, in the pyrene assay, polymerization is already completed, whereas in rheology G′ is still subject to change.
If the Arp2/3 complex is added together with its activator VCA in a three to five fold excess, a notable change in the rheological polymerization curve emerges. The Arp2/3 complex gives rise to a much faster polymerization, which can be seen in a steep slope. The more Arp2/3 complex is added, the steeper the slope is. After a couple of minutes the growth of G′ stagnates and decreases. This decrease is not as pronounced as the initial slope. Then again, the storage modulus growth is resumed, but at a much lower rate compared to the start of polymerization, until after about 40 min when it reaches its final value (Fig. 4.1a).
In pyrene assays using the same protein concentrations as in the rheology experiments, this local minimum can not be detected. Here, the polymerization is also accelerated through the addition of the Arp2/3 complex, which can be seen in the increased rise of the intensity during the first few minutes. Polymerization with the addition of 100 nM Arp2/3 complex is finished after 10 min, while with 333 nM Arp2/3 it takes only 4 min to completion (Fig. 4.1b).

For an easier and more direct graphical comparison of the polymerization rates, the pyrene curves were plotted in the same graph as the rheology curves after corrected for any occurring bleaching (Fig. 4.1c,d). For both 100 nM and 300 nM Arp2/3 complex the initial polymerization rates in the rheology curves are almost identical to the intensity curves of the pyrene assays. For 100 nM exactly when polymerization is completed G′ starts to decrease. Similar behavior can be observed for 333 nM Arp2/3 complex. As soon as the pyrene intensity reaches its maximum value, in rheology the onset to the local minimum starts (Fig. 4.1c,d).
Both Arp2/3 complex and VCA buffer contain 1 mM $MgCl_2$. The Mg^{2+} concentration has an accelerating influence on the polymerization rate [Frieden, 1983, Tobacman and Korn, 1983]. To be able to compare polymerization rates, all experiments were conducted with same buffer compositions adjusted to the maximal Arp2/3 complex and VCA concentration used.

The viscoelastic response of branched actin networks is determined by measuring the frequency-dependent viscoelastic moduli $G'(\omega)$ and $G''(\omega)$. The frequency dependence of both moduli of a branched actin network with either 100 nM or 300 nM Arp2/3 complex remain very similar to that of an unbranched actin network (Fig. 4.2a). The gradient of the storage modulus G′ and the loss modulus G′

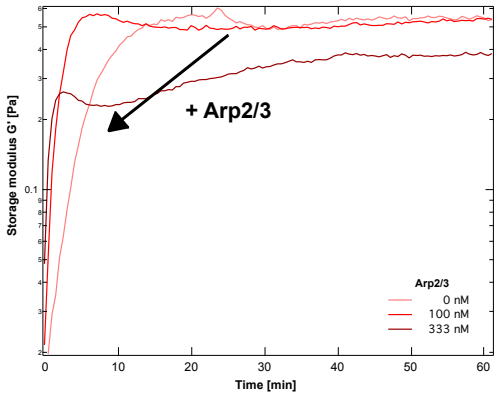

(a) Polymerization in rheology with Arp2/3 complex

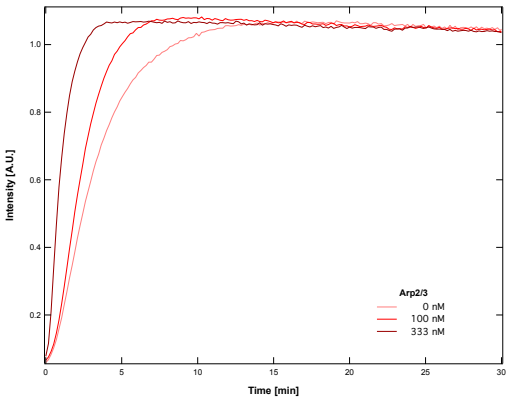

(b) Polymerization in pyrene assays with Arp2/3 complex

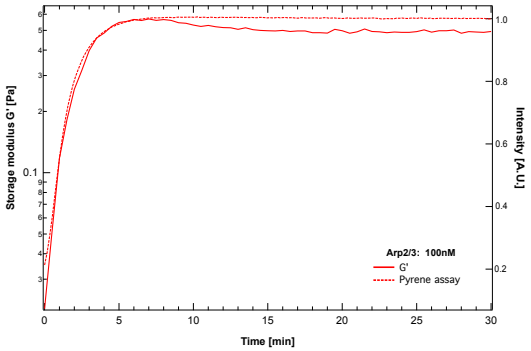

(c) Overlay: Rheology and pyrene data (100 nM Arp2/3 complex)

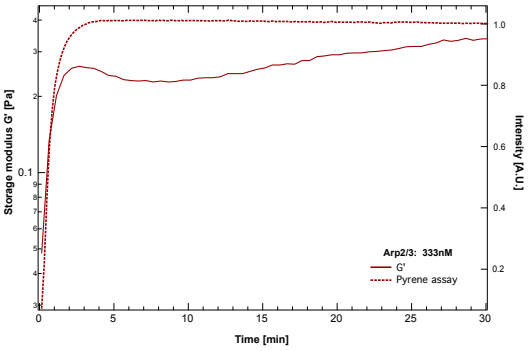

(d) Overlay: Rheology and pyrene data (333 nM Arp2/3 complex)

Figure 4.1: (a) The addition of Arp2/3 complex results in a local maximum, followed by a minimum in G′. (b) Pyrene assay of the polymerization of 10 µM actin with 20 % pyrene actin. Curves are normalized to a value of 1. Slight decrease in intensity is likely due to bleaching effects. (c), (d) Overlay of pyrene assay with the rheological data. Pyrene data is corrected for bleaching and normalized to final G′ value.

is almost equal and the total values differ only minimal. This is in within the G′ and G″ distribution, when identical samples are measured more often.

The non-linear response serves as an indicator for molecular interactions present in the network and can give helpful insights into the mechanics of the network. To examine the non-linear response of the actin and actin-Arp2/3 complex networks stress-strain experiments are conducted, where the network is deformed up to 500% with a constant shear rate ($\dot{\gamma} = 0.125\ \mathrm{s}^{-1}$). For all three networks a stiffening of the network can be observed, which can be seen in the change of gradient in the stress response. The onset of the stiffening is denoted by arrows (Fig. 4.2b). Stiffening

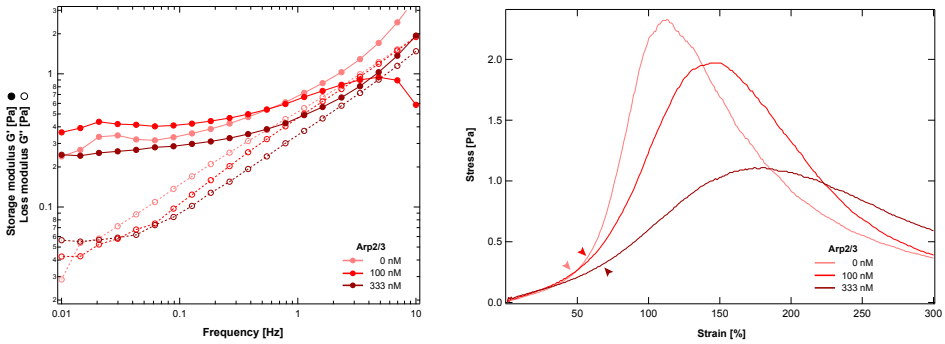

(a) Frequency dependence (b) Stress-strain relation

Figure 4.2: (a) Storage and loss moduli at different frequencies from 0.01 to 10 Hz and (b) non-linear response as obtained from constant shear experiments ($\dot{\gamma} = 0.125\ s^{-1}$) for pure actin solutions (10 µM actin) and with 100 nM and 333 nM Arp2/3 complex, respectively.

starts later, the more Arp2/3 complex is added to the system. Furthermore, the non-linear response is also less distinct with more Arp2/3 complex. The stiffening is weaker, which means that the networks is softer.

b) Discussion

The Arp2/3 complex has a large effect on the formation of the actin network. Both the pyrene assays and the rheology experiments show a steeper slope with Arp2/3 complex than without. This acceleration of the polymerization arises from the Arp2/3 complex nucleation ability. It was shown that the Arp2/3 complex forms branches on existing actin filaments at an angle of 70° [Mullins et al., 1998]. The rate of elongation at the barbed end does not change due to the Arp2/3 complex [Mullins et al., 1998], but the rate of overall polymerization does, since the Arp2/3 complex gives rise to many new barbed ends and as such accelerates by nucleation the polymerization in total. This nucleation ability of Arp2/3 complex has been shown many times [Welch et al., 1998, Blanchoin et al., 2000a, Beltzner and Pollard, 2008].

There is no Arp2/3 complex dependency in the frequency sweep, i.e. G′ stays very similar to the G′ of a pure actin network for all frequencies, while the non-linear response of branched actin networks appears softer. It was already shown that the experimental conditions, e.g. the filaments length, remarkably influences the occurrence and characteristics of the stiffening behavior. Even though the filament

length strongly affects the nonlinear response, it has no significant effect on the linear elastic response [Semmrich et al., 2007]. This can be seen here in the very similar G′ with and without Arp2/3 complex that is thus independent of the filament length. Furthermore, with shorter filaments a transition from strain-stiffening to strain-softening could be observed [Semmrich et al., 2008]. We detect the same trend in our data and we expect that with even more Arp2/3 complex, clear strain-softening will be detectable in the non-linear response.

Networks polymerized in the presence of Arp2/3 complex are highly branched. Since actin can elongate now from much more barbed ends, the monomer pool depletes much quicker from solution with Arp2/3 complex. Hence, due to the limited monomer pool the filaments cannot grow as long as they would do without the Arp2/3 complex. If we make a rough estimate by neglecting spontaneous nucleation and by assuming that only every Arp2/3 complex raises one daughter filaments, a concentration of 100 nM Arp2/3 complex would results in filaments at an average length of 270 nm at 10 µM actin (100 monomers per filament). Likewise, filaments polymerized with the presence of 333 nM Arp2/3 complex can only grow up to 81 nm on average. Since not all Arp2/3 complexes bind to actin filaments and nucleate new branches at the same time, the network will also exhibit some longer filaments. For this reason can some Arp2/3 complexes form no new branches, as actin monomers are all yet consumed. Nevertheless, Arp2/3 complex leads to many more but much shorter filaments that cannot entangle as much as unbranched straight actin filaments.

The mesh size ξ of unbranched actin filaments depends on the actin concentration and can be calculated with $\xi = 0.3\ \mu\text{m} \cdot (\frac{c_a}{\text{mg/ml}})^{-1/2}$ [MacKintosh et al., 1995]. So, a 10 µM actin network has a mesh size of about 0.5 µm, which must be composed by filaments longer that the mesh size. Hence, it is debatable if the term mesh size is even applicable to highly branched actin networks with short branches. Here, only the longest filaments can entangle and form a mesh and many of the shorter filaments do not contribute to the non-linear response.

Hence, we can conclude that the viscoelastic behavior of branched actin networks is a result of the averaged shortening of the filament length due to the Arp2/3 complex.

Time dependence of peak and local minimum If all polymerization curves of G′ are compared, it is clearly visible that the peak and also the following local minimum are shifted to earlier times, the higher the Arp2/3 complex concentration

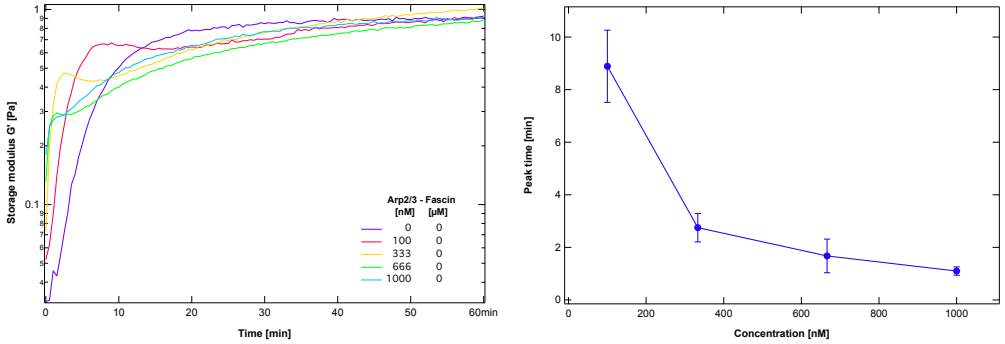

(a) (b)

Figure 4.3: (a) Polymerization of different Arp2/3 complex concentration. Rheology curves normalized in order to better compare the time dependence of the local minimum. (b) Times of peak for different Arp2/3 complex concentrations. Peak time is averaged from four different set of measurements.

(Fig. 4.3a). Furthermore, the duration of the non-monotonous behavior is shorter, i.e. the decrease is shorter with higher concentrations of the Arp2/3 complex.

To extract the polymerization time at which the maximum occurs, a gaussian was fitted to the graph around the peak and the peak time extracted from the gaussian maximum. A set of four measurement series, with the addition of 100 nM, 333 nM, 666 nM and 1000 nM Arp2/3 complex, were taken into account to extract and average the peak times.

4.1.2 Further experiments to investigate local minimum

To inquire, what causes and what happens during the local minimum further experiments are conducted.
Arp2/3 complex has two features. It acts as a nucleating agent for actin polymerization by providing rapidly new barbed ends of the daughter filaments. Additionally Arp2/3 complex branches the actin filaments and by this causes networks with a very different architecture to pure entangled networks.

Hypotheses Therefore, two different hypotheses might explain the local minimum. Either enhanced nucleation leads to this uncharacteristic behavior of the storage modulus or Arp2/3 complex's branching ability or mechanical rearrangements are

the underlying reason. For the latter, we propose that rapid dissociation of the newly formed daughter filaments might be the primary cause for the minimum.

a) Influence of nucleation seeds on G′ progression

To test weather the nucleating ability of the Arp2/3 complex is the reason for the unusual rheological behavior during the early polymerization process, nucleation seeds in form of very short prepolymerized and sheared actin filaments were added to the system without the Arp2/3 complex. If the nucleation is the only source for this behavior, we expect the same or a similar performance with seeds instead of the Arp2/3 complex.

Seeds in the absence of Arp2/3 complex When 1% or 5% of the total actin concentration is added in form of seeds to actin monomers a faster onset of the polymerization can be observed (Fig. 4.4a). Nucleation is the fundamental starting point for polymerization. Since actin nuclei consisting out of two or three actin monomers are extremely unstable [Sept and McCammon, 2001], the on-set of polymerization is temporally limited by nucleation. Hence, with seeds actin can start polymerizing immediately. It can also be seen from Fig. 4.4a that with more seeds, the final value of the storage modulus G′ is slightly reduced.
Furthermore, the networks with seeds all show a non-linear response in the stress-strain curve, even though this stiffening is less pronounced with more seeds (Fig. 4.4b, 5% seeds). It is very likely that with an even higher percentage of seeds, the non-linear response will transition from a strain-stiffening to a strain-softening.

However, none abnormal minimum in the polymerization curve could be detected for any percentage of seeds. Therefore, the nucleation ability of Arp2/3 complex cannot be the sole reason for the non-monotonic behavior of G′ detected in rheology.

Seeds in the presence of Arp2/3 complex How do seeds and consequently an enhanced nucleation influence the polymerization process in the presence of the Arp2/3 complex?
With 333 nM Arp2/3 complex and without seeds, a clear peak with a following local minimum is observable as described above. With 5% seeds, this non-monotonous behavior is highly diminished. Where the local minimum used to be without seeds,

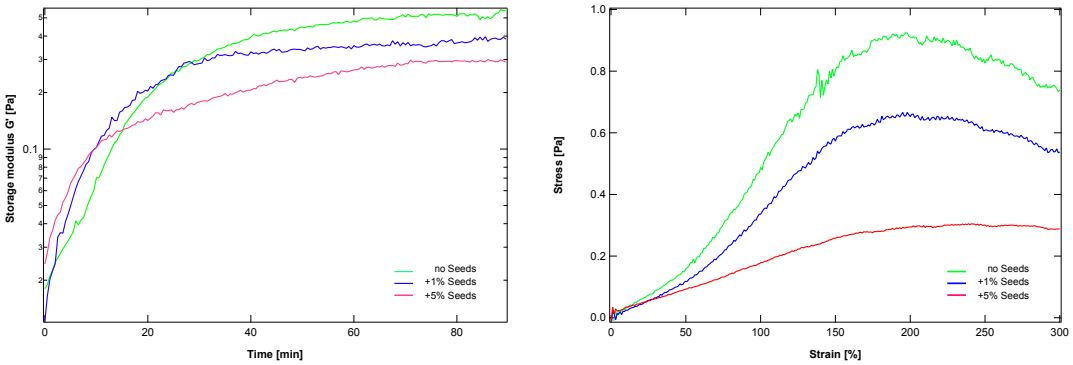

(a) Polymerization (b) Stress-strain relation

Figure 4.4: Rheological measurements with seeds on pure actin

now only a small change in slope is visible, indicated by an arrow (Fig. 4.5a). More seeds cause even this dent to disappear and with 25% seeds no trace of the non-monotonous behavior is detectable anymore, i.e. the polymerization is monotonically increasing. After about 10 min, when the local minimum without seeds passed, the polymerization speeds of all samples are almost identical, whether there are 5%, 25% or no seeds at all.

In addition, the seeds do not largely influence the final value of the storage modulus G′. Not even 25% seeds have a considerable impact on G′ at any frequency from 0.01 Hz to 10 Hz (Fig. 4.5c).

Furthermore, with seeds, the stress-strain curves show very different characteristics. Here, the typical strain-stiffening is now absent and cannot be observed anymore. Instead the stress builds up linearly or the sample exhibits stress-softening until it shows plastic deformations and detaches from the rheometer plates (Fig. 4.5b).

Discussion For an estimation of the amount of polymers that form without seeds, we modeled the kinetics of actin filament nucleation and growth following the simulation of Falzone et al. [2012]. Their model consists of a system of coupled rate equations describing the concentrations of actin monomers, dimers, trimers and filaments. Instead of their rate constants which Falzone et al. adjusted to their rather slowly polymerizing system, we used established rates for the kinetics [Paul and Pollard, 2008].

For 10 µM actin, the model calculates already 0.93 nM polymers after about 40 sec which ends in 1.1 nM after 80 sec, nearly the final amount of polymers. The model only takes into account pure actin nucleation and elongation and neither filament

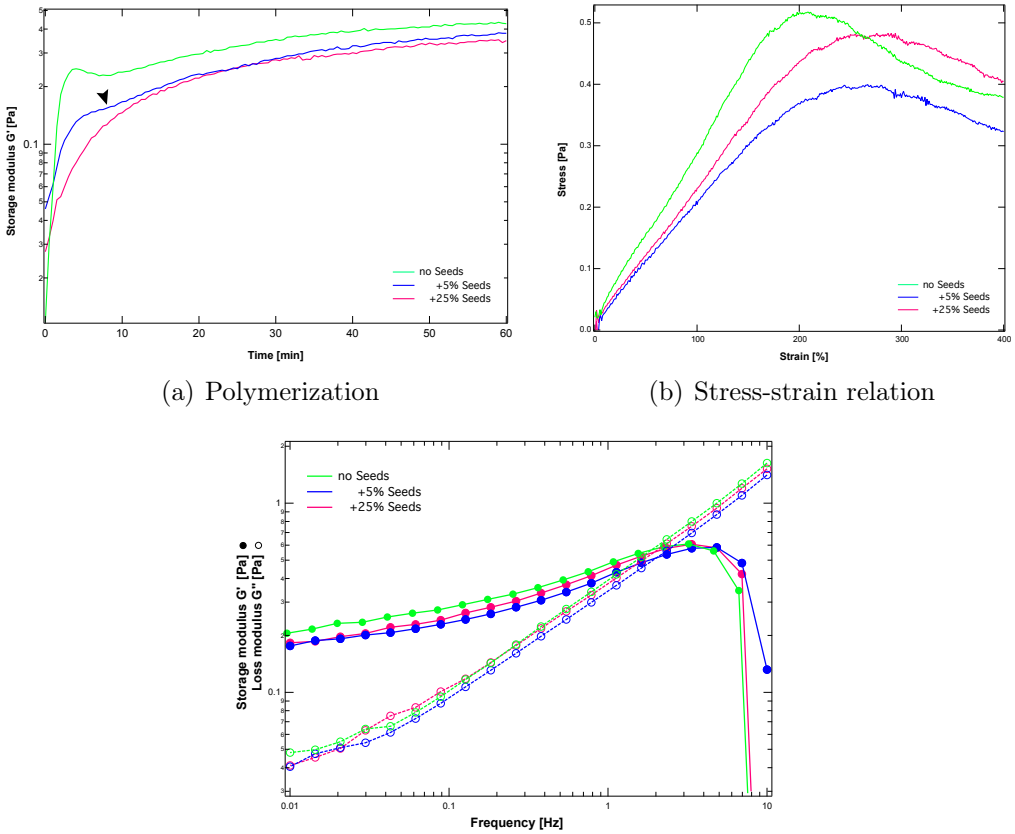

(a) Polymerization

(b) Stress-strain relation

(c) Frequency dependence

Figure 4.5: (a) Polymerization curve, (b) non-linear response and (c) frequency dependence of a branched network polymerized in the presence of seeds. $c_{Arp2/3} = 333\,\mathrm{nM}$.

fracturing, annealing nor nucleation by Arp2/3 complex.

To compare the number of polymers to the number of seeds that are added to the system, the amount of seed also need to be estimated. Assuming that filaments are sheared into seeds of roughly 1 µm length, which are assembled by 370 monomers, results in 1.3 nM seeds for 5% seeds in our assay. Likewise 25% result in 6.7 nM polymers.

So, 5% seeds outnumbers the filaments that would originate by actin nucleation and besides polymerization in the system happens highly simultaneously throughout the sample. This can be directly seen in the non-linear response of actin with seeds compared to actin networks formed without seeds (Fig. 4.4b). 5% seeds result in a much softer network with a minimal stiffening due to the simultaneous polymerization. Seeds lead to shorter filaments due to the excess of nucleation sites and hence simultaneous polymerization in the sample. Shorter filaments result in a

softer strain-stiffening as discussed above (Section 4.1.1b) [Semmrich et al., 2008], but has no influence on the linear response (Fig. 4.5c).
With the Arp2/3 complex this diminished stiffening is even further reduced (Fig. 4.5b) in the presence of seeds. Since Arp2/3 complex needs existing mother filaments to nucleate actin branches on its own, it can rapidly bind to existing seeds and thus start branching very early in the polymerization process. Therefore, with seeds Arp2/3 complex enhances the nucleation even more in the presence of seeds that seeds or Arp2/3 complex do on their own.
Hence, the lengths of filaments are even further reduced with seeds and Arp2/3 complex combined than with just of one of them. This decrease in length again does not show in the linear response of the frequency sweep, which is similar for Arp2/3 complex and both 5% and 25% seeds. But in the non-linear response with both Arp2/3 complex and seeds, the network is even softer with seeds. Here, the trend of a transition from stress-stiffening to stress-softening is visible due to the reduced length of filaments.
However, the difference in length that is due to both seeds and the Arp2/3 complex gives a good explanation for the different stress-strain responses, but does not explain why the peak during polymerization vanishes with seeds. Further details of our second hypothesis below will propose in a better explanation.

b) Influence of phalloidin on G′

If the nucleating ability of Arp2/3 complex is not the reason for the unexpected course of G′, it is most likely due to its branching ability. Therefore, our second hypothesis might explain the characteristic of G′ in detail.
During the first few minutes, a certain amount of branches that were formed by Arp2/3 complex might dissociate and thus lead to a reduced connectivity of the networks. Subsequent mechanical rearrangement through annealing of the dissociated branches can explain the drop in the storage modulus. Mechanical rearrangement of the branched network could primarily be caused by debranching of the daughter filaments. It was shown that the cyclic peptide phalloidin stabilizes branches of actin that were initiated by Arp2/3 complex [Mahaffy and Pollard, 2008]. Compared to an actin monomer, Arp2 has a similar binding site for phalloidin. Hence, the stabilization of branches by phalloidin resembles essentially the one of phalloidin between two actin monomers in F-actin. But for branches phalloidin links the Arp2 or Arp3

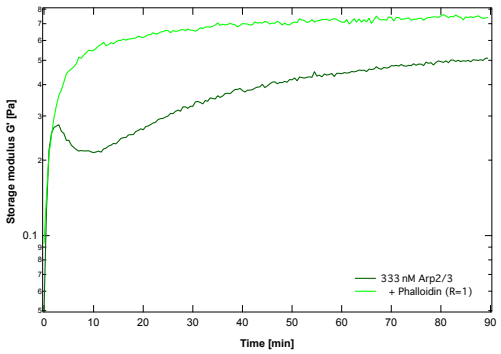

(a) Polymerization with Arp2/3 complex

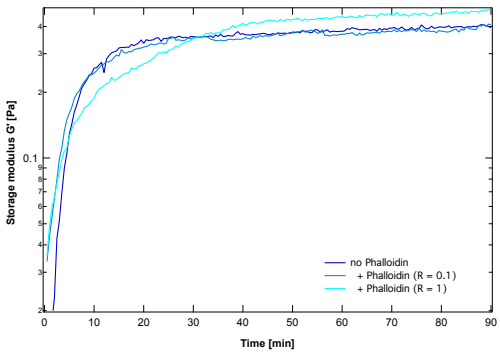

(b) Polymerization without Arp2/3 complex

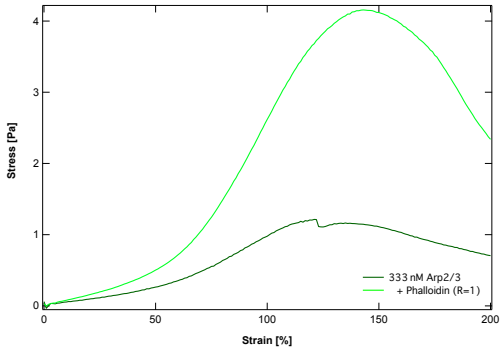

(c) Stress-strain response with Arp2/3 complex

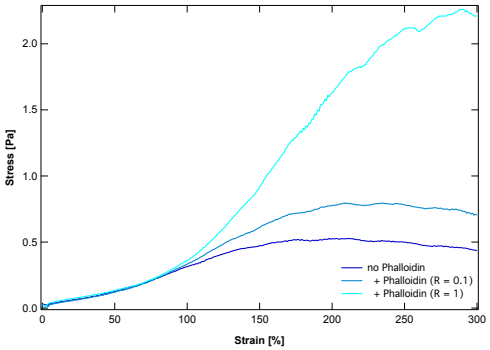

(d) Stress-strain response without Arp2/3 complex

Figure 4.6: Impact of phalloidin on polymerization and stress-strain response with (left, green) and without Arp2/3 complex (right, blue). (a) With phalloidin the local maximum vanishes during the polymerization process (dark green: R=0, light green: R=1). (b) Not much influence of phalloidin on pure actin networks during polymerization. (dark blue: R=0, medium blue: R=0.1, light blue: R=1) (c) Phalloidin increases stiffness and non-linear response of branched network. (d) Phalloidin has no impact on linear stress-response of purely entangled actin network, but on the non-linear response.

with the first actin monomer of the daughter filament.
Here, we present further evidence that strongly supports our hypothesis.

As discussed before, with 333 nM Arp2/3 complex and a three-fold excess rate of VCA a clear maximum between 2 and 3 min is visible for the storage modulus. It is then followed by a local minimum and the slow increase of G′. If now an identical sample is observed with additional phalloidin at equimolar ratio to actin (10 µM, R = 1), the non-linear behavior completely vanishes and G′ is monotonically rising. The final storage modulus with phalloidin is with 0.75 Pa a little higher that without (0.51 Pa). It has to be considered though that even after 90 min, the sample without

phalloidin has not reached its final G′ value, but is converging to it (Fig. 4.6a).
The stress-strain relations of the two samples also show very distinct behaviors. With phalloidin the sample is a lot stiffer and exhibits a much stronger strain-stiffening upon shearing than without phalloidin (Fig. 4.6c).

To exclude any effect that phalloidin might have on the storage modulus, its influence was also tested on actin without Arp2/3 complex. Here, the rheological data do not show a great influence of phalloidin. During polymerization G′ with 10% phalloidin is almost identical to the one of pure actin. At a equimolar ratio (R = 1), the polymerization curve of G′ differs a little, but not significantly (Fig. 4.6b). The linear behavior for R = 0.1 and R = 1 is equal to no phalloidin (R = 0). But the non-linear behavior indeed varies with phalloidin. More phalloidin results in a much stiffer non-linear response (Fig. 4.6d).

Discussion The peak with its following local minimum in rheological measurements cannot be detected in the pyrene assays. Here, the intensity curve is monotonically increasing without any dents (Fig. 4.1b). Fluorimeter assays and rheological assays measure different aspects of polymerization and the branching reactions. In pyrene assays, the only information that can be extracted is the total polymerization of the sample. Information about the network structure itself is not accessible.
Since no change in the polymerization degree can be observed, this already supports our assumption that the exceptional course of G′ in the rheology measurements has purely mechanical reasons. Either different processes happen on a different timescale or mechanical rearrangements lead to this behavior.

It has beed shown that the rigidity of actin filaments is increased about 2-fold by phalloidin [Pfaendtner et al., 2010]. Phalloidin increases the persistence length l_P of ADP-actin from 9-10 µm to 18 µm [Isambert et al., 1995]. Through control measurements, this increase in stiffness does not contribute to the higher final storage modulus that can be seen with phalloidin applied to an actin-Arp2/3 complex network (Fig. 4.6a,b). However, it indeed contributes to the pronounced strain-stiffening of the sample (Fig. 4.6c).

We propose that the decrease in G′ during the initial polymerization is due to vast debranching events in the network. Phalloidin inhibits this behavior and gives thus rise to a constantly increasing storage modulus.
It has been shown that phosphate release from the first subunits of the daughter

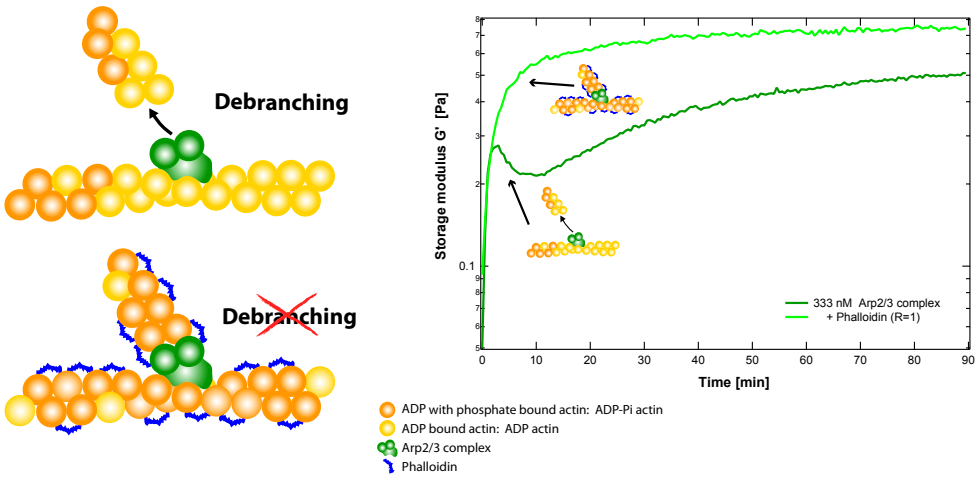

Figure 4.7: Phalloidin stabilizes branches. It couples neighboring actin monomers within a filament and inhibits the inorganic phosphate release of the subunits. Due to the similarity of Arp2 and Arp3 to actin, phalloidin most likely operates the same way here as well. Through binding to Arp2 and the adjacent subunit, phalloidin suppresses phosphate release and debranching of the daughter filament.

filaments favors dissociation of the daughter branch's pointed end from the Arp2/3 complex [Blanchoin et al., 2000b]. It is also know that phalloidin inhibits phosphate release from ADP-P_i-actin filaments [Dancker and Hess, 1990]. Phalloidin most likely stabilizes the interface between the Arp2 and Arp3 subunits to the respective adjacent actin monomers the same way, it stabilizes neighboring two actin monomers within a filament. Through binding to Arp2 and the adjacent subunit, phalloidin suppresses phosphate release and keeps the pointed end in the ADP-P_i-actin state. This state favors the stability of the connection between Arp2 and the branches (Fig. 4.7).
Since the local minimum cannot be detected with phalloidin in our rheological measurements, this is a first indication that the Arp2/3 complex's different affinity for ATP- and ADP-subunits is involved in the mechanism that accounts for the minimum. Ultimately, debranching is most likely the underlying reason for the course of G′ during polymerization.

It must also be mentioned that the nucleotide state of the mother filament and especially also of the Arp2/3 complex itself might also influence the stability of the branching point [Mahaffy and Pollard, 2006]. It was shown that the rate of branching from ADP-filaments as nearly the same as for newly polymerized filaments (ATP-filaments and ADP-P_i-filaments) [Blanchoin et al., 2000a], which suggests that

the nucleotide state of the mother filament displays only little importance for the branching initiation of Arp2/3 complex. However, this experiment does not reveal any relation between the nucleotide state of the mother filament and debranching events. Furthermore, the nucleotide state of Arp2 and Arp3 themselves might as well be of similar significance and crucial as the nucleotide state of the daughter filaments' first subunits.

Mahaffy and Pollard [2008] also reported that phalloidin increases the nucleation rate of actin alone and even more with Arp2/3 complex. They extracted their data from pyrene assays by calculation the amount of branched ends from the slope of the intensity. They argue that phalloidin might inhibit the dissociation of the spontaneously formed actin dimers and trimers and thus promote nucleation. Phalloidin also binds the Arp2 of the complex and by this means it is most likely that it stabilizes the interaction between Arp2 and the first actin subunit of the new daughter filament. In doing so, phalloidin helps stabilizing and activating the formation of new filaments, which results in faster nucleation.
This enhanced nucleation could not be verified in the rheological assays, we performed here. The rate of G′ increase is very much the same with and without phalloidin until it reaches the local maximum.

To conclude, the phosphate release is the key event that most likely triggers debranching. By adding phalloidin, we inhibit phosphate release, stabilize the branches and thus prevent debranching. This inhibition of debranching explains the constantly increasing storage modulus over time after the addition of phalloidin in contrast to the non-monotonous behavior of G′ without phalloidin.

4.1.3 Discussion

Here, we will now discuss the full course of G′ over time.

Increase of G′ due to fast polymerization In the beginning, fast polymerization can be observed. Arp2/3 complex serves as a nucleating factor as soon as enough mother filaments are present, where Arp2/3 complex can bind to and nucleate new daughter filaments. The more Arp2/3 complex is added to the system, the faster the nucleation is. This accelerated nucleation and polymerization leads to a rapid increase of G′ in the beginning (Fig. 4.8-1).

Decrease of G′ due to debranching In Section 4.1.1a, the unsteady slope of G′ during early polymerization was compared to the polymerization in pyrene assays and shown that the onset of the decrease in G′ coincides with the termination of polymerization. This is a strong indicator that mechanical rearrangements are the underlying reason for the behavior of G′. As it was already discussed in Section 4.1.2c, we arrive at the conclusion that debranching is the main reason that leads to the decrease in the course of G′. Debranching occurs most likely from the early beginning of polymerization and branching, but is being covered by the strong slope of G′. After polymerization terminates, ongoing debranching now dominates the course of G′ (Fig. 4.8-2).

It was reported several times that there is a discrepancy between the observation of the amount of barbed ends by microscopy compared to the detection and calculation of barbed ends in pyrene assays [Mahaffy and Pollard, 2008, 2006]. Microscopic assays detect only branches associated with their mother filaments. If branches dissociate very rapidly, the ex-daughter filaments will be observed as autonomous mother filaments. Hence, Mahaffy and Pollard arrived at the conclusion that many branches must dissociate from their mother filaments, before they can even be observed by microscopy. Their conclusion is in favor of our model.

The aging of ATP-actin within the actin filament to ADP-P_i- and ADP-actin might serve as a trigger for the debranching process. Mahaffy and Pollard [2006] have shown that ATP hydrolysis and γ-phosphate dissociation increase the rate of branch dissociation ∼10-fold as mother filaments age. Even though ATP hydrolysis occurs rapidly with a half time of 2 sec after actin monomer incorporation into filaments, the phosphate dissociation takes minutes. If we assume that the majority of Arp2/3 complex binds to mother filaments within seconds after sample preparation, half of the Arp2/3 complexes will dissociate from their aging mother filaments within 6 min and a large number already within the first minutes.

Increase of G′ due to annealing Now, the question rises, why G′ increases again and exceeds in all cases the local maximum, even though, polymerization is already completed as seen in the pyrene assays. One process that might explain this unexpected behavior is the annealing of short actin filaments into longer ones. We propose that the dissociated short daughter filaments diffuse and start to anneal over time. These longer filaments then entangle with other filaments and contribute to a rising G′ (Fig. 4.8-3).

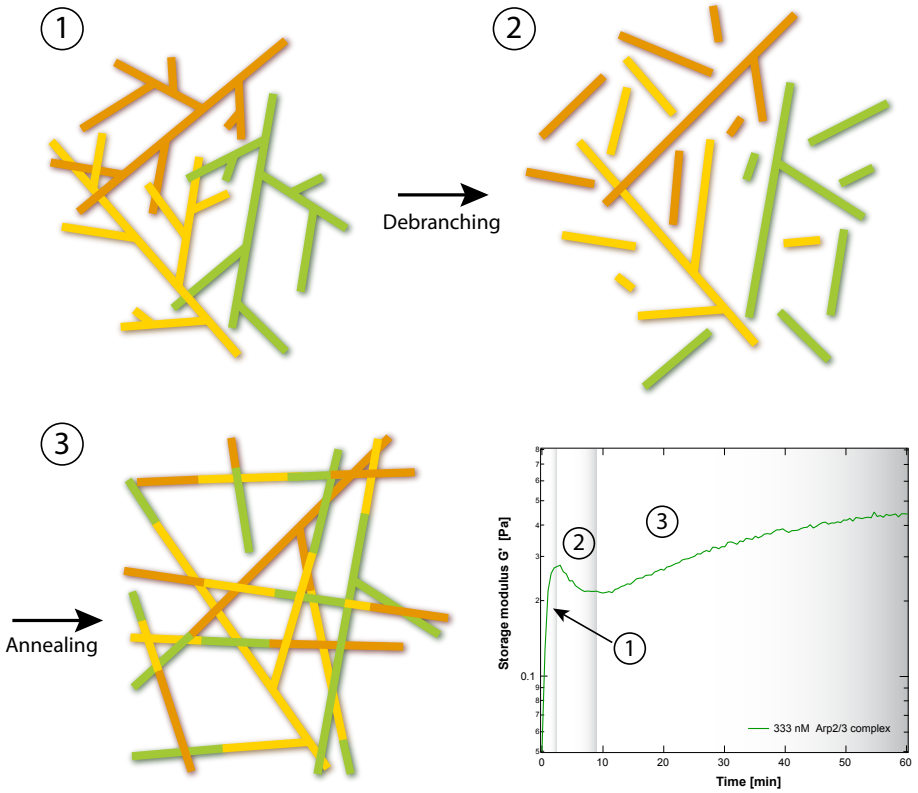

Figure 4.8: Bottom right: Storage modulus G′ plotted against time. In the beginning G′ increases due to polymerizing and branching of actin (1). After a short time, a majority of branches starts to dissociate (2), which results is a decrease of the storage modulus. Then the annealing of short dissociated branches into longer filaments (3) becomes predominant, which gives rise to another increase of G′.

For two filaments to anneal, a free barbed end and a free pointed end is required. Hence, this is only possible, if the daughter filament dissociates from the Arp2/3 complex. If Arp2/3 complex dissociates from the mother filament and remains at the daughter filament, it would cap the pointed end and annealing with another barbed end would not be feasible.

It is still a matter of debate, if the ATP hydrolysis and γ-phosphate release from either mother filaments, daughter filaments or Arp2/3 complex is responsible for the debranching process. Mahaffy and Pollard [2008] assume that phosphate dissociation of only one of the three mother filaments subunits which bind each Arp2/3 complex might be already sufficient to trigger debranching. From this assumption follows that the Arp2/3 complex remains with the pointed end of the daughter filament. Whereas other studies argue that debranching is due to the ATP hydrolysis and γ-phosphate release of the actin subunits in the daughter filament [Blanchoin et al.,

2000a]. In this case the daughter filament dissociates from the Arp2/3 complex and whether the Arp2/3 complex remains with the mother filament or not stays unclear [Blanchoin et al., 2000b].
For the annealing process it is inevitable that the Arp2/3 complex detaches from the daughter filament. Therefore, our model suggest the debranching occurs due to the dissociation of the daughter filament from the Arp2/3 complex as described by Blanchoin et al. [2000b]. However, it is also possible that the debranching process itself is triggered by the ATP hydrolysis and γ-phosphate release of actin in the mother filaments. This explanation is more likely, since the mother filaments had more time to age, release their γ-phosphate and trigger rapid debranching that the pointed ends of the daughter filaments. In this model Arp2/3 complex is still bound to the debranched daughter filaments and remains there. Only by liberation of pointed ends, annealing becomes possible and short dissociated branches can anneal to longer filaments.
The rapidity of debranching in our experiments suggest that branches detach with the Arp2/3 complex from the mother filament. Then, actin subunits of the pointed end release their phosphate and trigger Arp2/3 complex dissociation. Annealing is thus temporally delayed to the debranching process.

Furthermore, we showed that the final G' is about the same order for all Arp2/3 complex concentrations. This can be explained by the fact that after annealing the length distribution for all Arp2/3 complex concentrations are similar. It was already shown that the final distribution of filament lengths is nearly the same as that of an unfragmented sample after some hours [Andrianantoandro et al., 2001], which is in very good agreement to our model.
The non-linear response with Arp2/3 complex and seeds is much softer and instead of strain-stiffening they exhibit rather a strain-softening. Therefore, we conclude that even though filaments anneal, the entanglement and numbers of entanglement points will most likely not resemble the one of a pure actin network.

Our hypothesis of the rapidly debranching filaments and their subsequent annealing now also explains why the peak vanishes in the presence of seeds. As explained above the seeds lead to a simultaneous polymerization in the sample from the beginning (Section 4.1.2a). Arp2/3 complex can rapidly bind to seeds and give rise to daughter filaments. The polymerization also in the presence of Arp2/3 complex is without doubt faster completed with seeds than without. However, G' with seeds does not show a steeper rise in the polymerization (Fig. 4.5a), rather the contrary.

This can as well be explained with our hypothesis. We propose that with seeds the polymerization is completed very rapidly, but due to the low connectivity of the many highly branched clusters caused by the seeds, G′ is very low. Hence, the subsequent debranching of the very short daughter filaments is not visible in rheology as most of them are not strongly connected to the rest of the network. Then G′ slowly increases through annealing. Therefore, with seeds no peak is observable in the beginning and the rise of G′ has purely mechanical reasons.

We have shown that a lot of debranching occurs during the first few seconds to minutes, which is in good agreement with previous publications [Blanchoin et al., 2000b, Ichetovkin et al., 2002, Mahaffy and Pollard, 2008]. Furthermore, we suggest a model where subsequent annealing leads to a mechanical rearrangement that is vivid within branched actin networks *in vitro*. These insights have a huge impact on how we understand the assembly and disassembly of the highly branched network in the lamellipodium and requires further studies especially *in vivo*.

4.1.4 Outlook

Phalloidin stabilizes the branches directly, by binding both Arp2/3 complex and the first subunit of the daughter filament. But is also keeps the actin filaments in the ADP-P_i state. ATP hydrolysis plays a major part in the debranching and regulating mechanism of actin networks. Whether ATP hydrolysis and γ-phosphate release from mother filaments, daughter filaments or Arp2/3 complex is the reason for debranching is still controversial. Our findings affirm the mechanism of the debranching from the mother filaments during early stages with subsequent dissociation of the daughter filament from the Arp2/3 complex. An investigation of our assay with inhibition of hydrolysis and phosphate release otherwise would give further evidence.

ATP hydrolysis of Arp2 Contrasting models have been proposed for both the kinetics and the role of Arp2 hydrolysis in Arp2/3 complex-mediated actin-filament assembly [Kovar, 2006].
Whether the ATP hydrolysis of either one or both Arp subunits plays a significant role in nucleation or debranching is still highly controversial [Le Clainche et al., 2003, Martin et al., 2006]. The Arp2 subunit has been shown to hydrolyze ATP, but

the functional importance of this hydrolysis is not yet known. It has been proposed that the ATP hydrolysis is required for nucleation of the daughter filament [Dayel et al., 2001]. On the other hand is has also been proposed that Arp2 hydrolysis is associated with debranching [Le Clainche et al., 2003]. Though this controversial debate, it is verified that hydrolysis of the Arp2/3 complex has a great impact in regulating the branched network [Kovar, 2006].

One issue that might arise when attempts are made to inhibit the ATP hydrolysis of Arp2 with the help of the non-hydrolyzable ATP analogue AMP-PNP is the following: Arp2/3 complex loaded with AMP-PNP cannot nucleate actin-filament assembly [Dayel et al., 2001], and is as such not feasible for experiments aiming at the involvement of ATP hydrolysis of Arp2 in the debranching mechanism.

ATP hydrolysis of actin subunits It is also still a matter of debate if ATP hydrolysis of actin subunits in the mother filaments or the pointed end subunits in the daughter filament are triggering dissociation of branches in the actin-Arp2/3 complex network. Published results concerning this matter are inconsistent.

Actin filaments contain their own internal "timer", since their subunits hydrolyze bound ATP within seconds followed by the release of the γ-phosphate within minutes. This timing can influence the disassembly and rearrangement of the branched actin network. While some studies focus only on the ATP hydrolysis of Arp3 and Arp3 as a trigger for debranching [Le Clainche et al., 2003, Dayel et al., 2001], others focus mainly on the hydrolysis of the pointed end of the daughter filaments [Blanchoin et al., 2000a,b].

a) Influence of additional phosphate on polymerization

It was shown previously that ADP-actin filaments can be converted back into ADP-P_i filaments in the presence of high concentrations of inorganic phosphate [Rickard and Sheterline, 1986, Carlier and Pantaloni, 1988]. Furthermore, P_i has a lower tendency to dissociate from ADP-P_i-actin filaments, if there is an phosphate excess in solution.
The dissociation equilibrium constant for P_i from polymerized ADP-P_i subunits is in the low millimolar range, so some ADP-actin subunits may retain the γ-phosphate [Pollard et al., 2000].

First attempts were made, to investigate branched actin networks rheologically with the addition of inorganic phosphate. To verify this approach and that phosphate has no impact on actin polymerization, 25 mM phosphate was added to pure actin and the polymerization was monitored. The phosphate had almost no influence at all on the sample's polymerization. The final value of G′ was completely identical to the untreated sample. With phosphate, the nucleation was a little bit delayed, but the following rise in the storage modulus was again identical. Therefore, we conclude that phosphate does not have a significant effect on the simple actin polymerization. Experiments with Arp2/3 complex and inorganic phosphate excess were so far not successful. Polymerization curves as well as the non-linear responses give ambiguous information. One reason for that might be that inorganic phosphate is also a buffer substance and that slight changes in the pH leads to a malfunction of Arp2/3 complex or its activator VCA.

b) Influence of AMP-PNP actin on debranching

An similar effect, but more straight forward would be the use of the non-hydrolyzable ATP analogue AMP-PNP (adenylyl-imidodiphosphate). AMP-PNP-actin is be similar to ATP-actin and thus, debranching should also be inhibited or at least drastically reduced with AMP-PNP-actin.
Since a Arp2/3 complex bound to ADP or AMP-PNP cannot nucleate actin filaments [Dayel et al., 2001], it is crucial that only the actin monomers are in the AMP-PNP state and not Arp2/3 complex.

First attempts were already made, but the AMP-PNP state of actin did not polymerize any other to ADP-actin. AMP-PNP actin is made subsequently out of ADP-actin. So, we conclude that the ADP to AMP-PNP exchange was not successful.

4.1.5 Impacts on viscoelastic properties of branched networks

a) Aging effects of actin

This rheological effect of a local recess during the polymerization process is even more pronounced, if the G-actin is a more than two weeks old. If this is the case,

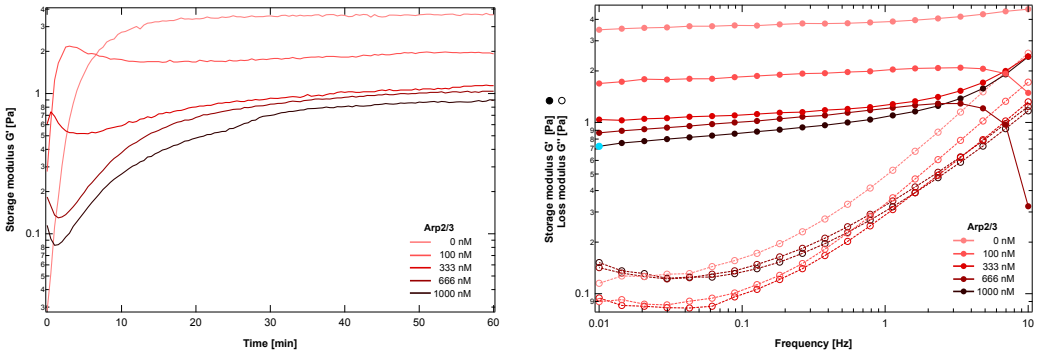

(a) Polymerization (b) Frequency dependence

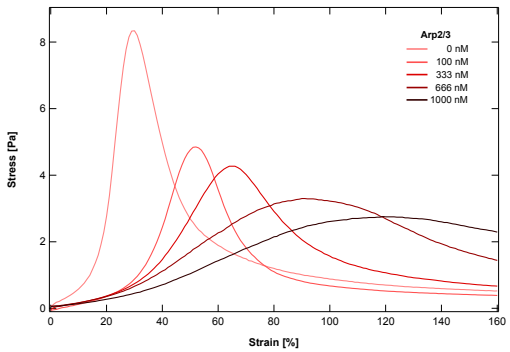

(c) Stress-strain relation

Figure 4.9: (a) Polymerization, (b) frequency dependence of the storage and loss modulus, and (c) non-linear response of branched actin networks assembled with aged actin monomers. G′ is almost independent of the frequency, while the non-linear response exhibits a very stiff networks with stresses up to 8 Pa.

the local minima in the beginning is deeper and the gradient is strong for the appropriate Arp2/3 complex concentration (Fig. 4.9a, compare Fig. 4.3a). If now the frequency dependence of these samples are closely examined, it can be seen that the storage modulus G′ is nearly independent of the frequency (Fig. 4.9b).

This pronounced plateau in the storage modulus G′ is rather characteristic for cross-linked networks and was not detected for branched and unbranched actin networks assembled from actin monomers that were less than a week old after purification (Fig. 4.2a).

This frequency independence of G′ is an indicator that now attractive forces exist between the actin filaments and the network is not purely entangled anymore [Mezger, 2006]. Very probable with aged actin the friction forces are greatly increased to an extent where the steadiness of the bonds act almost like cross-linking bonds (Section 2.2.4c).

The non-linear response is extraordinarily stiff compared to branched actin networks polymerized from new actin monomers (Fig. 4.9c). This is another indicator that some attractive effects of aged actin come into play. Therefore, it is very important to only work with freshly purified actin which is regularly tested on aging effects.

b) Purity of Arp2/3 complex

The purification protocol for the Arp2/3 complex was later fundamentally changed and based on another protocol (2.1.3c, improved protocol). With this adapted purification both the purity and the activity of the Arp2/3 complex is much higher. In the pyrene assay, the same amount of Arp2/3 complex, here 30 nM, activated by 100 nM VCA, gave rise to a 2-fold accelerated actin polymerization compared to Arp2/3 complex purified after the old protocol. The whole network is already entirely polymerized after about 3 min. Arp2/3 complex purified after the old protocol takes ca. 6 min to do the same (Fig. 4.10a).
When the Arp2/3 complex, purified by the new protocol, is used in the rheological measurements, the local minimum is much more pronounced while employed the same concentrations as above, such as 100 nM, 333 nM and 666 nM, respectively (Fig. 4.10b). This is especially the case for the addition of 666 nM Arp2/3 complex. Here, G′ drops almost one magnitude of order.
At the same time, the peak is shifted to earlier times for all Arp2/3 complex concentrations. It is shifted so much that it could not be measured in the rheometer. It has to be noted that from start of polymerization which is when actin is added to the solution until the first measurement can take place, it takes several tens of seconds. First of all to mix and pipette the sample on the rheometer plate take roughly 10 sec and then the rheometer delays the start of the measurement by about 30 sec due to mechanical and software reasons. Thus, the real polymerization time actually has an offset of about 40 sec. This is usually neglected, since polymerization without Arp2/3 complex occurs on a much slower time scale. But here, this should be taken into account. Furthermore, one data point takes on top 30 sec to be acquired. Thus, at the first data point of 30 sec the sample is actually more that 1 min old.
In addition, the local minimum is now later instead of earlier. For a concentration of the Arp2/3 complex of 100 nM the minimum appears around 1 min, for 333 nM around 2 min and for 666 nM it is at 3.5 min. This is opposite to the experiments described in Section 4.1.1. Here, the time of the peaks were determined (Fig. 4.3b),

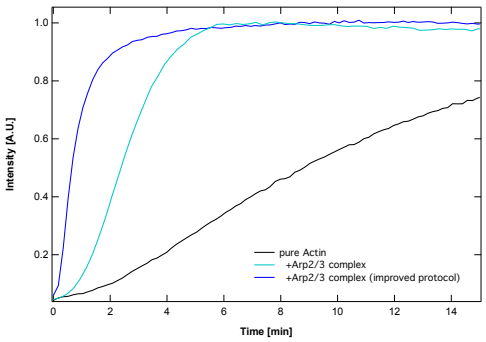

(a) Polymerization curves measured by pyrene assay with Arp2/3 complex

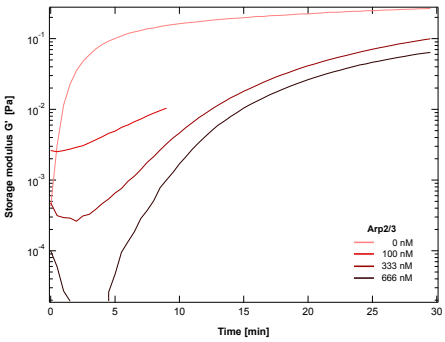

(b) Polymerization curves measured rheologically with Arp2/3 complex purified by an improved protocol

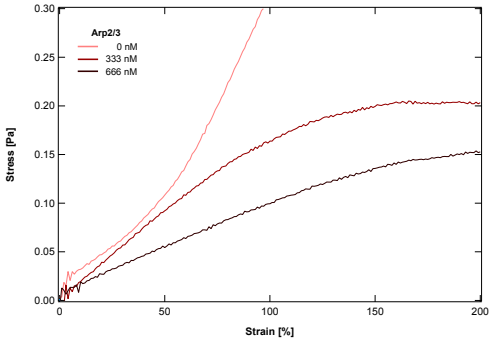

(c) Stress-strain relations with Arp2/3 complex purified by an improved protocol

Figure 4.10: (a) Pyrene assay with 3 µM actin, 30 nM Arp2/3 complex, 100 nM VCA. (Experiments performed by Katharina Henneberg). (b) With Arp2/3 complex that is more active local minimum is more pronounced. For 666 nM Arp2/3 complex the sensitivity of the rheometer is not sufficient to detect values of G′ below 20 µPa. (c) Networks with purer Arp2/3 complex do not exhibit any strain-stiffening anymore.

but the same trend to earlier times with more Arp2/3 complex hold also true for the local minima (Fig. 4.3a).

For the new purification of Arp2/3 complex, strain-stiffening is not anymore observable at any concentration (Fig. 4.10c), whereas for the purification after the old protocol, for both 100 nM and 333 nM Arp2/3 complex the branched networks exhibit a clear stiffening is observable (Fig. 4.2b). This is another indication that the improved purification protocol leads to much more active and as shown in Chapter 2 (Fig. 2.4) much purer Arp2/3 complex.

4.2 Rheological investigation of branched and bundled actin networks

During cellular migration, actin assembly takes place at the leading edge, while disassembly occurs in the cell interior. Filopodia with thick actin bundles emerge from the highly branched network in the lamellipodia. To gain further understanding of the structural transition of lamellipodia to filopodia and of the self-assembly of the network there, we performed macrorheological experiments with proteins that are mainly involved in the assembly of lamellipodia and filopodia: the Arp2/3 complex with its activator VCA and the bundling protein fascin.

4.2.1 Temporal development of G′

Note: Curves and microscopy pictures in this chapter are color coded for easier comparison. Red: 0 µM fascin. Yellow: 0.5 µM fascin. Green: 1 µM fascin. Blue: 3 µM fascin.

While the activated Arp2/3 complex induces a decrease in the storage modulus after a few minutes of polymerization followed by a slow, but steady increase for pure actin networks, the addition of fascin to this branched network changes the behavior of G′ again fundamentally.
With Arp2/3 complex and fascin G′ rapidly rises to a value depending on the concentration of fascin. This is about 80 Pa for 3 µM fascin, 40 Pa for 1 µM and 8 Pa for 0.5 µM. After this, instead of being followed by an increase as observed for non cross-linked branched, the storage modulus decreases monotonously (Fig. 4.11a). This clear peak could be observed more or less pronounced for any positive concentrations of Arp2/3 complex and fascin together. In Fig. 4.11a unbundled branched actin networks show here only a small minimum, but these are the same data as in Fig. 4.1a. The logarithmic scaling of G′ diminishes the clarity of the course though. If more Arp2/3 complex is added to the assay at the same fascin concentration, the final storage modulus is reduced, but also the peak is shifted to earlier times (Fig. 4.11b).
The cross-linked branched networks exhibit a quite regular frequency dependence. G′ as well as G′’ increase with the addition of fascin, but the loss modulus loses

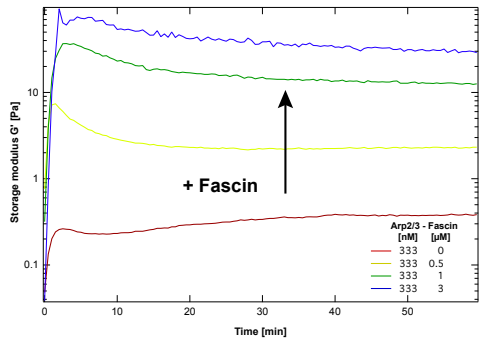

(a) Polymerization with Arp2/3 complex and fascin concentration gradient

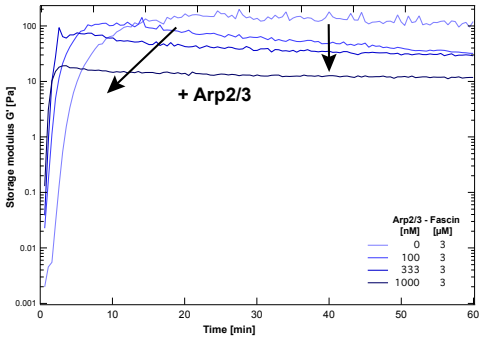

(b) Polymerization with Arp2/3 complex concentration gradient

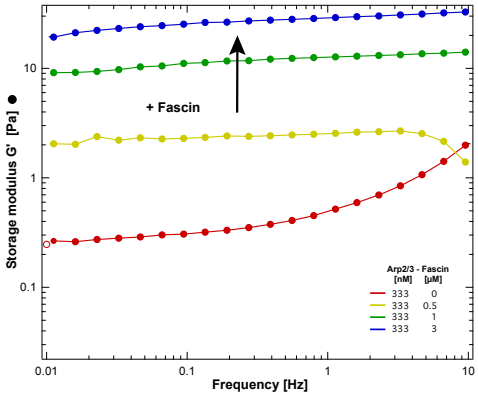

(c) Frequency dependence of G′

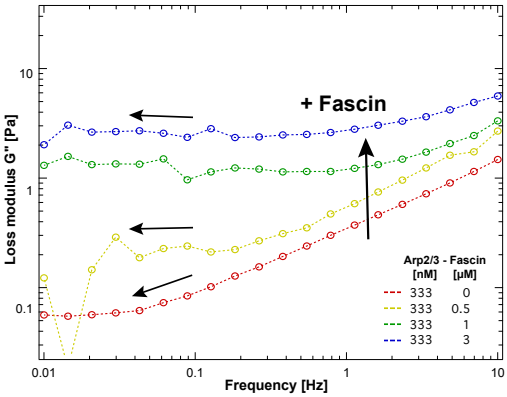

(d) Frequency dependence of G″

Figure 4.11: (a) Polymerization of branched actin networks with the addition of fascin. (b) With more Arp2/3 complex the final value of G′ decreases and the peak is shifted to earlier times. (c, d) Frequency dependence of the storage and loss modulus. With fascin both G′ and G″ increase and lose their dependency with more fascin, which even more pronounced for the loss modulus.

its dependence with more fascin and becomes quite flat. Both is an indication that the rheology of the network is rather dominated by the bundled regime than the branched regime.

4.2.2 Microscopical investigation of branched bundled networks

Cross-linked actin bundles can be easily examined with fluorescence microscopy. Compared to actin filaments, actin bundles have a higher intensity and a better signal-to-noise ratio. That makes actin-fascin networks good candidates to also

visualize them and further investigate, how bundled branched networks differ from purely branched networks and purely bundled networks.

a) Covalently labeled actin and labeled phalloidin

Covalently labeled actin To visualize the networks, a direct approach is of course the use of covalently labeled actin. Covalently labeled actin does not interfere much with the kinetics of polymerization and depolymerization. Furthermore, it was shown that phalloidin has also a large impact on the stability of branches formed by Arp2/3 complex [Mahaffy and Pollard, 2008], This property was already discussed in detail in Section 4.1.2b.
Therefore, covalently labeled actin would be the natural choice for visualizing branched networks. However, with labeled actin we encounters even more artifacts, so that phalloidin at a very low ratio was chosen for labeling.

To test covalently labeled actin, 20% actin was labeled for imaging. Protein concentrations matched the ones of the rheological experiments (10 µM actin, 333 nM Arp2/3 complex, 3 µM fascin). As shown in Fig. 4.12, differently labeled dyes have a different impact on the network. Actin labeled with Atto-647N leads to a much denser network compared to actin that is labeled with Atto-532. All other experimental conditions were kept constant.
If the differences in dyes affect the resulting networks on such a large scale, the question arises, which of those two dye pictures the network truthfully and has less unwanted side effects. None of those two dyes show any abnormality in rheology, when tested with pure actin.

Labeling with phalloidin Phalloidin has a great impact on the stability of actin filaments branches, which was especially shown at a equimolar concentration (Section 4.1.2b). To test whether labeling with phalloidin changes the rheological behavior of our system even at a smaller ratio, experiments were carried out with and without the incorporation of phalloidin.

The ratios at which the effect of phalloidin was examined were at 1%, 10% and 100% (R = 0.01, 0.1 and 1). Here, unlabeled phalloidin is used, since R = 1 is not possible with labeled phalloidin for our concentrations. If only little phalloidin is mixed with the sample, almost no difference could be detected in both the polymerization

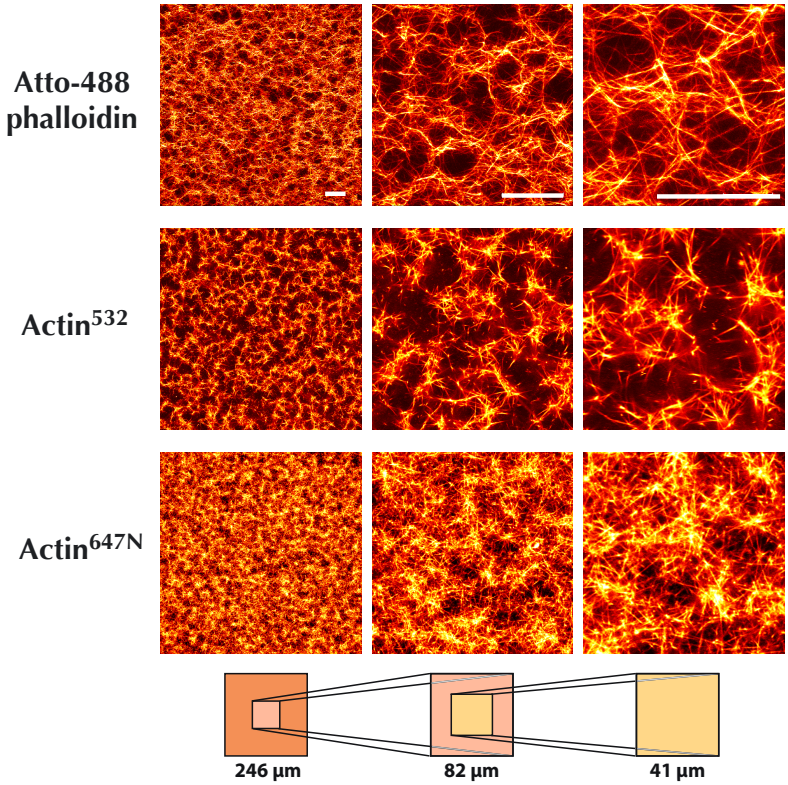

Figure 4.12: Branched bundled actin networks labeled with different dyes at increasing zoom levels. Up: actin labeled with 1% phalloidin AlexaFlour-488. Middle: 20% actin labeled covalently with Atto-532. Down: 20% actin labeled covalently with Atto-647N. 333 nM Arp2/3 complex, 3 µM fascin. Scale bar 25 µm.

process and the frequency dependence of G′. The data is nearly identical to actin without any phalloidin at all. Whereas at an equimolar ratio of phalloidin, the steep decay of G′ is prevented.

Therefore, we conclude that phalloidin at a low ratio (R = 0.01) does not affect largely the rheological behavior of the samples with fascin and contributes most likely to less artifacts than covalently labeled actin. Thus, low concentrated phalloidin-488 is suitable to visualize the sample.

b) Visualization of bundled branched networks

Imaging of bundled networks by the means of confocal microscopy is a straight forward approach to learn more about the structure of networks. Especially interesting is the imaging of the time course of polymerization: What happens structurally

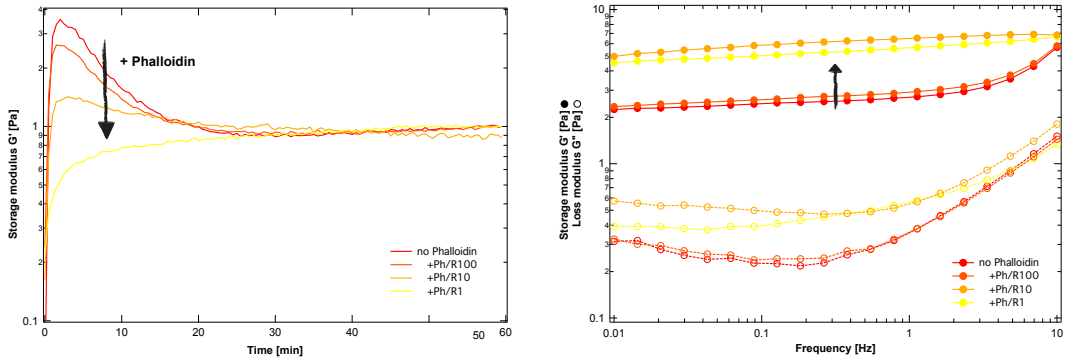

(a) Polymerization (b) Frequency Sweep

Figure 4.13: Rheological measurement of polymerization and the frequency dependence with different amounts of unlabeled phalloidin. Rheology curves of polymerization are normalized to their final value for a better visual comparison of phalloidin's impact on the storage modulus.

during the first 10 min to the network that results in this large decrease of G′?

Dependency of Arp2/3 complex concentration First of all, we examined how different amounts of Arp2/3 complex affect the structure of the network. In Section 4.2.1, it was already mentioned that the final G′ value decreases with increasing Arp2/3 complex concentration, besides exhibiting an earlier peak after that G′ drops (Fig. 4.11b).

Here, we imaged samples of 10 µM actin and 3 µM fascin. Arp2/3 complex is added at 100 nM, 333 nM, 666 nM, and 1000 nM while VCA is available in each case in a 3-fold excess.

Without Arp2/3 complex the network consists of long straight bundles that are relatively homogeneously distributed. The addition of Arp2/3 complex results in shorter bundles, since more nucleation sites allow rapid polymerization. The more Arp2/3 complex is added to the sample, the more disrupted the network seems. At high concentrations the network rather consists of individual clusters rather than an intermeshing network. Images at higher zoom levels however, reveal that these clusters are indeed still connected to their neighbors (Fig. 4.14). Clusters appear starlike, with a high density of actin bundles at the center of the clusters and short outwards facing bundles.

100 nM of Arp2/3 complex does not have a big impact on the structure of the network with 3 µM fascin. Bundles still appear rather long and straight. Transition

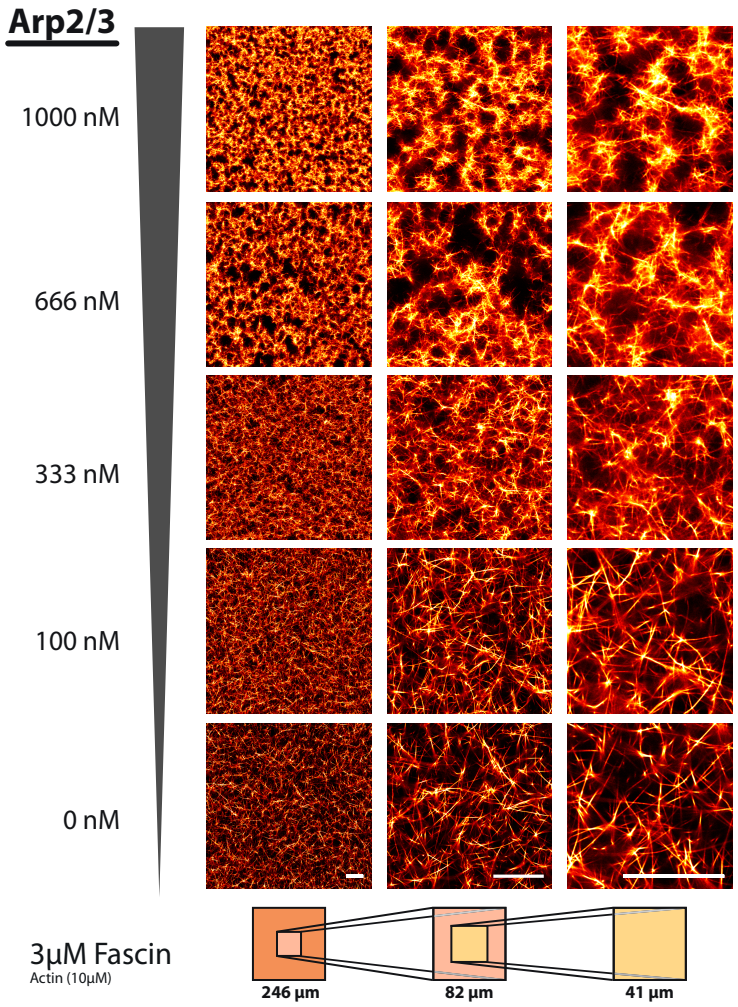

Figure 4.14: Confocal images of branched bundled networks at increasing zoom levels. The more Arp2/3 complex is added to the sample, the more disrupted and clustered the network appears. Protein concentrations: 10 µM actin, 3 µM fascin. Scale bar 25 µm.

into starlike cluster starts at 333 nM. Here, straight bundles are starting to disappear and shorter bundles emerge that are well connected. Magnified views indicate that bundle thickness is also reduced. Number of connections between bundles seem to be enhanced.

The character of networks fundamentally change above a concentration of 333 nM Arp2/3 complex. With 666 nM and 1000 nM, distinct clusters emerge. In their center a high density of actin bundles emerge and short bundles are facing starlike into the surroundings. Bundle thickness is further reduced. Bundle lengths rarely exceed the size of a cluster. Connections are only made between exterior bundles (Fig. 4.14).

Dependency on fascin concentration How does the concentration of fascin now impact the bundled branched networks?

To get a complete picture of the interplay of the two actin binding proteins, the impact of Arp2/3 complex without fascin is also investigated. In Section 4.1, we described in detail the rheological properties of purely branched actin networks. Here, we now also visualize those networks.
Pure actin networks are a dense meshwork of actin filaments. Single filaments are adumbrate but cannot really be distinguished. Actin networks appear highly marbled and on a large scale to some extent homogeneous, with some filaments sticking out from the background. Here again, the addition of 100 nM Arp2/3 complex does not have a big impact on the structure. Branches cannot be differentiated from actin filament crossings. Little islets with higher filament concentration form for 333 nM. Single filaments are not slightly visible any more and filament lengths are decreasing as well. For higher concentrations of Arp2/3 complex, the branched actin network again fundamentally changes its structure. Large clusters of short actin filaments form and the networks appears not as network anymore, but rather as a conglomerate of filament fragments (Fig. 4.15).

The differences between the fascin concentrations are not as intense as expected. For 0.5 µM, 1 µM and 3 µM 100 nM Arp2/3 complex does not show any significant impact. Precursors of clusters start to appear with 333 nM Arp2/3 complex. With more Arp2/3 complex clusters develop even further and with 1000 nM they appear starlike. For 3 µM fascin both the onset of the clusters and also their formation occurs at a lower Arp2/3 complex concentration. The onset is already much more pronounced at 333 nM and clusters are very starlike at 666 nM Arp2/3 complex.

Super-resolution imaging To get a better understanding of how the asteroidal clusters are assembled in the network and how they vary between the different concentrations of Arp2/3 complex and fascin, super-resolution microscopy is applied to our samples.
Only specific dyes work with the STED (Stimulated Emission Depletion) set-up, so here, covalently labeled actin (Atto-647N) must be used. Actin networks were imaged at a STED set-up build in our lab. A direct comparison of a standard confocal image to a STED image reveals that the STED image has unsurprisingly a better resolution. Actin bundles appear thinner and the clusters are better defined. However, the structure of the cluster is not much better resolved, since there are too

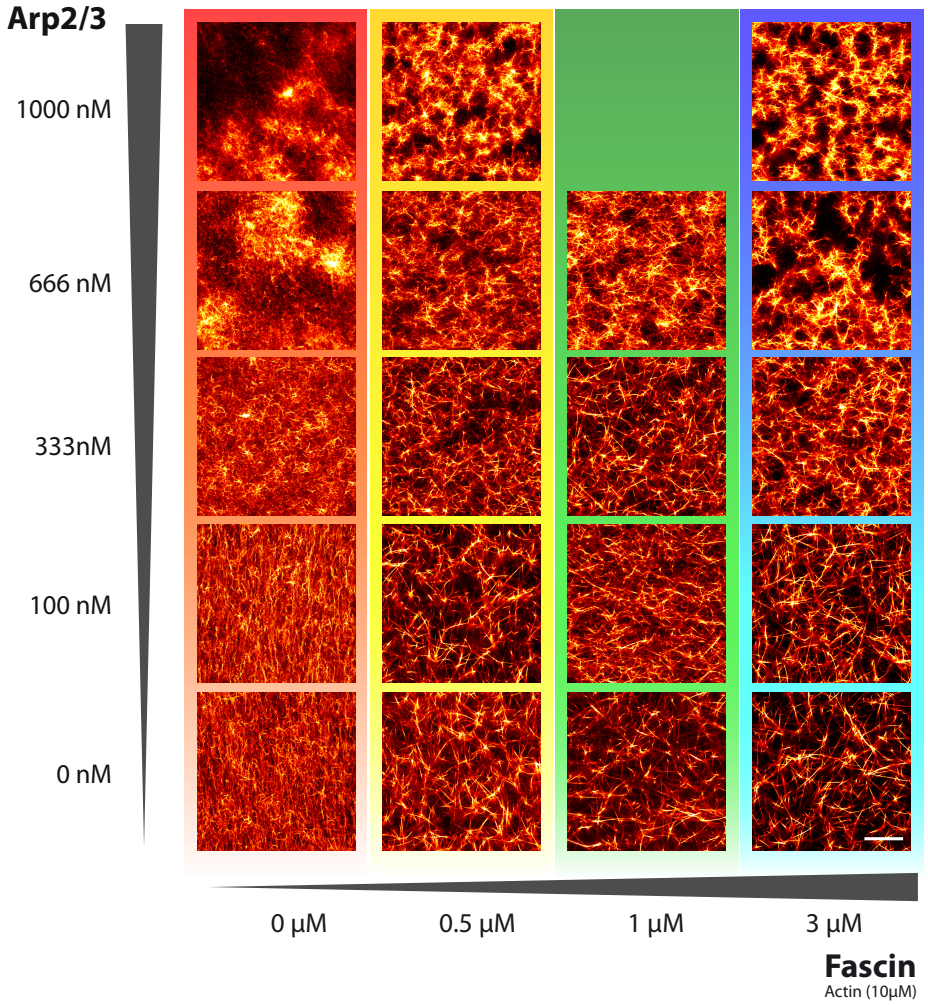

Figure 4.15: Phase space of branched bundled networks. Actin networks are imaged as a function of the Arp2/3 complex concentration and the fascin concentration. To get a better impression of the 3D networks, here a projection of a 15 µm thick z-stack is depicted. Red: 0 µM fascin. Yellow: 0.5 µM fascin. Green: 1 µM fascin. Blue: 3 µM fascin. Scale bar 20 µm.

many bundles, which makes it hard to detect the structure.
For qualitative data of the interior of the clusters STED imaging does not bring any further information than confocal imaging. Furthermore, due to the long recording process and sample bleaching is not practicable for the screening of samples.

Time course of bundled branched network To investigate, what is happening with G′ after the peak, we imaged the sample from the very beginning of polymerization.

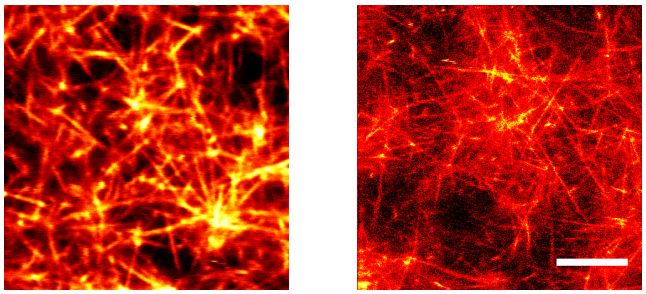

(a) Confocal image (b) STED image

Figure 4.16: Direct comparison of the same sample imaged with a confocal microscope (a) and with a STED set-up (b). 333 nM Arp2/3 complex, 3 µMfascin. Scale bar 5 µm.

To assure fast imaging, it is necessary to acquire the pictures at a high repetition rate. This high repetition results in a short exposure time. Combined with a very low phalloidin concentration (R = 0.01) that has only minor impact on the development of the network, the quality of the images are poor. The low intensity and a short exposure time result in a very high signal-to-noise ratio. Here, the main structure of the network is visible but the weak connection between the clusters can not be resolved (Fig. 4.17). However, these connections are the main reason for G′ and most likely also for its drop.

Hence, confocal imaging will not enlighten the structural change the network undergoes within the first few minutes during polymerization. To resolve both the interior structure of the clusters and the structure of the network at different points in time, it will be more revealing to generate images by the means of transmission electron microscopy (TEM), or any other microscopy technique that does not require fluorescence dyes that can cause labeling artifacts.

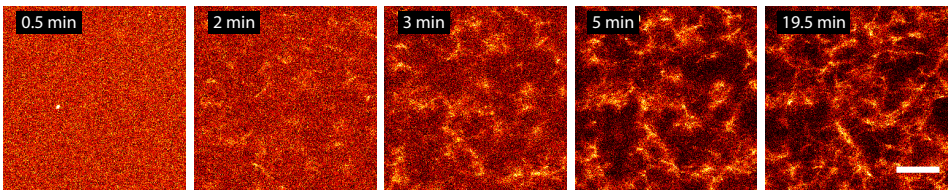

Figure 4.17: Time resolved images of the polymerization of branched bundles networks. Protein concentrations: 10 µM actin, 333 nM Arp2/3 complex, 3-fold excess VCA, 0.5 µM fascin, 0.1 µM Atto-488 phalloidin (R = 0.01). Scale bar 20 µM.

4.2.3 Discussion

Branched bundled network Here, it was shown that the interplay of the branching protein Arp2/3 complex and the bundling protein fascin results in starlike clusters. In the absence of fascin the structure of the actin network is dominated by Arp2/3 complex nucleation and branching activity. At low Arp2/3 complex concentration the network does not differ much to a pure actin network. With more Arp2/3 complex present the system organizes into diffuse clouds of actin at high density. If fascin is also added to the system with both fascin and Arp2/3 complex at high concentrations, the system self-assembles into a dense network of stars.

It was recently shown and modeled by Kinetic Monte Carlo simulation, how these starlike structures develop [Ideses et al., 2008, Brill Karniely and Ideses, 2009, Haviv et al., 2006]. According to this study, in the early stages of actin polymerization fascin is passive while Arp2/3 complex mediates the formation of dense and highly branched starlike networks of actin. If the filaments in the periphery of the asters grew long enough, fascin becomes active and cross-links the filaments into bundles which then emanate radially from the aster's surface. This leads to the starlike structures.

In their study [Ideses et al., 2008], they use similar protein concentrations of actin (7 µM), Arp2/3 complex, VCA and fascin, yet they only observe single very distant asters, regardless of the Arp2/3 complex concentration. The fully developed stars upon addition of fascin are also far apart. They only studied in the formation of single asters or stars, but neither the distribution of the material in bulk nor the connectivity of the stars.

Our result differ very much to their findings, except that with much fascin we also enter a starlike structural regime. However, we observed in all cases a dense network of either diffuse clouds or interconnected stars. This reproduces much better the transition from the lamellipodia to filopodia, since in the lamellipodia a highly branched network exists instead of just single cores, from where the filopodia emerge.

Furthermore, Haviv et al. [2006] do not include debranching in their simulations, because they argue debranching is relatively slow. Even though they show that their aster and stars develop over the time of several minutes. In addition information lacks about the activity of their Arp2/3 complex with VCA with pyrene assays. We have shown in our experiments (Section 4.1) that the first wave of debranching occurs shortly after polymerization initialization. This will strongly change the

simulations and lead to a better understanding of the transition from lamellipodia to filopodia.

Rheology with fascin and Arp2/3 complex Neither STED imaging nor time resolved confocal imaging could bring any further information to the clarification why G′ suddenly drops during the early polymerization. The addition of phalloidin however gives a some indication. Along with the discussion about the initial polymerization of purely branched networks (Section 4.1.3), we propose the following explanation for the decrease of the storage modulus after few minutes of polymerization.

Here, the polymerization is twofold enhanced. First due to the addition of Arp2/3 complex, but also due to the cross-linker fascin. Then, debranching is happening exactly as without fascin. During the first seconds to minutes newly formed branches are dissociating from their mother filaments. Both with and without fascin, the storage modulus decreases, but without fascin G′ does increase again. We concluded that this increase is due to the annealing of short filaments into longer ones (Section 4.1.3). However, with fascin this annealing is not possible anymore. The daughter filaments are bundled by fascin near their barbed end, if they are long enough that the binding energy gained due to actin-fascin-fascin links between filaments exceed the unfavorable bending energy required to bring those filaments into contact [Haviv et al., 2006]. So, if daughter filaments from the same or different mother filaments are cross-linked into one thick bundle and one of them detaches from its mother filaments the structure cannot rearrange on a large scale, since it is stabilized by its cross-links. For the annealing process without fascin, those short dissociated filaments diffuse around until they make contact to another filament with a matching pointed or barbed end. This is not possible for bundled dissociated filaments and that is why the storage modulus can only decrease monotonically.
A strong support for this proposal comes from the experiments with phalloidin. Phalloidin inhibits the debranching of the daughter filaments. As with experiments on purely branched networks, G′ does not decrease with phalloidin as well. G′ increases monotonically without any peak and drop of its value (Fig. 4.13a). Very likely without the stabilizing effect of phalloidin G′ loses a lot of connections over time which gave rise to its high value. By losing them without building new ones G′ can just degrade. So, here with fascin we propose that there is no mechanical rearrangement as in a purely branched network, only dissipation of connections

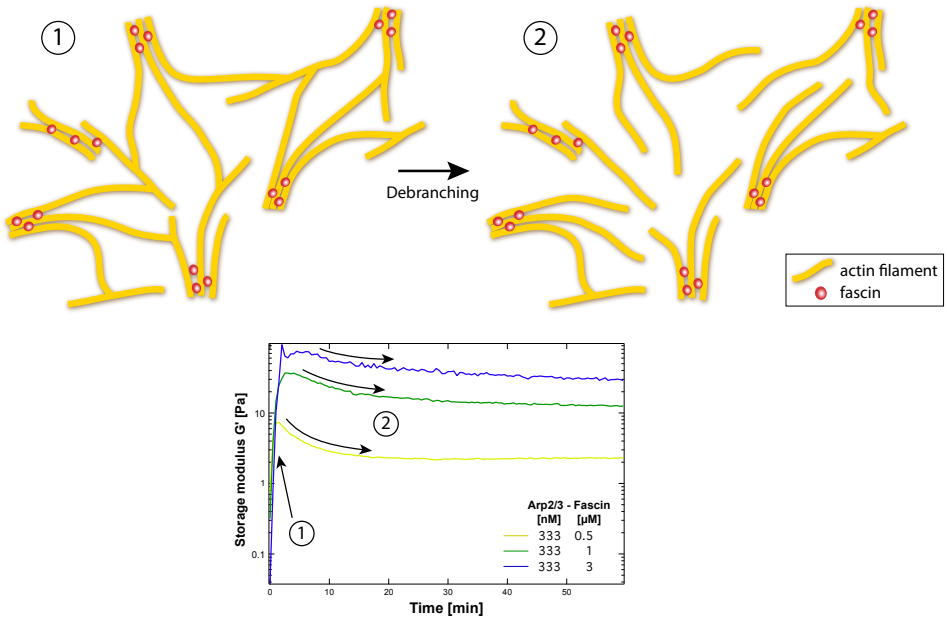

Figure 4.18: Bottom: Storage modulus G′ plotted against time with different concentrations of Arp2/3 complex. In the beginning G′ increases due to polymerizing, branching and cross-linking of actin (1). After a short time, a majority of branches starts to dissociate (2), which results again is a decrease of the storage modulus similar to pure branched actin networks (Section 4.1). Unlike in those networks, here branches dissociate from their mother filament, but cannot diffuse and anneal due to their filament ends that are cross-linked in bundles. Connections are lost and thereby networks becomes softer, which results in a continuously decreasing G′ until no more debranching occurs and G′ reaches steady state.

between mother and daughter filaments.

These new findings contribute to a better understanding of individual effects of the proteins involved in filopodia mechanics. They provide new perspectives on how filopodia are initiated and how forces are generated.

4.3 Protein interplay reacts very sensitive

The interplay of the different proteins is very sensitive. Rheological measurements, but also microscopic recordings differ sometimes a little to a lot within several measurements throughout time with different batches of proteins. This makes it very hard to get always consistent data in every experiment. We have seen that also different purification protocols give rise to different activity of the Arp2/3 complex.

Moreover, even Blanchoin et al. [2000b] mentioned that the fractions of branched filaments at each point in time varied a lot between experiments, because of experimental factor that they cannot fully control.
Another reason for the variations in out experiments might be the aging of one of the proteins involved. That can already happen during one to few days. Except actin, proteins were never used for longer than five days, usually less. A further change in can be observed, if a new purification batch of one of the proteins is used. This is not to say that, the quality of our proteins is below average. In other experiments, none of these changes occur. It rather indicates that the dissociation process and thus the interplay of the involved proteins is highly sensitive to any kind of small changes. Due to the amounts of proteins needed for rheology, it is not possible to conduct all required experiments and controls within the same batches.

4.4 Outlook

Our results and their interpretation fits very well to the findings of other published results. However, to quantify the rheological data, we need to develop a model with rates that describes and reproduces our data. Since not all rates of the dynamic interplay of these proteins are known, further experiments need to be conducted.

For that, the developmental phase of the starlike cluster should be visualized to get a more detailed knowledge about the rates of debranching and annealing.
To get a detailed picture about the length distribution of the branches and their mother filaments, further experiments must be performed. This can be achieved for example by terminating the polymerization of the sample by dilution and fixation with phalloidin at different points in time. By imaging the stabilized and labeled filaments further information about the lengths distributions at specific polymerization times can be acquired. With this method results can be easily achieved but it has to be verified that the sample will not be damaged due to the shear flow in the pipette tip and thus impair the results.
Furthermore, to reveal the internal structure of the starlike clusters with fascin and the asters without fascin a better method is provided by transmission electron microscopy (TEM). Here a much higher resolution of single filaments is possible even in dense clusters.
With this new information about the rates our model can then be quantified and

the dynamics can be simulated.

In addition to that, different Arp2/3 complexes purified from different organisms should be compared. It has beed reported that e.g. bovine Arp2 hydrolyzes bound ATP on a minute timescale well after branches form [Le Clainche et al., 2003], while others found that Arp2 purified from yeast or amoeba hydrolyzes bound ATP rapidly in less that 1 min with [Dayel et al., 2001, Martin et al., 2006]. This shows that Arp2/3 complex from different organism might have different debranching, dissociation and nucleation rates. Thus, current available rates that have been published so far need to be applied with care.
Besides that, experiments with yeast, platelet or brain Arp2/3 complex have been done with muscle actin only with rare exceptions [Pollard, 2007]. That is to say that also the origin of the actin monomers might have also an impact on the branching and debranching rates. Relative changes in filament branching rate and dissociation rate by changes in Arp2/3 complex isoforms will drive changes in the actin networks.

To even better reproduce the structural transition from lamellipodia to filopodia, we propose a successive addition of the cross-linker fascin to a fully developed branched network. Similar to our set up of Chapter 3, where we attached the nucleator formin to NiNTA beads, we can attach the activator VCA to these beads. By this, Arp2/3 complex should only be activated at the surface of the bead and the branched network will grow from there. A similar system was implemented by Galland et al. [2013] with additional capping protein. If fascin was now added to this branched and capped network, it would replicate the transition of a branched network to parallel bundled fingerlike protrusions. With this a further understanding of transition could be gained. It will be also interesting to see if such phenomena can be explored in the assembly of cytoskeletal structures *in vivo*.

Bibliography

Amann, K. J. and Pollard, T. D. (2001). Direct real-time observation of actin filament branching mediated by Arp2/3 complex using total internal reflection fluorescence microscopy. *Proceedings of the National Academy Of Sciences*, 98(26):15009–15013.

Andrianantoandro, E., Blanchoin, L., Sept, D., McCammon, J. A., and Pollard, T. D. (2001). Kinetic mechanism of end-to-end annealing of actin filaments. *Journal of Molecular Biology*, 312:721–730.

Applewhite, D. A., Barzik, M., Kojima, S. i., Svitkina, T. M., Gertler, F. B., and Borisy, G. G. (2007). Ena/VASP Proteins Have an Anti-Capping Independent Function in Filopodia Formation. *Molecular Biology of the Cell*, 18(7):2579–2591.

Beltzner, C. C. and Pollard, T. D. (2008). Pathway of actin filament branch formation by Arp2/3 complex. *Journal of Biological Chemistry*, 283(11):7135–7144.

Blanchoin, L., Amann, K. J., Higgs, H. N., Marchand, J. B., Kaiser, D. A., and Pollard, T. D. (2000a). Direct observation of dendritic actin filament networks nucleated by Arp2/3 complex and WASP/Scar proteins. *Nature*, 404(6781):1007–1011.

Blanchoin, L., Pollard, T., and Mullins, R. (2000b). Interactions of ADF/cofilin, Arp2/3 complex, capping protein and profilin in remodeling of branched actin filament networks. *Current Biology*, 10:1273–1282.

Brackmann, M. (2011). Analysis of the photosensitivity of a LOV-N-Wasp construct as an activator of the actin polymerization and characterization of the folding conformation. *Technische Universität München*.

Brill Karniely, Y. and Ideses, Y. (2009). From branched networks of actin filaments to bundles. *ChemPhysChem*, 10:2818–2827.

Carlier, M. F. and Pantaloni, D. (1988). Binding of phosphate to F-ADP-actin and role of F-ADP-Pi-actin in ATP- actin polymerization. *Journal of Biological Chemistry*, 263(2):817–825.

Claessens, M., Tharmann, R., Kroy, K., and Bausch, A. (2006). Microstructure and viscoelasticity of confined semiflexible polymer networks. *Nature Physics*, 2:186–189.

Claessens, M. M. A. E., Semmrich, C., Ramos, L., and Bausch, A. R. (2008). Helical twist controls the thickness of F-actin bundles. *Proceedings of the National Academy Of Sciences*, 105(26):8819–8822.

Cooper, J. A. and Schafer, D. A. (2000). Control of actin assembly and disassembly at filament ends. *Current Opinion in Cell Biology*.

Cooper, J. A., Walker, S. B., and Pollard, T. D. (1983). Pyrene actin: documentation of the validity of a sensitive assay for actin polymerization. *Journal of Muscle Research and Cell Motility*, 4(2):253–262.

Craig, S. W., Lancashire, C. L., and Cooper, J. A. (1982). Preparation of smooth muscle α-actinin. *Methods in Enzymology*, 85:316–321.

Dancker, P. and Hess, L. (1990). Phalloidin reduces the release of inorganic phosphate during actin polymerization. *Biochimica et Biophysica Acta*, 1035:197–200.

Dancker, P., Löw, I., Hasselbach, W., and Wieland, T. (1975). Interaction of actin with phalloidin: Polymerization and stabilization of F-actin. *Biochimica et Biophysica Acta*, 400(2):407–414.

Dayel, M. J., Holleran, E. A., and Mullins, R. D. (2001). Arp2/3 complex requires hydrolyzable ATP for nucleation of new actin filaments. *Proceedings of the National Academy Of Sciences*, 98(26):14871–14876.

Egile, C., Loisel, T. P., Laurent, V., Li, R., Pantaloni, D., Sansonetti, P. J., and Carlier, M.-F. (1999). Activation of the Cdc42 Effector N-Wasp by the Shigella flexneri Icsa Protein Promotes Actin Nucleation by Arp2/3 Complex and Bacterial Actin-Based Motility. *The Journal of Cell Biology*, 146(6):1319.

Egile, C., Rouiller, I., Xu, X.-P., Volkmann, N., Li, R., and Hanein, D. (2005). Mechanism of Filament Nucleation and Branch Stability Revealed by the Structure of the Arp2/3 Complex at Actin Branch Junctions. *PLoS Biology*, 3(11):e383.

Falzone, T., Lenz, M., Kovar, D., and Gardel, M. (2012). Assembly kinetics determine the architecture of alpha-actinin crosslinked F-actin networks. *Nature Communications*, 3:861.

Falzone, T. T., Oakes, P. W., Sees, J., Kovar, D. R., and Gardel, M. L. (2013). Actin Assembly Factors Regulate the Gelation Kinetics and Architecture of F-actin Networks. *Biophysical Journal*, 104(8):1709–1719.

Footer, M. J., Kerssemakers, J. W. J., Theriot, J. A., and Dogterom, M. (2007). Direct measurement of force generation by actin filament polymerization using an optical trap. *Proceedings of the National Academy Of Sciences*, 104(7):2181–2186.

Frieden, C. (1983). Polymerization of actin: mechanism of the Mg2+-induced process at pH 8 and 20 degrees C. In *Proceedings of the National Academy Of Sciences*, pages 6513–6517.

Galland, R., Leduc, P., Guérin, C., Peyrade, D., Blanchoin, L., and Théry, M. (2013). Fabrication of three-dimensional electrical connections by means of directed actin self-organization. *Nature Materials*, 12(5):416–421.

Gardel, M. L., Valentine, M. T., Crocker, J. C., Bausch, A. R., and Weitz, D. A. (2003). Microrheology of Entangled F-Actin Solutions. *Physical Review Letters*, 91(15):158302.

Gebhardt, J. C. M., Bornschlogl, T., and Rief, M. (2010). Full distance-resolved folding energy landscape of one single protein molecule. *Proceedings of the National Academy Of Sciences*, 107(5):2013–2018.

Gerbal, F., Laurent, V., Ott, A., Carlier, M. F., Chaikin, P., and Prost, J. (2000). Measurement of the elasticity of the actin tail of Listeria monocytogenes. *European Biophysics Journal*, 29(2):134–140.

Goley, E. and Welch, M. (2006). The ARP2/3 complex: an actin nucleator comes of age. *Nature Reviews Molecular Cell Biology*, 7:713–726.

Gordon, D. J., Yang, Y. Z., and Korn, E. D. (1976). Polymerization of Acanthamoeba actin. Kinetics, thermodynamics, and co-polymerization with muscle actin. *Journal of Biological Chemistry*, 251(23):7474–7479.

Gordon, R., editor (1994). *Mechanical Engineering of the Cytoskeleton in Developmental Biology*. Academic Press.

Gupton, S. L. and Gertler, F. B. (2007). Filopodia: The Fingers That Do the Walking. *Science Signaling*, 2007(400):5.

Haviv, L., Brill-Karniely, Y., Mahaffy, R., backouche, F., Ben-Shaul, A., Pollard, T. D., and Bernheim-Groswasser, A. (2006). Reconstitution of the transition from lamellipodium to filopodium in a membrane-free system. *Proceedings of the National Academy Of Sciences*, 103(13):4906–4911.

Hill, T. L. and Kirschner, M. W. (1982). Bioenergetics and Kinetics of Microtubule and Actin Filament Assembly-Disassembly. *International Review of Cytology-a Survey of Cell Biology*, 78:1–125.

Hinner, B., Tempel, M., Sackmann, E., Kroy, K., and Frey, E. (1998). Entanglement, elasticity and viscous relaxation of actin solutions. *Physical Review Letters*, 81:2614.

Ichetovkin, I., Grant, W., and Condeelis, J. (2002). Cofilin Produces Newly Polymerized Actin Filaments that Are Preferred for Dendritic Nucleation by the Arp2/3 Complex. *Current Biology*, 12(1):79–84.

Ideses, Y., Brill-Karniely, Y., Haviv, L., Ben-Shaul, A., and Bernheim-Groswasser, A. (2008). Arp2/3 Branched Actin Network Mediates Filopodia-Like Bundles Formation In Vitro. *Plos One*, 3(9):e3297.

Isambert, H., Venier, P., Maggs, A., Fattoum, A., Kassab, R., Pantaloni, D., and Carlier, M. F. (1995). Flexibility of actin filaments derived from thermal fluctuations. Effect of bound nucleotide, phalloidin, and muscle regulatory proteins. *Journal of Biological Chemistry*, 270(12):11437–11444.

Kellogg, D. R., Mitchison, T. J., and Alberts, B. M. (1988). Behaviour of microtubules and actin filaments in living Drosophila embryos. *Development*, 103:675–686.

Kilimann, M. W. and Isenberg, G. (1982). Actin filament capping protein from bovine brain. *The EMBO Journal*, 1(7):889.

Kinoshita, M., Field, C. M., Coughlin, M. L., and Straight, A. F. (2002). Self- and Actin-Templated Assembly of Mammalian Septins. *Developmental cell*, 3:791–802.

Korobova, F. and Svitkina, T. (2008). Arp2/3 Complex Is Important for Filopodia Formation, Growth Cone Motility, and Neuritogenesis in Neuronal Cells. *Molecular Biology of the Cell*, 19:1561–1574.

Kouyama, T. and Mihashi, K. (1981). Fluorimetry Study of N-(1-Pyrenyl)iodoacetamide-Labelled F-Actin. *European Journal of Biochemistry*, 114:33–38.

Kovar, D. R. (2006). Arp2/3 ATP hydrolysis: to branch or to debranch? *Nature Cell Biology*, 8(8):783–785.

Kovar, D. R., Harris, E. S., Mahaffy, R., Higgs, H. N., and Pollard, T. D. (2006). Control of the assembly of ATP- and ADP-actin by formins and profilin. *Cell*, 124(2):423–435.

Kovar, D. R., Kuhn, J. R., Tichy, A. L., and Pollard, T. D. (2003). The fission yeast cytokinesis formin Cdc12p is a barbed end actin filament capping protein gated by profilin. *Journal of Cell Biology*, 161(5):875–887.

Kovar, D. R. and Pollard, T. D. (2004a). Insertional assembly of actin filament barbed ends in association with formins produces piconewton forces. *Proceedings of the National Academy Of Sciences*, 101(41):14725–14730.

Kovar, D. R. and Pollard, T. D. (2004b). Progressing actin: Formin as a processive elongation machine. *Nature Cell Biology*, 6(12):1158–1159.

Kovar, D. R., Wu, J.-Q., and Pollard, T. D. (2005). Profilin-mediated Competition between Capping Protein and Formin Cdc12p during Cytokinesis in Fission Yeast. *Molecular Biology of the Cell*, 16:2313–2324.

Kramers, H. A. (1940). Brownian motion in a field of force and the diffusion model of chemical reactions. *Physica*, 7(4):284–304.

Le Clainche, C., Didry, D., Carlier, M.-F., and Pantaloni, D. (2001). Activation of Arp2/3 Complex by Wiskott-Aldrich Syndrome Protein Is Linked to Enhanced Binding of ATP to Arp2. *Journal of Biological Chemistry*, 276(50):46689–46692.

Le Clainche, C., Pantaloni, D., and Carlier, M. F. (2003). ATP hydrolysis on actin-related protein 2/3 complex causes debranching of dendritic actin arrays. *Proceedings of the National Academy Of Sciences*, 100(11):6337–6342.

Lewis, A. K. and Bridgman, P. C. (1992). Nerve growth cone lamellipodia contain two populations of actin filaments that differ in organization and polarity. *The Journal of Cell Biology*, 119(5):1219–1243.

Lieleg, O., Claessens, M. M. A. E., Heussinger, C., Frey, E., and Bausch, A. R. (2007). Mechanics of bundled semiflexible polymer networks. *Physical Review Letters*, 99(8):088102.

Machesky, L. M. and Insall, R. H. (1998). Scar1 and the related Wiskott–Aldrich syndrome protein, WASP, regulate the actin cytoskeleton through the Arp2/3 complex. *Current Biology*, 8:1347–1356.

MacKintosh, F. C., Käs, J., and Janmey, P. (1995). Elasticity of Semiflexible Biopolymer Networks. *Physical Review Letters*, 75(24):4425–4428.

MacLean-Fletcher, S. and Pollard, T. D. (1980). Identification of a factor in conventional muscle actin preparations which inhibits actin filament self-association. *Biochemical and Biophysical Research Communications*, 96(1):18–27.

Mahaffy, R. and Pollard, T. (2006). Kinetics of the formation and dissociation of actin filament branches mediated by Arp2/3 complex. *Biophysical Journal*, 91:3519–3528.

Mahaffy, R. and Pollard, T. (2008). Influence of Phalloidin on the Formation of Actin Filament Branches by Arp2/3 Complex. *Biochemistry*, 47:6460–6467.

Maier, V. (2014). Charakterisierung von Keratin mit der optischen Pinzette. *Technische Universität München.*

Marchand, J.-B., Kaiser, D. A., Pollard, T. D., and Higgs, H. N. (2000). Interaction of WASP/Scar proteins with actin and vertebrate Arp2/3 complex. *Nature Cell Biology*, 3(1):76–82.

Martin, A. C., Welch, M. D., and Drubin, D. G. (2006). Arp2/3 ATP hydrolysis-catalysed branch dissociation is critical for endocytic force generation. *Nature Cell Biology*, 8(8):826–833.

Mattila, P. K. and Lappalainen, P. (2008). Filopodia: molecular architecture and cellular functions. *Nature Reviews Molecular Cell Biology*, 9(6):446–454.

May, R. C., Hall, M. E., Higgs, H. N., Pollard, T. D., Chakraborty, T., Wehland, J., Machesky, L. M., and Sechi, A. S. (1999). The Arp2/3 complex is essential for the actin-based motility of Listeria monocytogenes. *Current Biology*, 9(14):759–762.

Mejillano, M. R., Kojima, S., Applewhite, D. A., and Gertler, F. B. (2004). Lamellipodial Versus Filopodial Mode of the Actin Nanomachinery: Pivotal Role of the Filament Barbed End. *Cell*, 118:363–373.

Mezger, T. G. (2006). *The Rheology Handbook*. For Users of Rotational and Oscillatory Rheometers. Vincentz Network GmbH & Co KG.

Mogilner, A. and Oster, G. (1996). Cell motility driven by actin polymerization. *Biophysical Journal*, 71(6):3030–3045.

Mogilner, A. and Rubinstein, B. (2005). The Physics of Filopodial Protrusion. *Biophysical Journal*, 89(2):782–795.

Mullins, R. D., Heuser, J. A., and Pollard, T. D. (1998). The interaction of Arp2/3 complex with actin: Nucleation, high affinity pointed end capping, and formation of branching networks of filaments. *Proceedings of the National Academy Of Sciences*, 95:6181–6186.

Noireaux, V., Golsteyn, R. M., Friederich, E., Prost, J., Antony, C., Louvard, D., and Sykes, C. (2000). Growing an Actin Gel on Spherical Surfaces. *Biophysical Journal*, 78(3):1643–1654.

Ono, S., Yamakita, Y., Yamashiro, S., Matsudaira, P. T., Gnarra, J. R., Obinata, T., and Matsumura, F. (1997). Identification of an Actin Binding Region and a Protein Kinase C Phosphorylation Site on Human Fascin. *Journal of Biological Chemistry*, 272:2527–2533.

Pantaloni, D., Boujemaa, R., Didry, D., Gounon, P., and Carlier, M. F. (2000). The Arp2/3 complex branches filament barbed ends: functional antagonism with capping proteins. *Nature Cell Biology*, 2(7):385–391.

Paul, A. and Pollard, T. (2008). The role of the FH1 domain and profilin in formin-mediated actin-filament elongation and nucleation. *Current Biology*, 18(1):9–19.

Peskin, C. S., Odell, G. M., and Oster, G. (1993). Cellular Motions and Thermal Fluctuations - the Brownian Ratchet. *Biophysical Journal*, 65(1):316–324.

Pfaendtner, J., Lyman, E., Pollard, T., and Voth, G. (2010). Structure and dynamics of the actin filament. *Journal of Molecular Biology*, 396:252–263.

Pollard, T. and Borisy, G. (2003). Cellular motility driven by assembly and disassembly of actin filaments. *Cell*, 112(4):453–465.

Pollard, T. D. (1986). Rate constants for the reactions of ATP- and ADP-actin with the ends of actin filaments. *The Journal of Cell Biology*, 103(6):2747–2754.

Pollard, T. D. (2007). Regulation of actin filament assembly by Arp2/3 complex and formins. *Annual Review of Biophysics and Biomolecular Structure*, 36:451–477.

Pollard, T. D., Blanchoin, L., and Mullins, R. D. (2000). Molecular mechanisms controlling actin filament dynamics in nonmuscle cells. *Annual Review of Biophysics and Biomolecular Structure*, 29:545–576.

Pollard, T. D. and Earnshaw, W. C. (2004). *Cell Biology*. Elsevier, 1st edition.

Resch, G. P., Goldie, K. N., Krebs, A., Hoenger, A., and Small, J. V. (2002). Visualisation of the actin cytoskeleton by cryo-electron microscopy. *Journal of Cell Science*, 115(9):1877–1882.

Rickard, J. E. and Sheterline, P. (1986). Cytoplasmic concentrations of inorganic phosphate affect the critical concentration for assembly of actin in the presence of cytochalasin D or ADP. *Journal of Molecular Biology*, 191(2):273–280.

Romero, S., Le Clainche, C., Didry, D., Egile, C., Pantaloni, D., and Carlier, M.-F. (2004). Formin Is a Processive Motor that Requires Profilin to Accelerate Actin Assembly and Associated ATP Hydrolysis. *Cell*, 119(3):419–429.

Rouiller, I., Xu, X.-P., Amann, K. J., Egile, C., Nickell, S., Nicastro, D., Li, R., Pollard, T. D., Volkmann, N., and Hanein, D. (2008). The structural basis of actin filament branching by the Arp2/3 complex. *The Journal of Cell Biology*, 180(5):887–895.

Schafer, D. A. (2004). Cell biology: Barbed ends rule. *Nature Cell Biology*, 430(7001):734–735.

Schafer, D. A., Jennings, P. B., and Cooper, J. A. (1996). Dynamics of capping protein and actin assembly in vitro: uncapping barbed ends by polyphosphoinositides. *The Journal of Cell Biology*, 135(1):169–179.

Schirenbeck, A., Bretschneider, T., Arasada, R., Schleicher, M., and Faix, J. (2005). The Diaphanous-related formin dDia2 is required for the formation and maintenance of filopodia. *Nature Cell Biology*, 7(6):619–625.

Schmoller, K., Lieleg, O., and Bausch, A. (2009). Structural and viscoelastic properties of actin/filamin networks: cross-linked versus bundled networks. *Biophysical Journal*, 97:83–89.

Semmrich, C., Larsen, R. J., and Bausch, A. R. (2008). Nonlinear mechanics of entangled F-actin solutions. *Soft Matter*, 4(8):1675–1680.

Semmrich, C., Storz, T., Glaser, J., Merkel, R., Bausch, A. R., and Kroy, K. (2007). Glass transition and rheological redundancy in F-actin solutions. *Proceedings of the National Academy Of Sciences*, 104(51):20199–20203.

Sept, D. and McCammon, J. A. (2001). Thermodynamics and Kinetics of Actin Filament Nucleation. *Biophysical Journal*, 81(2):667–674.

Shaw, T. J. and Martin, P. (2009). Wound repair at a glance. *Journal of Cell Science*, 122(18):3209–3213.

Sheetz, M. P. (2001). Cell control by membrane–cytoskeleton adhesion. *Nature Reviews Molecular Cell Biology*, 2(5):392–396.

Sjöblom, B., Salmazo, A., and Djinović-Carugo, K. (2008). α-Actinin structure and regulation. *Cell and Molecular Life Sciences*, 65(17):2688–2701.

Spudich, J. A. and Watt, S. (1971). The Regulation of Rabbit Skeletal Muscle Contraction. *Journal of Biological Chemistry*, 246(15):4866–4871.

Storm, C., Pastore, J. J., MacKintosh, F. C., Lubensky, T. C., and Janmey, P. A. (2004). Nonlinear Elasticity in Biological Gels. *Nature*, 435:192–194.

Svitkina, T., Bulanova, E., and Chaga, O. (2003). Mechanism of filopodia initiation by reorganization of a dendritic network. *The Journal of Cell Biology*, 160:409–421.

Svitkina, T. M. (1999). Arp2/3 Complex and Actin Depolymerizing Factor/Cofilin in Dendritic Organization and Treadmilling of Actin Filament Array in Lamellipodia. *The Journal of Cell Biology*, 145(5):1009–1026.

Takenawa, T. and Miki, H. (2001). WASP and WAVE family proteins: key molecules for rapid rearrangement of cortical actin filaments and cell movement. *Journal of Cell Science*, 114(10):1801–1809.

Tobacman, L. S. and Korn, E. D. (1983). The kinetics of actin nucleation and polymerization. *Journal of Biological Chemistry*, 258:3207–3214.

Vignjevic, D., Kojima, S.-i., Svitkina, T., and Borisy, G. G. (2006). Role of fascin in filopodial protrusion. *Journal of Cell Biology*, 174(6):863–875.

Vignjevic, D., Yarar, D., Welch, M. D., Peloquin, J., Svitkina, T., and Borisy, G. G. (2003). Formation of filopodia-like bundles in vitro from a dendritic network. *The Journal of Cell Biology*, 160(6):951–962.

Welch, M. (1997). Actin dynamics in vivo. *Current Opinion in Cell Biology*, 9(1):54–61.

Welch, M. D., Rosenblatt, J., Skoble, J., Portnoy, D. A., and Mitchison, T. J. (1998). Interaction of human Arp2/3 complex and the Listeria monocytogenes ActA protein in actin filament nucleation. *Science*, 281(5373):105–108.

Yang, C., Czech, L., Gerboth, S., Kojima, S., and Scita, G. (2007). PLOS Biology: Novel Roles of Formin mDia2 in Lamellipodia and Filopodia Formation in Motile Cells. *PLoS Biology*, 5(11):e317.

Yang, C. and Svitkina, T. (2011). Filopodia initiation: Focus on the Arp2/3 complex and formins. *Cell Adhesion & Migration*, 5(5):402–408.

Ziemann, F., Radler, J., and Sackmann, E. (1994). Local measurements of viscoelastic moduli of entangled actin networks using an oscillating magnetic bead micro-rheometer. *Biophysical Journal*, 66:2210–2216.

Acknowledgments

Die Jahre der Doktorarbeit sind immer geprägt von vielen Menschen, die mich unterstützt haben und den Weg teilweise mit mir gemeinsam gegangen sind.

DANKE....

Meinem Doktorvater **Prof. Dr. Andreas Bausch**, dafür, dass ich meine Doktorarbeit bei dir schreiben durfte, du mir alle Freiheiten gelassen hast und mich über die letzten Jahre so gut betreut hast.

Martina – Supergirl! Die beste Bürokollegin der letzten vier Jahre. Allein durch das Zuhören meines Problems hast du mir oft geholfen, es auch direkt zu lösen und Argumentationsknoten zu lockern. Lass uns die Verteidigung zusammen rocken!

Katharina und **Felix** – Für die hilfreichen Diskussionen der Experimente und der Ergebnisse. Für das kritische und detaillierte Korrekturlesen. Felix, auch für deine spontane Hilfe zu Matlab Simulationen und ImageJ Auswertungen.

Anja – Du hast mir viel Details zur Biochemie beigebracht, mir in einem 1-wöchigen Crashkurs alles, wirklich alles zur Proteinaufreinigung und Klonieren gezeigt und hattest für alle Fragen stets eine Antwort.

Schuppi – Dafür, dass wir die Experimente an deiner Falle gemacht haben und die Auswertung der Daten gemeinsam diskutiert haben.

TAs – Lieben Dank an Moni, Gabi, Karin und Hieu für die unermüdliche Proteinaufreinigung. Ohne euch läuft im Labor halt einfach nichts!

Lorenz – Danke für die Salsa-Abende, für die Rotwein-Abende am Königplatz und besonders dafür, uns regelmäßig in die bezaubernde Welt des Piemont, des guten Essens und der erstklassigen Gesellschaft mitzunehmen. Die Weinvorräte müssen jährlich aufgestockt werden ;)

Alex – Danke für's bekochen, mich abends mit Häppchen und Vitaminen versorgen, wenn meine Essensvorräte mal wieder ausgegangen sind und für die Feierabendbiere. Für's zuhören, für's motivieren, für angeregte, interessante und manchmal auch hitzige Gespräche und einfach für's da sein. Es ist schön, dass sich unsere Wege gekreuzt haben.

Allen von E22/E27 und den fleißigen Kuchenbäckern – Die Atmosphäre war einfach unbeschreiblich toll und der Zusammenhalt auch außerhalb der Laborgänge bemerkenswert - sei es auf der Wiesn, auf der Hütte oder auf'm Nockherberg.

Danke, **Mama und Papa**, dass ihr mich immer meinen Weg gehen gelassen habt und auch an meine **Schwester Christiane** für eure unermüdliche Unterstützung über all die Jahre hinweg. Ich freu mich sehr, dass wir endlich wieder alle in einer Stadt wohnen und der Weg zu euch nicht mehr so lang ist.

Danke auch an meinen Lama **Ole Nydahl**, dessen Tatkraft, Freude und Energie eine Inspiration ist. Er hat mich gelehrt, worauf es im Leben ankommt und mir den Weg gezeigt.

Besonderen Dank gebührt auch den zwei wichtigen Frauen in meinem Leben:
Sofia und **Eva**. Für's reden, lachen, inspirieren, zuhören, feiern, spazieren gehen, diskutieren, erzählen. Für euren Input und euren Rückhalt. Danke, dass ihr immer für mich da seid!

Und vor allem **Robert** – Das Leben mit dir zu teilen ist einfach wunderschön. Unserer liebevolle unerschütterliche Partnerschaft ist eine kostbare Bereicherung, in der wir uns ständig weiterentwickeln und die uns eine tiefe Kraft gibt. Mögen wir unseren Weg weiterhin gemeinsam in die richtige Richtung gehen.